KUKHA HAWEZ, H.R. 2023. *Coupled geomechanics and transient multiphase flow at fracture-matrix interface in tight reservoirs*. Robert Gordon University, PhD thesis. Hosted on OpenAIR [online]. Available from: https://doi.org/10.48526/rgu-wt-1987869

Coupled geomechanics and transient multiphase flow at fracture-matrix interface in tight reservoirs.

KUKHA HAWEZ, H.R.

2023

The author of this thesis retains the right to be identified as such on any occasion in which content from this thesis is referenced or re-used. The licence under which this thesis is distributed applies to the text and any original images only – re-use of any third-party content must still be cleared with the original copyright holder.

OpenAIR @RGU

This document was downloaded from https://openair.rgu.ac.uk

BY NC

Coupled Geomechanics and Transient Multiphase Flow at Fracture-Matrix Interface in Tight Reservoirs

Haval Rostam Kukha Hawez

PhD 2023

Coupled Geomechanics and Transient Multiphase Flow at Fracture-Matrix Interface in Tight Reservoirs

Haval Rostam Kukha Hawez

A thesis is submitted in partial fulfilment of the requirements of
Robert Gordon University
For the degree of Doctor of Philosophy

January 2023

To my Father and Mother

Abstract

Fractured hydrocarbon reservoirs play a significant role in the world economy and energy markets. Fluid injection (normally water) forces the hydrocarbons out of the reservoirs. Geomechanics, externally applied stress on the rock, play a significant role in the oil recovery from fractured reservoirs. Subsurface fluid injection modifies pore pressure and in-situ stresses locally. In response to the pressure/stress combined effects, the pores and fracture regions undergo deformation. Similarly, it is a well-known fact that pore volume significantly impacts the absolute and relative permeability of fractured tight reservoirs. The governing factors that characterize multiphase fluid flow mechanism in naturally fractured tight reservoirs, such as wellbore stability, CO_2 sequestration, and improved hydrocarbon recovery, are relative permeability and capillary pressure. Although the effects of geomechanical parameters on single-phase fluid flow in naturally fractured tight reservoirs are well documented, the interdependence between geomechanical and multiphase flows are severely lacking. This study aims to bridge this knowledge gap using advanced numerical techniques, focusing on accurately capturing complex flow phenomena at the fracture-matrix interface to enhance the accuracy of predicting oil recovery from naturally fractured tight reservoirs, leading towards more efficient operations and reduced costs.

Extensive set of numerical investigations have been carried out in the present study, using advanced Computational Fluid Dynamics (CFD) solver, to accurately capture transient multiphase flow (oil and water) phenomena within naturally

fractured tight reservoirs. Special attention has been paid towards accurate multiphase flow modelling and characterisation at the fracture-matrix interface. The numerical models have been validated against Berea Sandstone experimental data. Two separate numerical models have been developed with the aim to identify the most appropriate modelling technique for accurate numerical predictions of multiphase flow in naturally fractured tight reservoirs. These two models are based on duct flow theory and flow through porous medium theory, respectively, while Brooks and Corey method has been utilised to compute fluid saturation, relative permeability, and capillary pressure at the fracture-matrix interface. The results obtained show that the difference between the numerical and experimental results is 30 % when duct flow model is considered, while it is 2.57 % when porous medium is considered.

In order to critically evaluate the dependence of multiphase flow on the geomechanical parameters of naturally fractured tight reservoirs, a one-way FEA-CFD coupling scheme has been implemented in the present study, not taking into consideration the pore pressure. The effects of externally applied stress loading on the geomechanical (porosity and fracture aperture) and multiphase flow characteristics (permeability, capillary pressure, relative permeability, and fluid saturation), at the fracture-matrix interface, have been thoroughly analysed. For accurate modelling and numerical predictions in naturally fractured tight reservoirs, a viscous loss term has been incorporated in the momentum conservation equations. The numerical predictions from the one-way coupled model matches well with Clashach core flooding experimental data, with 9 % average difference between the two. The results obtained clearly indicate that external stress loading has significant impact on the geomechanical and multiphase flow characteristics at the fracture-matrix interface.

Finally, a novel numerical model has been developed based on the full coupling scheme, with the aim to enhance the accuracy of the numerical predictions regarding oil recovery from naturally fractured tight reservoirs for efficient and cost effective operations. The porous elasticity interface is coupled with multiphase flow in porous media where the mass conservation of each phase, and an extended Darcy's equation, underpin multiphase flow characteristics. The fully coupled model takes into consideration the pore pressure and has been validated against Clashach core flooding experimental data. The developed model has been shown to significantly enhance the prediction accuracy from 9 %, for one-way coupled model, to 4 %, and has the ability to capture complex multiphase flow phenomena at the fracture-matrix interface. Moreover, the novel model accurately predicts the effects of geomechanical parameters on multiphase flow characteristics. It is envisaged that the novel fully coupled model developed in this study will pave the way for future scientific research in the area of geomechanical-fluid flow coupling for enhanced oil recovery in naturally fractured tight reservoirs.

Declaration

I hereby certify that the research report in this thesis is original and that I (Haval Kukha Hawez) performed it independently under the supervision of Dr Taimoor Asim and Prof Nadimul Haque Faisal. This PhD thesis has not been submitted for consideration for any other degree or professional qualification.

Acknowledgements

Completing the requirements for a Doctor of Philosophy (PhD) degree reminds me a lot of running a marathon. It takes time, effort, planning, training, and equipment. It, like a marathon, has benefited from spectator support along the way. Although there are too many to name, you know who you are. Past professors, co-workers, friends, and families have all impacted me, some of which have been positive! Your investment in me has contributed to my achievement. Certain people, however, were critical to finishing this marathon.

My deepest gratitude to Dr Taimoor Asim, Prof Nadimul Haque Faisal, and Dr Reza Sanaee, for allowing me to work on this PhD I have had more than three years of guidance, encouragement, criticism, support, humour, and constant motivation from the three of you. I have achieved excellence, thanks to your advice. Your support, coaching approach, and vast knowledge have made a lasting impression on me. I am blessed to have you all as my friends and coaches.

Thank my devoted wife, Shayee Omar, for her assistance during this research endeavour. My friends Dr Auwalu Mohammad, Dr Yakubu Balogun, Dr Haidar Al-Mashhadani, and Dr Maryam Heidaran deserve special thanks.

I also thank Dr Rosslyn Shanks, Mrs Kirsty Stevenson, and Mrs. Petrena Morrison. I thank the technicians, friends, and colleagues (N436) from the School of Engineering, Graduate School, and library personnel.

Contents

List of Figures

List of Tables

List of Publications

1. Hawez, H., Sanaee, R., Faisal, N.H. (2020). Coupled Reservoir Geomechanics and Multiphase Flow in Fractured Porous Media. ETP Annual Conference.

2. Hawez, H.K., Sanaee, R., Faisal, N.H., 2021. A critical review on coupled geomechanics and fluid flow in naturally fractured reservoirs. J. Nat. Gas Sci. Eng. 95, 104150. https://doi.org/10.1016/j.jngse.2021.104150

3. Hawez, H., Sanaee, R., Faisal, N.H., 2021. Multiphase Flow Modelling in Fractured Reservoirs using a Novel Computational Fluid Dynamics Approach, in Paper Presented at the 55th U.S. Rock Mechanics/Geomechanics Symposium, Virtual. https://doi.org/ARMA-2021-1077

Nomenclature

φ	*Porosity (-)*
φ_a	*Absolute porosity (-)*
φ_e	*Effective porosity (-)*
q_β	*Flow rate of the phase β (m^3/s)*
A	*Cross-sectional area (m^2)*
k_β	*Permeability of the phase β (mD or D)*
ΔP	*Pressure difference across the sample (Pa)*
μ	*Dynamic viscosity (Pa.s)*
L	*Length of the sample (m)*
k_f	*Fracture permeability (D)*
k_{i-f}	*Initial fracture permeability (D)*
h	*Fracture aperture (µm)*
S_β	*Saturation of the phase β (-)*
S_w	*Water saturation (-)*
S_o	*Oil saturation (-)*

S_g	*Gas saturation (-)*
S_{gc}	*Gas condensate saturation (-)*
S_{wc}	*Connate water saturation (-)*
Kr_{β}	*Relative permeability of the phase* β *(-)*
$k_{e\beta}$	*Effective permeability of the phase* β *(mD or D)*
k_a	*Absolute permeability (mD or D)*
Kr_w, Kr_o, Kr_g	*Water, oil and gas relative permeability, respectively (-)*
S_{oi}	*Initial oil saturation (-)*
S_{or}	*Residual oil saturation (-)*
S_{wi}	*Irreducible water saturation (-)*
η	*Darcy velocity (m/s)*
ρ	*Density (kg/m^3)*
g	*Gravitational acceleration (m/s^2)*
D	*Depth of the datum and dimeter of the core sample (m)*
t	*Time (s)*
Ψ	*Source or sink term (N/m^3)*
Pc	*Capillary pressure (kPa)*

Pec	*Entry capillary pressure (Pa)*
P_o, P_w	*Oil and water pressure (Pa)*
λ_β	*Mobility of the phase β (m^2/Pa.s)*
P_p	*Pore pressure (Pa)*
c	*Consolidation coefficient (m^2/s)*
σ	*Total stress (MPa)*
σ'	*Effective stress (MPa)*
δ	*Kronecker delta (-)*
α_B	*Biot-Willis coefficient (-)*
K_d	*Drained bulk modulus (MPa)*
K_s	*Solid bulk modulus (MPa)*
e	*Void ratio (-)*
e_i	*Initial void ratio (-)*
ε_{vol}	*Volumetric strain (-)*
k_{mat}	*Matrix permeability (mD)*
$k_{i\text{-}mat}$	*Initial matrix permeability (mD)*
ν	*Poisson's ratio (-)*

E	Young modulus (GPa)
u, v, and w	Flow velocities (m/s) in x, y, and z direction respectively
Ψ_x, Ψ_y and Ψ_z	The source terms (N/m^3) in x, y and z direction respectively
U	Flow velocity (m/s)
$\vec{U}_{superficial}$	Superficial velocity (m/s)
$\vec{U}_{physical}$	Physical velocity (m/s)
ρ_m	Mixture density (kg/m^3)
μ_m	Mixture dynamic viscosity (Pa.s)
λ_p	Pore size distribution index (-)
σ^{el}	Elastic stress (MPa)
ε^{el}	Elastic strain (-)
K_b	Bulk modulus (MPa)
R	Shear modulus (MPa)
X	Rock swell index (-)
p	Mean effective stress (MPa)
p_t^{el}	Elastic limit of tensile strength (MPa)
ε_{vol}^{el}	Elastic volumetric strain (-)

M	*Storage model (1/Pa)*
d	*Displacement (μm)*
Qc	*Cumulative oil volume (m^3/s)*
$P_{c\beta}^{l}$	*Capillary pressure (kPa) of the phase β on low permeable side*
$P_{ec\beta}^{l}$	*Entry Capillary pressure (kPa) of the phase β on low permeable*
$P_{c\beta}^{h}$	*Capillary pressure (kPa) of the phase β on high permeable side*
S_{β}^{l}	*Saturation of the phase β on low permeable side (-)*
S_{β}^{h}	*Saturation of the phase β on low permeable side (-)*

Chapter 1
Introduction to Naturally Fractured Tight Reservoirs

Naturally fractured tight hydrocarbon reservoirs play a significant role in the global economy and energy. To successfully study the underlying complicated multiphase flow phenomena occurring in naturally fractured tight reservoirs, it is necessary first to understand fractured rock composition and key hydraulic parameters of naturally fractured tight reservoirs. Also discussed in this chapter are the factors affecting multiphase flows in naturally fractured tight reservoirs. The motivation and aims of this research study are the highlights of this chapter.

1.1 Introduction

Since the beginning of the nineteenth century's industrial revolution, man has relied increasingly on mineral fuels to provide the energy required to run the machines. The first oil-only commercial well was built in the United States in 1859. After its success, the extraction and processing of petroleum in the United States and European countries rapidly became very famous (Craig et al., 2018; Soeder, 2021). Despite society's decreased reliance on fossil fuels, oil and natural gas, which together are commonly referred to as hydrocarbons, have continued to be crucial for decades. As the energy mix diversifies, customer choice expands, and needs for integration across various fuels and energy services rise. Today, fossil fuels are powerful in meeting the world's energy needs. Even though their contribution to the energy mixture is anticipated to decline, it will still be more than 80 % up to 2035. Thus, the oil will continue to play the dominant role in the energy mix, maintaining its proportion above 30 %, albeit gradually declining, as shown in Figure 1.1 (British Petroleum Company, 2017).

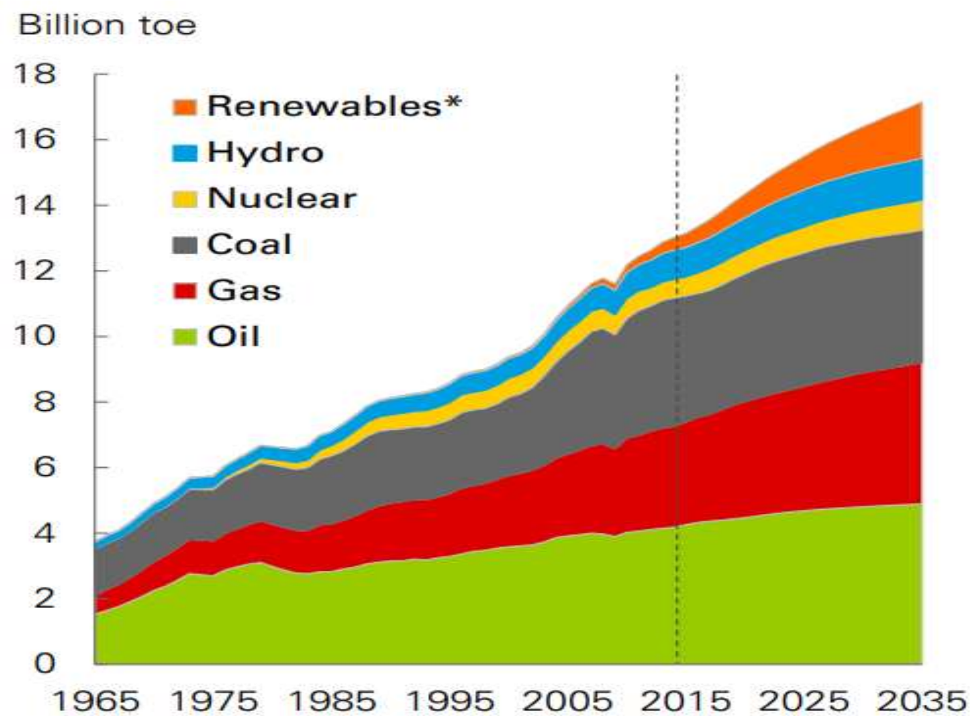

Figure 1.1. Global primary energy supply by fuel type (British Petroleum Company, 2017)

Naturally fractured tight hydrocarbon reservoirs play a significant role in the world economy and energy. Naturally fractured tight hydrocarbon reservoirs, such as the Ain Zalah and Kirkuk oil fields in Iraq, the Dukhan oil field in Qatar as depicted in Figure 1.2, the Asmari limestone reservoir in Iran, the vugular carbonate reservoirs in Mexico, the group of the chalk reservoirs in the North Sea, and more than 400 billion barrels of hydrocarbon reserves in Canada, provide more than 20 % of the reserves and production (Jalali and Dusseault 2012). These are frequently impacted by complicated production histories, uncertain well coupling, quickly fluctuating flow rates, early water breakthrough, and low final recovery.

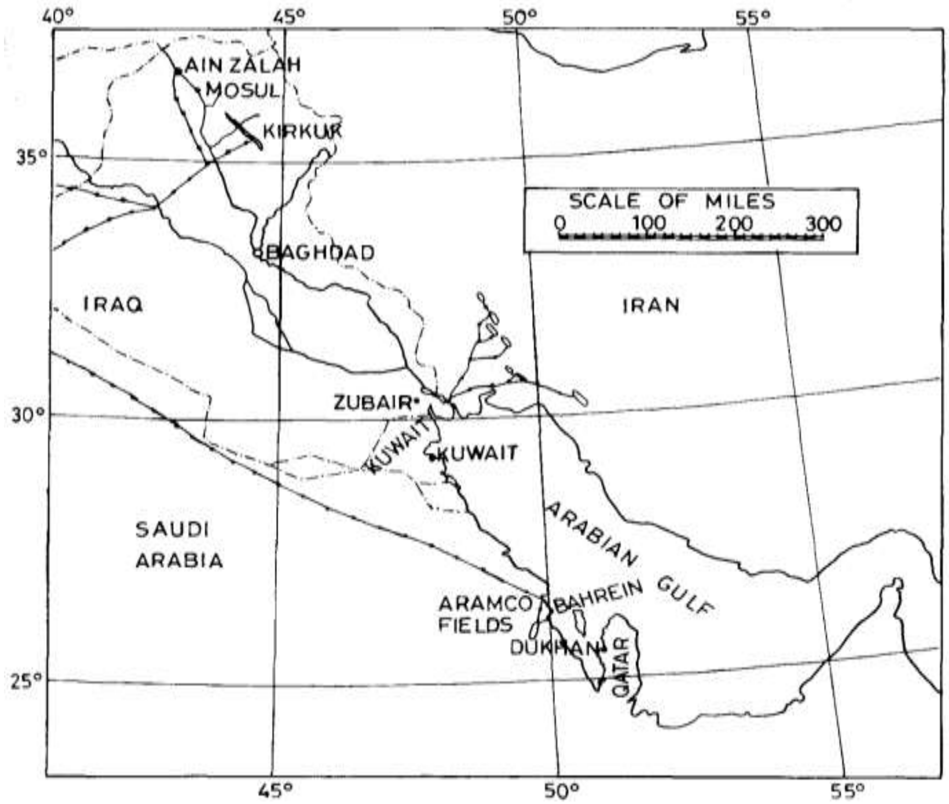

Figure 1.2. Middle East general map indicating the locations of the Ain Zalah, Kirkuk, and Dukhan reservoirs (Daniel, 1954)

1.2 Composition of Naturally Fractured Tight Reservoirs

Rock is a porous medium, containing fractures. Tectonic activity results in some degree of fracture in subsurface rocks. Fluid flow is critically dependent on fractured systems, particularly in tight rock reservoirs. Predominantly, fracture network patterns are the primary conduits for fluid flow and improve permeability in tight formations, while the porous matrix controls the main reservoir storage capacity.

Natural fractures, such as joints, faults, and fissures, are common in the subsurface. Generally, a fracture is a discontinuity that divides rock beds into blocks along fractures, fissures, and joints. Along this, there is no displacement parallel with the discontinuity planes. These innate discontinuities frequently involve intricate networks and produce disorganized geological settings. Fractures are important conduits or obstacles for fluid flows. For domains ranging from millimetres to hundreds of kilometres, distinct forms of porous media are characterized by fractures that affect flow and transport, as shown in Figure 1.3.

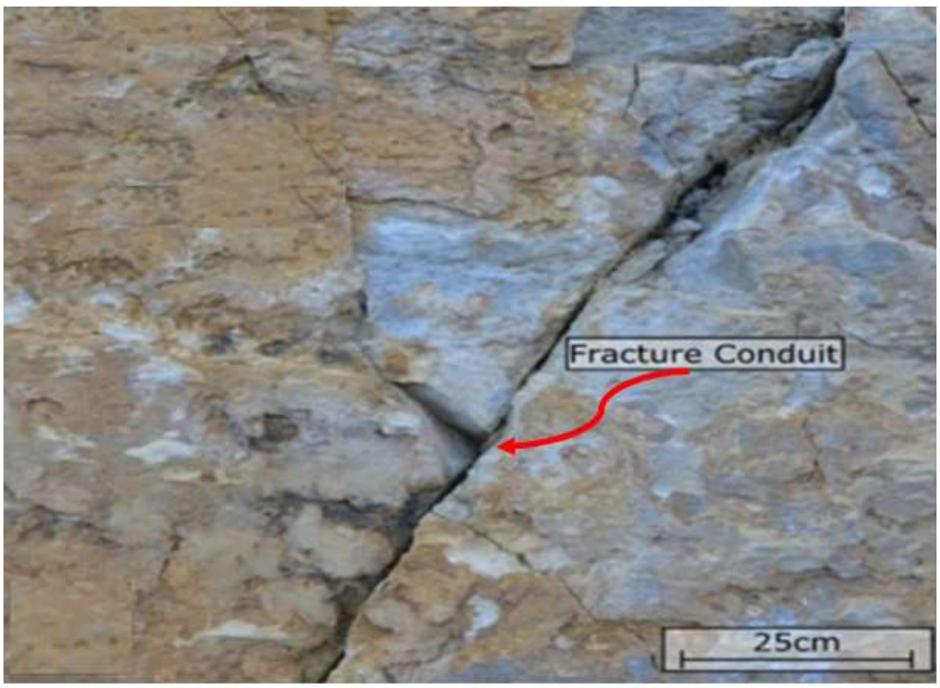

Figure 1.3. A fracture conduit (Smith et al., 2022)

The most common fractures are identified through their size, density, orientation (and aperture), and spatial association (Golf-Racht, 1982). The lognormal, exponential, and gamma distributions, among others, are frequently good descriptions of these characteristics. The traditional theory of a rock fracture considers two parallel, smooth plates. Such a framework is helpful for quantitative analyses in particular. Examining the meaning of fracture aperture in light of fracture wall roughness is only natural. In quantitative flow and transport modelling attempts, an aperture must be defined as a parameter. The definition, an aperture, is a function of the physical process (such as fluid flow or solute transport) for which it is required. In many naturally fractured tight reservoirs, fracture systems are crucial components that support better reservoir characteristics and flow. Numerous scales can be used to analyse fracture systems, including seismic and dynamic field data, analogues from outcrops, well data, and laboratory studies. The stability and fracture reactions of a rock structure can be impacted by fluid mechanics.

1.3 Key Hydraulic Parameters of Naturally Fractured Tight Reservoirs

In a single-phase system, a single fluid (such as water) or a combination of many miscible fluids (such as fresh water and saltwater) fills the void area of the porous media. In a multiphase system, two or more fluids that are immiscible with one another, that is, they retain a clear border between them (for example, water and oil fill the fractured pore spaces). Since gases are always entirely miscible, there may only be one gaseous phase. Formally, the fractured rocks can also be considered a phase with the name solid phase. Individual phases have a specific volume fraction and flow velocity field in a multiphase scenario in a naturally fractured tight reservoirs (Carrillo et al., 2020). The principals involved in simulating multiphase fluid flow through naturally fractured tight reservoirs are outlined in the following subsections.

1.3.1 Porosity

Porosity is the amount of space available for storing hydrocarbons and is one of the essential rock qualities from the perspective of reservoir engineering. Porosity is a quantitative proportion of pore volume to total volume (or bulk volume). The following generalized relationship provides a mathematical formula for this crucial rock attribute.

$$\varphi = \frac{pore\ volume}{bulk\ volume} = \frac{bulk\ volume - grain\ volume}{bulk\ volume} \tag{1.1}$$

where φ is the porosity.

The pore structure of the rock is incredibly intricate, and the texture of the rock is made up of mineral grains of all sizes and shapes. The shape and distance between these grains are the two most crucial components of the pore structure. This is because the fluids that create connection or storage pores are primarily transported or stored in the gaps between these grains.

Naturally fractured tight reservoirs comprise of two distinct types of porosities. The first type of porosity is called Primary or Intergranular porosity. The second type of porosity is called Secondary porosity. Primary porosity is formed by void spaces between the rock grains, while the secondary porosity is composed of void spaces of fractures and vugs. Both the porosity systems are shown in Figure 1.4. (Golf-Racht, 1982).

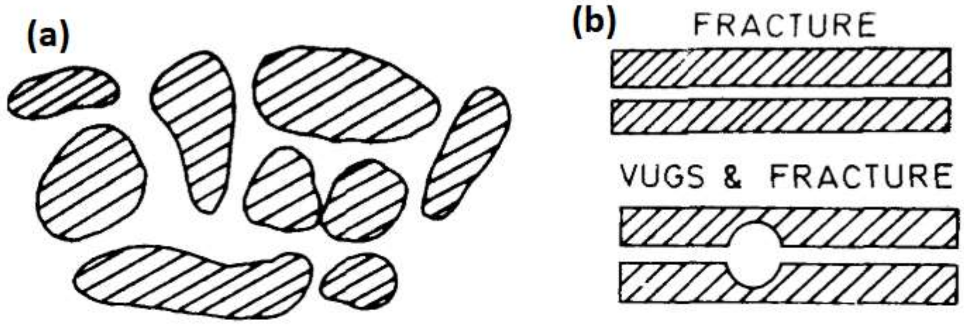

Figure 1.4. Porosity in naturally fractured tight reservoirs (a) Primary porosity (b) Secondary porosity (Golf-Racht, 1982)

Primary porosity is common in sandstone or limestone. Secondary porosity exclusively applies to vugs or fractures (Maniscalco et al., 2022). The secondary porosity is typically found in brittle, compact rocks with little intergranular porosity, such as schists, siltstones, compact limestone, shales, and shaly sandstones. Typical causes of secondary porosity include the fracturing, jointing, and water-induced dissolving of rocks. During ancient geological periods, void spaces were formed within tight reservoirs and the rocks became isolated from other void spaces by excessive cementation. As a result, whereas specific pore spaces were entirely isolated, numerous empty spaces were connected, as shown in Figure 1.5. Consequently, there are two kinds of primary porosity i.e. absolute and effective porosity.

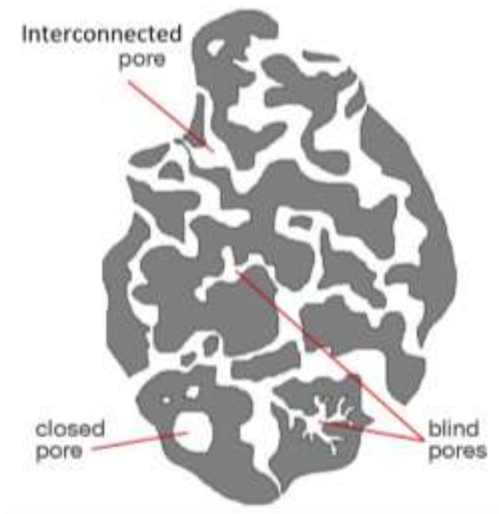

Figure 1.5. A porous solid

The ratio of the amount of pore space in the rock to its bulk volume is known as absolute porosity. Despite having significant absolute porosity, a rock may not have appreciable fluid conductivity due to a lack of pore connectivity (Ahmed, 2019). The following mathematical relationships often represent the absolute porosity:

$$\varphi_a = \frac{total\ pore\ volume}{bulk\ volume} \tag{1.2}$$

where φ_a is the absolute porosity.

Only interconnected pores are important from flow through porous media perspective. Effective porosity is defined as the proportion of interconnected pore space to the bulk volume.

$$\varphi_e = \frac{interconnected\ pore\ volume}{bulk\ volume} \tag{1.3}$$

where φ_e is the effective porosity.

1.3.2 Permeability

Permeability is the ability of fluid to flow through the porous medium. Because it regulates the direction and flow rate of the reservoir fluids in the formation, the rock's permeability, or k, is an important rock attribute (Hommel et al., 2018). Henry Darcy (1856) provided the first mathematical definition of permeability as:

$$q_\beta = \frac{A\, k_\beta \Delta P}{\mu L} \tag{1.4}$$

where q is the flow rate (m^3/s) of the phase β, k is the permeability (mD or millidarcy), A is the cross sectional area (m^2), μ is the viscosity (Pa.s), L is the length of the sample (m) and ΔP is the differential pressure (Pa) across the sample.

In the case of a naturally fractured tight reservoir, the fundamentals of permeability established in a conventional reservoir (fractured reservoir) still hold true. However, permeability may be redefined as matrix permeability, fracture permeability, and system (fracture-matrix) permeability in the presence of fractures in matrix (Golf-Racht, 1982). This revised definition of permeability could lead to certain misunderstandings, particularly concerning fracture permeability, which can be understood as either single fracture permeability or fracture network permeability, or occasionally as fracture permeability of fracture-bulk volume (Lamur et al., 2017). As a result, the various permeability expressions will be thoroughly explored and analysed. The intrinsic fracture permeability is correlated with the conductivity observed during fluid passage through a single fracture or a network of fractures, independent of the rock surrounding the fracture (matrix) (Mohais et al., 2012). Specifically, it is the conductivity of a single channel (fracture) or a collection of channels (fracture network). Only the fracture void areas in this instance represent the flow cross-section (excluding the surrounding matrix area). For simplification, imagine a block where the fracture runs parallel to the flow direction (Xu et al., 2021).

The fracture permeability can be calculated directly to be isotropic in the case of an idealized representation of a conductive fracture as a channel between two parallel planes separated by a constant distance h, as well as additional assumptions of incompressible flow and no-slip conditions on the confining planes (Berre et al., 2019). Since the permeability of the rock matrix is often low to extremely low, many conventional and unconventional reservoirs (hydrocarbons in the unconventional reservoirs were formed inside the rock and have never migrated) produce hydrocarbons primarily through a network of fractures. The permeability of the fractures can range from hundreds of millidarcies to a Darcy or more, which is several orders of magnitude higher than matrix permeability (Satter and Iqbal, 2016). The following equation links fracture permeability to fracture width:

$$k_f = \frac{h^2}{12} \tag{1.5}$$

where k_f is the fracture permeability and h is the fracture's hydraulic aperture (μm). The permeability of more general conductive fractures exhibits a nonlinear relationship with the aperture, making it a crucial characteristic. How accurately the aperture, including macroscale local fluctuations along the fracture, and the accompanying fracture permeability is represented is a vital factor in the development of an appropriate numerical model (Berre et al., 2019).

1.3.3 Fluid Saturation

The percentage of the pore volume that a specific fluid occupies in a system is known as saturation (oil, gas, or water). Most oil formations are thought to have been completely saturated with water before oil migrated through and became trapped in the formation (Ahmed, 2019). Less dense hydrocarbons are considered to migrate to hydrostatic and dynamic equilibrium positions by displacing the original water. However, oil did not replace all the water in these pores. Consequently, reservoir rocks typically contain water and hydrocarbons. The percentage of pore capacity that a specific fluid occupies is considered as that fluid's saturated. The following mathematical expression represents fluid saturation:

$$fluid\ saturation = \frac{total\ volume\ of\ the\ fluid}{pore\ volume} \tag{1.6}$$

Therefore, all saturation values are based on the pore volume instead of the gross reservoir volume. Each phase's saturation varies from zero to one hundred percent (Chapman, 1983). Since the cumulative saturations is 100 % by definition, this means:

$$\sum S_\beta = S_w + S_o + S_g = 1 \tag{1.7}$$

where S is the saturation (or volume fraction) of phase β. The subscripts w, o and g represent water, oil, and gas, respectively.

The matrix's fluid saturation in a fractured tight reservoir is comparable to that in a standard reservoir. The same method can be used to evaluate saturation in the laboratory using direct measurements or indirect logs. The saturation of hydrocarbons per unit of volume is unaffected by secondary porosity's low value (fracture network, vugs) compared to the primary porosity (Bauer et al., 2017). In any case, it is possible to consider that the fluids of the corresponding zones have entirely saturated the fractures (water in the water zone, oil in the oil zone, etc.). However, a double porosity system must be used to examine fluid saturation in a fractured reservoir (Golf-Racht, 1982). Oil saturation levels in conventional oil reservoirs typically vary from 65 % to 85 %. There are several oil reservoirs with measurable gas saturation in the gas cap. Natural gases, notably heavier ones like ethane and methane, are typically highly saturated in dry gas reserves. Table 1.1 lists a few typical examples of water, gas, and oil saturations (Ahmed, 2019).

Table 1.1. Examples of saturations in petroleum reservoirs (Ahmed, 2019)

Reservoir type	Oil without a gas cap	Oil with a gas cap	Dry gas	Gas condensate
Oil saturation (S_o,%)	65 - 85	60 - 70	0	0
Gas saturation (S_w,%)	0	5 - 15	70 - 85	40 - 60
Gas condensate saturation (S_{gc},%)	0	0	0	20 - 40
Connate water saturation (S_{wc},%)	15 - 35	20 - 30	15 - 30	20

Note: The data in the table should only be used as a general guide as it contains approximations.

1.3.4 Relative Permeability

The relative permeability of a phase in multiphase flow systems is calculated as the difference between the absolute permeability of the porous medium and the phase's effective permeability (Satter and Iqbal, 2016). The following is an expression for a phase's relative permeability:

$$Kr_{\beta} = \frac{k_{e\beta}}{k_a} \tag{1.8}$$

where *Kr* is the relative permeability of the phase β.

The concept of relative permeability is an extension of Darcy's law to allow for the presence and flow of multiple fluids within the pore spaces. In the presence of two or more immiscible fluids, the flows of these fluids interact. When a fluid is present at 100 % saturation, permeability is said to be absolute (Ahmed, 2001). When two or more fluids are present in the pore spaces, a porous material's effective permeability represents its capacity to allow a fluid to pass through it while being subjected to a potential gradient. Each fluid has a lower effective permeability than absolute permeability.

The cumulative relative permeability of gas, water, and oil in a multiphase flow system is between 0 and 1, or $Kr_w + Kr_o + Kr_g \leq 1$. Figure 1.6 shows a representative example of oil-water relative permeability. The relative permeability to the oil phase decreases as the water saturation increases, whereas the relative permeability to the water phase increases until it approaches the residual oil saturation (S_{or}), at which point, the oil phase becomes immobile (Ganat, 2019). Typical relative permeability curve analysis reveals that:

a. There is a nonlinear relationship between relative permeability and phase saturation due to the non-uniform distribution of the pore spaces.
b. The irreducible water saturation (S_{wi}) for the water phase is the saturation endpoint at which the enclosed water is immobile, and the relative permeability is zero.
c. The residual oil saturation (S_{or}), where the relative permeability of the oil is zero, and the oil no longer flows through the porous medium, is the corresponding point in case of oil phase.
d. Oil and water flowing concurrently result in K_{ro} and K_{rw} values between 0 and 1.

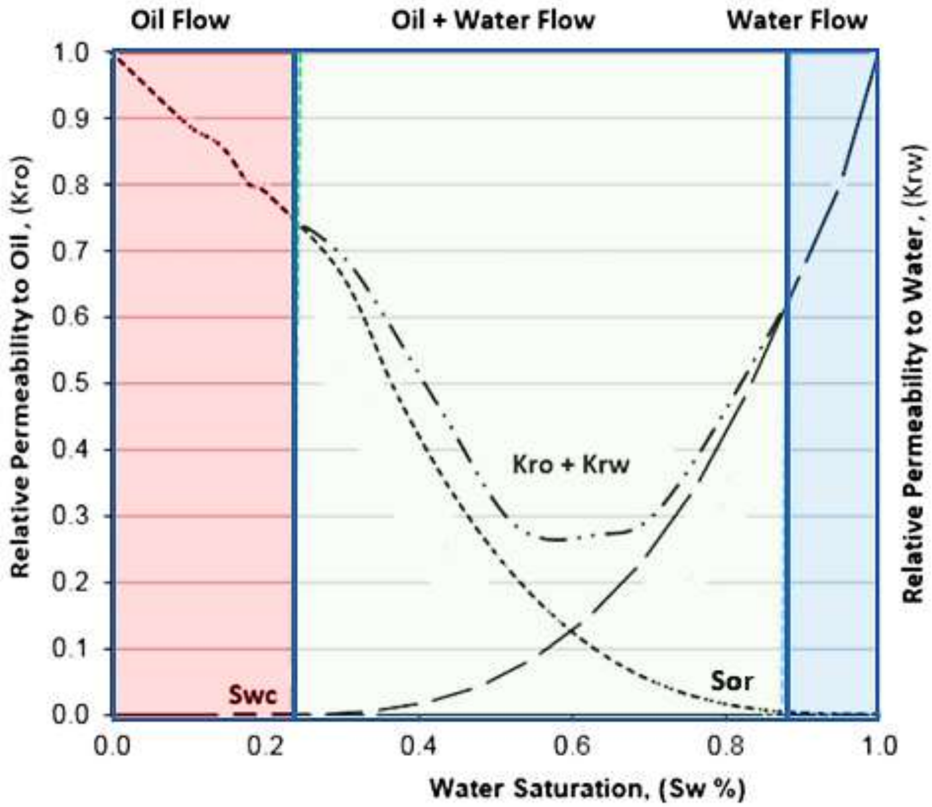

Figure 1.6. Typical relative permeability curve for water-oil system (Ganat, 2019)

A special core analysis is used to determine the relative permeability in a naturally fractured tight reservoir. Because of the nature of the double porosity system in a naturally fractured tight reservoir, where the fracture plane between two matrix units generates a discontinuity in the multiphase flowing process, evaluating relative permeability is challenging. The relative permeability of an incredibly naturally fractured tight reservoir is rarely researched in the literature, while heterogeneity within a porous media and its impact on relative permeability have been thoroughly investigated (Feng et al., 2019). Using water flooding to determine the relative permeability of heterogeneous rocks carries the danger of being inaccurate if a previous water breakthrough has already occurred. This means that if the water breakout through fractures or vugs occur earlier than the main moving front in the matrix, the results become inexplicable. Due to a piston-like displacement in some fractures, the fracture-matrix relative permeability curve resembles the curve shape shown in Figure 1.7.

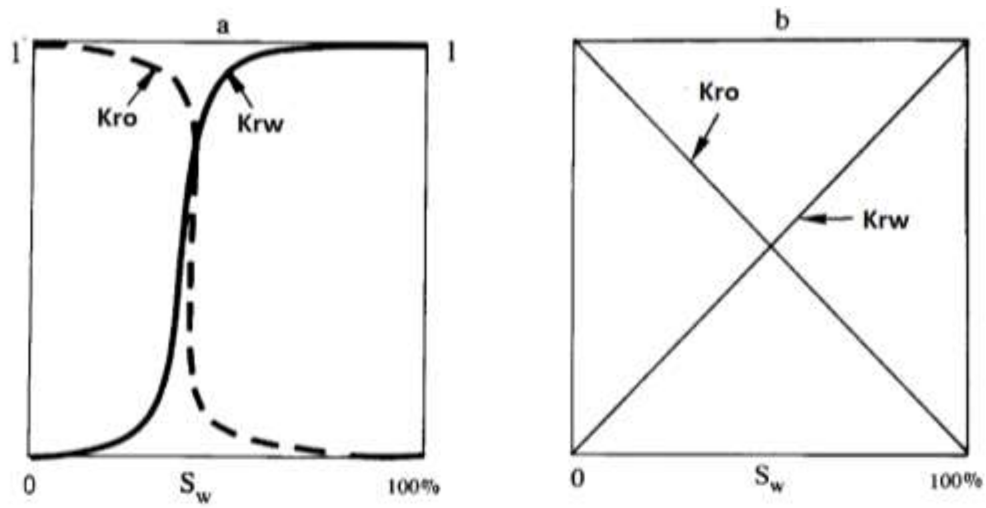

Figure 1.7. Relative permeability curve forms for fractures that are either (a) not along the core axis, or (b) along the core axis (Golf-Racht, 1982)

The relationship between relative permeability and fluid phase saturation for an oil reservoir undergoing water injection, without any free gas present, is summarized in table 1.2.

Table 1.2. Relationship between saturation and relative permeability (Satter and Iqbal, 2016)

Stage of water flood	At the start of water flood	During water flood	At the end of water flood
Oil phase saturation ($\boldsymbol{S_o}$)	S_{oi}	$S_{oi} < S_o < S_{or}$	$S_{or}{}^*$
Oil phase relative permeability ($\boldsymbol{Kr_o}$)	1	$0 < k_{ro} < 1$	0
Water phase saturation ($\boldsymbol{S_w}$)	$S_{wi}{}^*$	$S_{wi} < S_w < 1 - S_{or}$	$1 - S_{or}$
Water phase relative permeability ($\boldsymbol{Kr_w}$)	0	$0 < Kr_w < 1$	1

*End point saturation

1.3.5 Wettability

The tendency of one fluid to spread-on or cling-to a solid surface, while additional immiscible liquids are present, is known as wettability, as shown in Figure 1.8. In order to measure the wettability, mercury, oil, and water are placed in tiny drops on a spotless glass plate, and three drops are examined from one side. The oil droplet assumes a roughly hemispherical shape; the mercury maintains its spherical shape while the water spreads over the glass surface. The propensity of a liquid to spread across the surface of a solid is a sign of the liquid's wetting property. By measuring the angle of contact at the liquid-solid interface, the liquid’s spreading tendency can be estimated. The contact angle is always measured from the solid through the liquid. The contact angle has grown in importance as a wettability indicator.

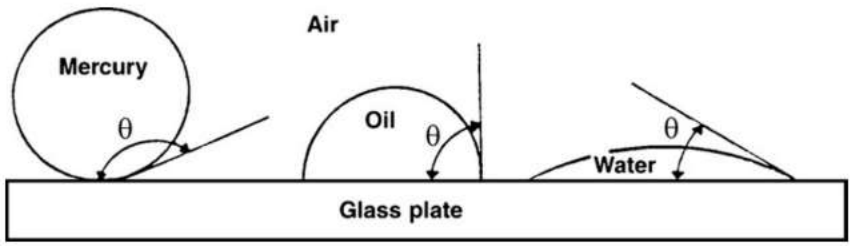

Figure 1.8. Wettability (Ahmed, 2019)

Figure 1.8 also demonstrates how the wetting property of a liquid grows as the contact angle decreases. A contact angle of zero would indicate complete wettability, whereas a contact angle of 180° would indicate complete non-wetting. There are many definitions of intermediate wettability, but the published literature demonstrates that contact angles between 60° and 90° tend to make liquids want to resist one other. The matrix fluid displacement process in naturally fractured tight reservoirs is influenced by fluid saturation in the matrix, fractures, and preferential wettability.

1.3.6 Capillary Pressure

Capillarity is the propensity of a liquid to rise or sink in a capillary tube due to adhesive tension (Alyafei, 2021). Capillary forces are produced in an oil reservoir by the interaction of the reservoir fluids' surface and interfacial tensions, aperture size and shape, and wetting characteristics. As two immiscible fluids available in the aperture of the reservoir rock, one phase is classified as a wetting phase and the other as a non-wetting phase. The curvature of the interface, which separates the two immiscible fluids, causes a pressure discontinuity between them when they are in contact. Capillary pressure (*Pc*) is used to describe this pressure difference (Ganat, 2019). The pressure difference between the non-wetting and wetting phases in a porous medium is known as capillary pressure, and it is never zero. It can be stated as follows:

$$Pc = \textit{pressure of non-wetting phase} - \textit{pressure of wetting phase} \qquad (1.9)$$

The capillary pressure in a typical porous medium depends on the medium's wettability state, pore size, geometry, and combined influence of surface and interfacial tensions. The surface forces of capillary pressure either help or hinder the displacement of one fluid by another in the pores of a porous media (Yang et al., 2019). Therefore, it is essential to keep the pressure of the non-wetting fluid at a value greater than that in the wetting fluid to retain the porous medium partially saturated with non-wetting fluid. At the same time, the medium is also exposed to wetting fluid (Ahmed, 2001). The drainage capillary pressure curve is considered to comprehend how height-saturation data can identify fluid distribution, zonation, and fluid contacts in a reservoir. The data for this curve has been converted to reservoir conditions (for an oil-water system) and then to height-saturation, as shown in Figure 1.9. In essence, it depicts water saturation distribution in an oil-water system.

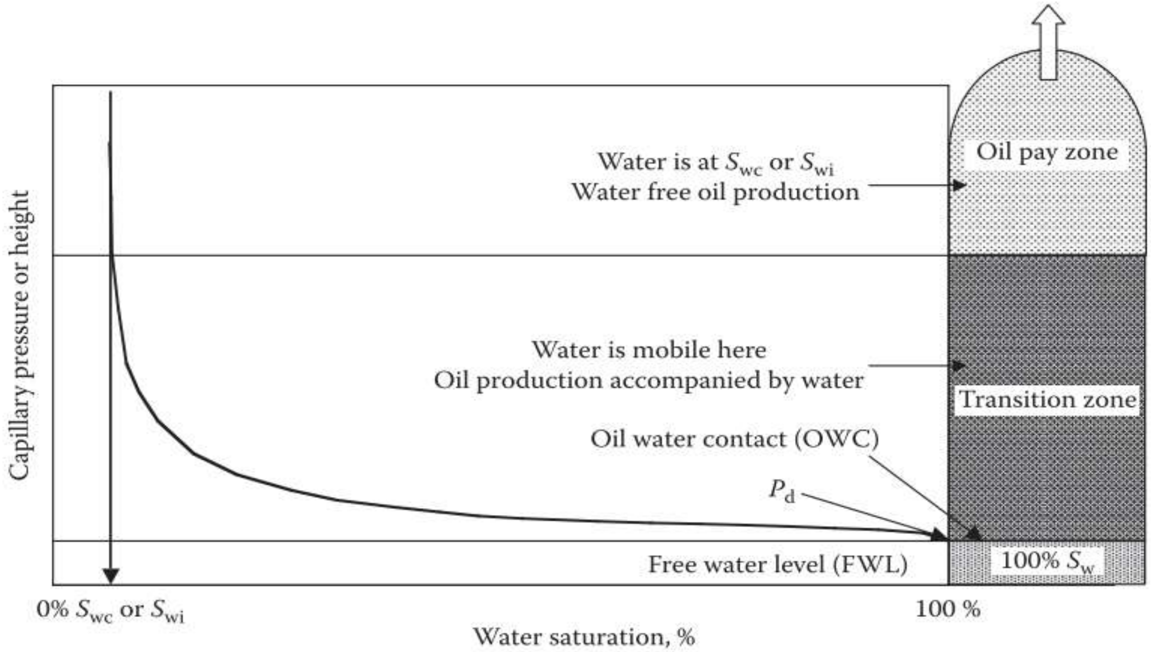

Figure 1.9. Capillary pressure w.r.t water saturation (Dandekar, 2013)

1.4 Flow in Naturally Fractured Tight Reservoirs

The mathematical expression for fluid flow and transport in porous media are derived based on Darcy's Law. As discussed earlier, the scale of tight reservoirs can be in kilometres, which obviously is not suitable for modelling fluid flows. Bear (1972) solved the scaling issue by defining Representative Elementary Volume (REV). The grain size and pore-scale geometry, which are micro-scale characteristics of porous media, are represented by an equivalent continuum on a larger scale defined by new attributes through volume averaging. The REV must be both large enough to prevent undesirable fluctuations in the average characteristics and small enough to preserve the spatial dependence of these properties. Figure 1.10 illustrates the relationship between volumetric porosity and

REV and the fact that porosity measurement changes with sample volume and the domain of the REV.

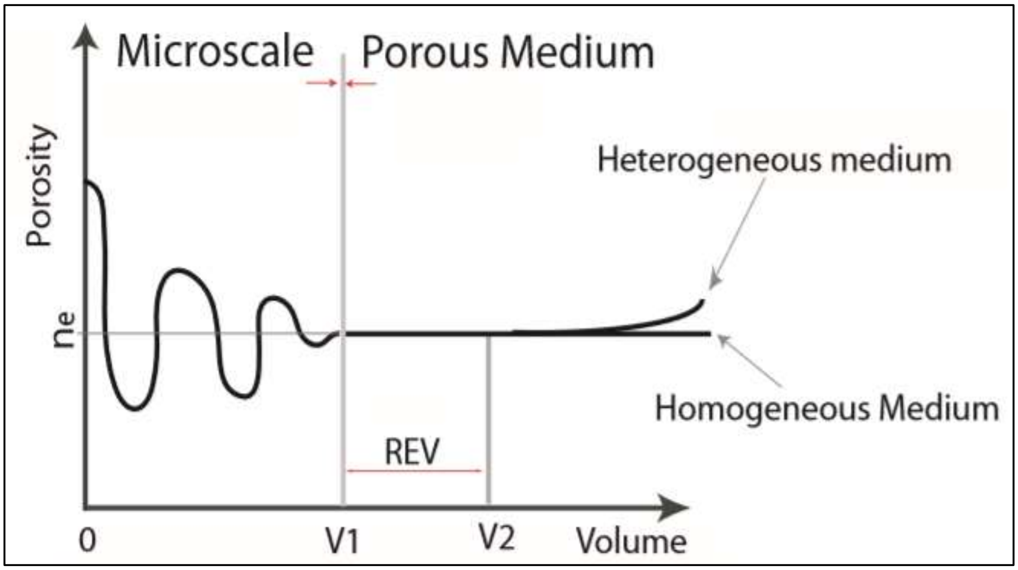

Figure 1.10. Illustration of the REV concept (Nick, 2010)

1.4.1 Single-Phase Flow in Naturally Fractured Tight Reservoirs

Darcy transport equation is widely applicable for single, two, and three-phase flow. Eq. (1.10) represents the Darcy transport equation where the pressure gradient (∇P) is the primary driving force for single-phase flow.

$$\eta = -\frac{k}{\mu}\,(\nabla P - \rho\; g\; \nabla D) \tag{1.10}$$

The mass conservation equation is normally expressed by Eq. (1.11) for single-phase flow in the naturally fractured tight reservoir.

$$\frac{\partial}{\partial t}(\rho\;\varphi) + \nabla.(\rho\;\eta) = \Psi \tag{1.11}$$

where η is the Darcy velocity (m/s), ρ is the density of the fluid (kg/m^3), μ is the dynamic viscosity of the fluid (Pa.s), k is the permeability of the formation (mD), g is the gravitational acceleration(m/s^2), D is the depth of the datum (m), φ is the rock porosity (fraction), and Ψ is the source term for viscous losses.

1.4.2 Multiphase Flow in Naturally Fractured Tight Reservoirs

In isothermal multiphase flow conditions, multi-mass components and mass balance equations are needed to describe the flow in fracture and matrix reservoir rocks for each phase separately. The mass conservation equation is given as Eq. (1.12).

$$\frac{\partial}{\partial t}\left(\varphi\, S_\beta\, \rho_\beta\right) = -\nabla.\left(\rho_\beta\, \eta_\beta\right) + \Psi_\beta \tag{1.12}$$

here $S_\beta, \rho_{\beta,}\, \eta_\beta$ are the saturation, density and velocity of the phase respectively (β=*g* for gas, β=*w* for water, and β=*o* for oil).

The extended Darcy law is also widely applied for considering the effect of density, viscosity and pressure gradient for multiphase flow in the naturally fractured tight reservoirs, as shown in Eq. (1.13).

$$\eta_\beta = -\frac{k_a\, Kr_\beta}{\mu_\beta}\left(\nabla P_\beta - \rho_\beta\, g\, \nabla D\right) \tag{1.13}$$

where k_a is the absolute permeability of the formation and Kr_β is the relative permeability of the phase.

Multiphase (two and three phases) flow modelling is still challenging. To describe multiphase flow in naturally fractured tight reservoirs, description of saturation, relative permeability, and capillary pressure is important. In multiphase flow's presence, fluids filling the porous medium indicate the relation, as shown in Eq. (1.14) (Zhangxin et al., 2006).

$$\sum S_\beta - 1 = 0 \tag{1.14}$$

When multi-immiscible fluids exist in a naturally fractured tight reservoir, the distinct pressure between the non-wetting and wetting phases is called capillary pressure (Eq. (1.15)); across the interface, pressure arises from the capillary forces and these capillary forces originate from the surface and interfacial tension (Pyrak-Nolte et al., 2008; Soares et al., 2015).

$$Pc = P_o - P_w \tag{1.15}$$

where Pc is the capillary pressure (Pa), P_o and P_w are the oil (non-wetting) and water (wetting) phases' pressures respectively.

In immiscible multiphase flows, the presence of the non-wetting phase decreases the cross-sectional area for the flow of wetting fluid and vice versa. Therefore, the ability of fluid to flow reduces within the porous media domain and thus, the relative permeability decreases (Falode and Manuel, 2014; Honarpour et al., 1986; Jerauld and Salter, 1990).

$$Kr_\beta = \frac{k_\beta}{k_a} \tag{1.16}$$

$$\lambda_{\beta} = \frac{Kr_{\beta}\, k_a}{\mu_{\beta}} \tag{1.17}$$

where k_{β} is the effect permeability of the phase and λ_{β} is the mobility of the phase (fraction).

Adding Eqs. (1.16) and (1.17) to Eq. (1.13), we get the equation that describes multiphase incompressible fluid flow in naturally fractured tight reservoirs.

$$\frac{\partial}{\partial t}\left(\varphi\, S_{\beta}\, \rho_{\beta}\right) = \nabla.\left(\rho_{\beta}\, \lambda_{\beta}(\nabla P_{\beta} - \rho_{\beta}\, g\, \nabla D)\right) + \Psi_{\beta} \tag{1.18}$$

However, flow behaviour cannot be applied alone by Eq. (1.18) in different continuums. Therefore, it is essential to specify the initial and boundary condition. The continuity equation must be applied at other interfaces between separate continua in terms of pressures, concentrations, and mass fluxes (Martin et al., 2017). Figure 1.11 (a) represents the flow term evaluation, spatial discretization, and grid block connections within a multi-continuum system between two neighbour grid blocks (i, j) directly based on the integrated finite difference approach. Figure 1.11 (b) illustrates the effects of the periodic domain system *(Ω)*, which is the effect of fracture length on the contaminant transport in the fractured rock at the macroscopic scale where multiple fracture scales exist, and where Ω_f is the fracture domain, Ω_m is the matrix domain, Ω is the periodic domain, l is the microscopic characteristics length, l_p is the pore length scale and Γ is the fracture-matrix boundary or interface.

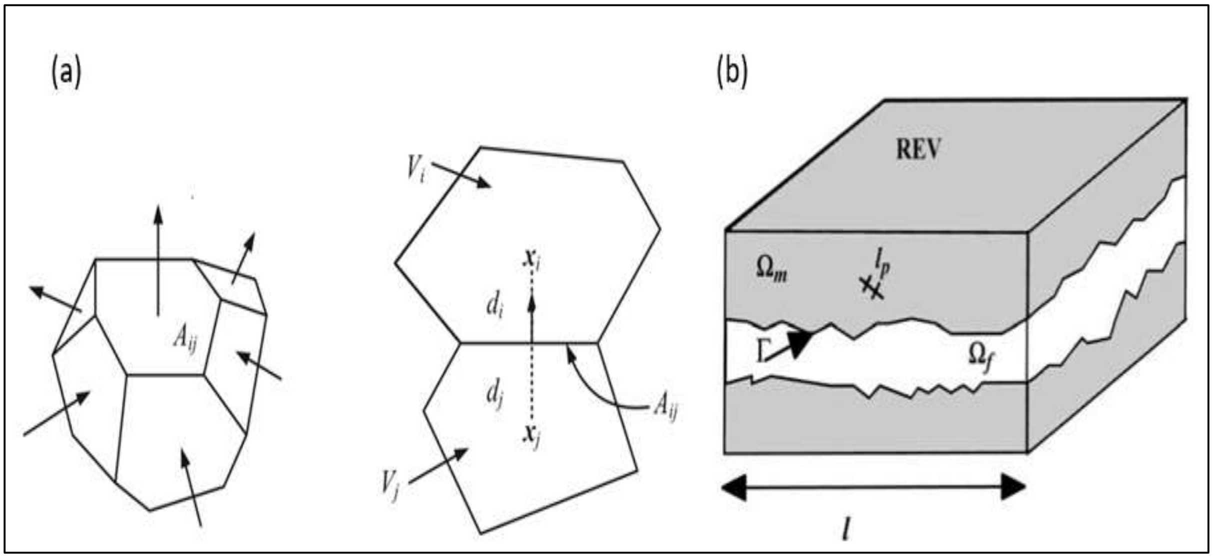

Figure 1.11. (a) 2D Finite difference integration for flow term evaluation, spatial discretization and connection (Wu 2016); (b) Fractured rock domain (Royer et al., 2002)

1.5 Factors Affecting Multiphase Flow in Naturally Fractured Tight Reservoirs

Geomechanical studies show that variations in stress, pressure, and temperature cause subsurface rocks to deform or fail. Geomechanical observations can be traced back to 77 AD when two men observed that the level of water in a well corresponded to the ocean tides (Melchior, 1983). Since then, geomechanical research has progressed consistently. As petroleum exploration and production significantly increased, more physical phenomena related to geomechanics have been observed in the oil and gas reservoirs in the early 20th century. For instance, the Goose Creek oil field was reported to sink into water in 1918, and this subsidence was caused by oil and gas extraction (Pratt and Johnson, 1926). Later, the physical hypothesis was developed by Biot (1941) and other scientists behind various observations in the petroleum industry. This physical hypothesis is based on the constitutive geomechanical relationships.

1.5.1 Constitutive Geomechanical Relationships

The constitutive relationships describe how the material deforms under loading. Three key geomechanical constitutive relationships frequently utilized in reservoir simulations include elastic, poroelastic, and thermoporoelasticity models. Based on observations, the behaviour of a material under load is complex. The constitutive laws can all be stated mathematically in either linear or nonlinear forms, depending on the application.

Through a series of laboratory experiments, the geomechanical hypothesis was first presented by Terzaghi et al. (1940). In these laboratory experiments, a constant load was applied laterally for a saturated soil sample. The following equation depicted this hypothesis:

$$\frac{\partial P_p}{\partial t} = c\,\frac{\partial^2 P_p}{\partial L^2} \tag{1.19}$$

where P_p is the pore pressure (Pa), t is time (s), c is the consolidation coefficient and L is the length of the sample.

The concept and definition of effective stress was then defined by Karl Terzaghi, as he noticed that effective stress, which is the difference between pore pressure and externally applied stress, controls the behaviour of the saturated soil samples, as depicted in Figure 1.12 (Zoback, 2007).

$$\sigma_{i,j} = \sigma'_{i,j} \pm \delta_{i,j}\, P_p \tag{1.20}$$

where $\sigma_{i,j}$ is the total stress (Pa), $\sigma'_{i,j}$ is the effective stress, P_p is the pore pressure (Pa), $\delta_{i,j}$ is the Kronecker delta in i and j volume respectively.

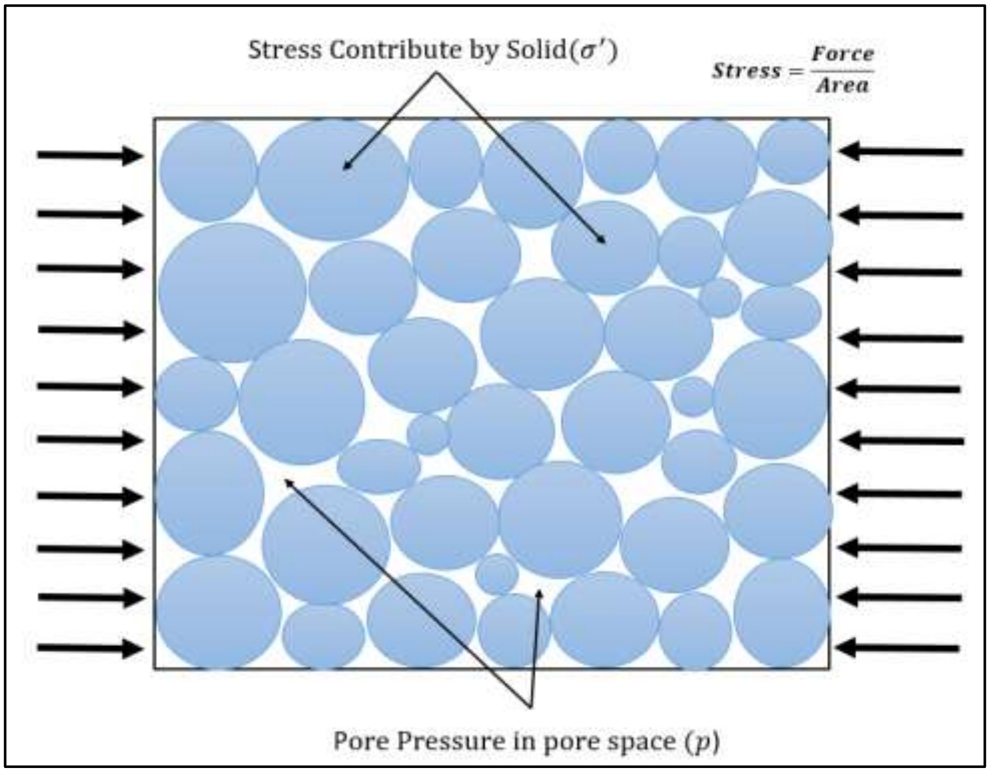

Figure 1.12. Effective stress and pore pressure (Zoback, 2007)

The + and – signs depend on the direction of externally applied stress. The Biot Willis coefficient (α_B) is defined as a function of the drained and solid bulk moduli of material (Garg and Nur, 1973; Nur and Simmons, 1969). Biot Willis coefficient can be calculated as:

$$\alpha_B = 1 - \frac{K_d}{K_s} \tag{1.21}$$

where K_d is the drained bulk moduli of material (MPa) and K_s is the solid bulk moduli of material (MPa) (Biot 1962). The typical value of α is between 0 and 1. For the compacted and nearly solid rocks, the value of α_B is zero when there are no interconnected pores, and pore pressure has no impact on rock behaviour, such as in quartzite. In contrast, the value of α is equal to one for highly interconnected pores and indicates pore pressure has a maximum influence such as in the case of uncemented sands (Zoback, 2007).

The fundamental constitutive relations above (equations 1.19-1.21) describe porous material's deformation behaviour under different stress loading. Due to the complexity of the porous material behaviour under different stress loading, some simplifications to the geomechanical constitutive relations are made based on natural geomechanical phenomena. The linear poroelasticity model is widely used in naturally fractured tight reservoirs to investigate the mechanical changes due to the pressure depletion in the naturally fractured tight reservoirs (Bagheri and Settari, 2005; Bai et al., 2019; Garipov et al., 2016; Ren et al., 2018; Sanaee et al., 2013; Sangnimnuan et al., 2018; Yang et al., 2018). Another significant use of geomechanical constitutive relations is to inform when the material reaches plasticity behaviour and eventually collapses. From the reservoir point of view, this phenomenon is significant in recovering oil and gas when the fracture is the main path available for the flow in the naturally fractured tight reservoirs.

1.6 Modelling of Multiphase Flow and Geomechanics in Naturally Fractured Tight Reservoirs

Modelling of flow and transport processes in naturally fractured tight reservoirs have come a long way since the 1960s (Wu, 2016). The modelling of fluid flow in naturally fractured tight reservoirs is complex due to the stark contrast between the permeability of the matrix, the fractures and the small fracture volumes. As a result, numerous approaches have been developed to model fluid flow in naturally fractured tight reservoirs. For instance, Computational Fluid Dynamics (CFD) solvers like TOUGH2 and Eclipse simulate fluid flows in naturally fractured tight reservoir however, they are generally inaccurate in predicting multiphase flow exchange at the fracture-matrix interface. Various advanced CFD solvers like ANSYS® and Abaqus are based on Finite Volume method (FVM) and Finite Element method (FEM) and are considered more accurate in numerical prediction related to multiphase flow and geomechanics in naturally fractured tight reservoirs, especially at the fracture-matrix interface.

The physical connection between geomechanical properties and fluid flow phenomena is referred to as coupling in earth sciences. Geomechanical and fluid flow characterisations are frequently observed in geological media because these materials (such as soils and rocks) have pores and fractures that can be fluid-filled and flexible. Geomechanical and fluid flow characterisation in subsurfaces have been observed since the late 1800s (Rutqvist and Stephansson, 2003). Early observations included the response of water levels in wells due to tidal loading from the ocean (solid-fluid coupling), as well as the sinking of the ground surface brought on by the extraction of water, oil, and gas. In general, either a change in the external load or a difference in the internal pore-fluid pressure can cause fluid saturation and porous medium (rock) fracture or deform, as shown in Figure 1.13. When one needs to analyse stress changes induced by production/injection, and investigate how these stress changes affect the fluid flow in the reservoir, coupling is frequently utilized in geomechanical simulations. There are many different types of coupling that can be employed, like one-way coupling, two-way coupling, iterative coupling and full coupling.

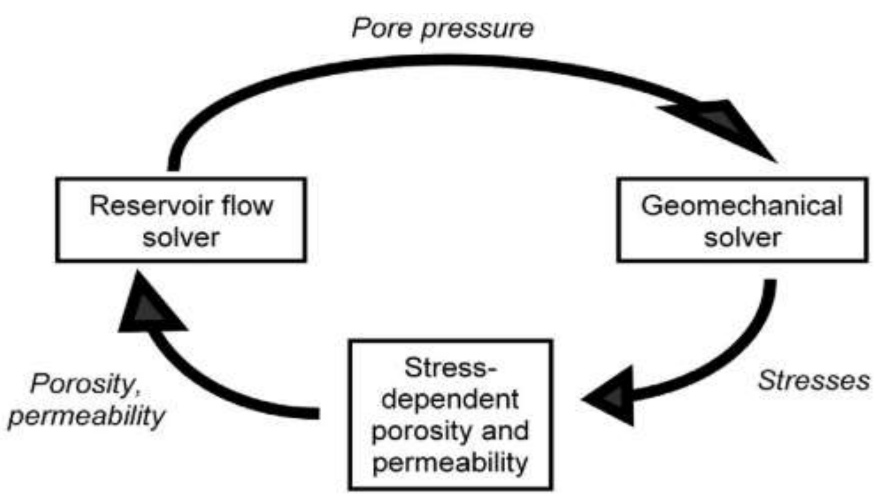

Figure 1.13. Coupling of geomechanics and multiphase flows (Shojaei and Shao, 2017)

Changes in the pore pressure brought on by production (or injection, or both) affect the effective and total stresses and the overburden in the reservoir. These stress fluctuations then impact the reservoir's porosity and permeability, which are its hydraulic qualities. In contrast, a stiffer material may also be produced through pore volume decrease because more connections between nearby grains are formed. These modifications suggest that geomechanics and fluid flow can influence one another by altering the material's properties. As a result of stress loading, the porous medium will be crushed to a lower bulk volume, and pore volume. The smaller pore capacity caused by the rapid application of the external load will tend to compress the pore fluid, increasing the pore-fluid pressure because the fluid has no chance to escape. However, if the external load is applied slowly, the fluid has time to exit the compressed volume. Therefore, there is essentially no increase in fluid pressure, similar to how a drop in fluid pressure or volume can result in the settlement of porous media and a corresponding reduction in bulk and pore volume. These are some of the challenges faced while accurately modelling geomechanics and multiphase flows in naturally fractured tight reservoirs.

1.7 Research Rationale

There is a significant number of unexploited resources that result in considerably lower hydrocarbon production and recovery factor. The under exploitation of these resources is primarily due to lack of understanding of the complex multiphase flow phenomena occurring at the fracture-matrix interface, which essentially controls flow dynamics in naturally fractured tight reservoirs. It is essential to analyse multiphase flow exchange at the fracture-matrix interface, which is directly related to the key hydraulic parameters of naturally fractured tight reservoirs. Thus, a better understanding of these important flow variables, like capillary pressure and relative permeability, forms the basis of multiphase flow analysis within tight reservoirs and helps to improve hydrocarbon recovery in the oil and gas industry.

Pore pressures and in-situ stresses alter as reservoirs go through voidage or switch from one recovery mechanism to another. The geomechanical characteristics of the rock and the combined impact of changes in pore pressure and stress state determine the volumetric response these changes cause in the reservoir rock. These complicated multiphysics processes include fluid interaction in the porous material. The material of interest may spread across the fracture network and the porous matrix due to the flow mechanism, combined with the transport phenomena. Moreover, forced water addition to a reservoir alters the stress state and pore pressure, possibly leading to the dilatation of the rock matrix. Porosity, permeability, water saturation and fluid movement are all altered by dilation. Therefore, the bulk volume will change as the reservoir adjusts to the combined effect of change in pore pressure and stress state, altering the dependent parameters such as porosity, absolute permeability, relative permeability, phase saturations and capillary pressure. The reservoir and the surrounding rock mass change due to the interaction of these characteristics and the dynamic effects of production and injection. It is crucial to underline that the same rock features that govern pore connectivity and geometry affect fluid distribution and movement within reservoirs.

It is essential to couple the multiphase flow characteristics (like fluid saturation) with the geomechanical features of the rock (like stress, etc.) in order to address these complex engineering problems. Coupled geomechanics and multiphase flow characteristics can be realised only when the specific interdependencies between the two are analysed thoroughly. This motivated the author to carry out extensive parametric investigations to evaluate the dependency of multiphase flow parameters on externally applied stress. The issue is further compounded by the complicated interactions occurring between the different phases at the fracture-matrix interface.

Modern numerical modelling solvers are capable of predicting multiphase flow behaviour in naturally fractured tight reservoirs, subjected to external stresses. However, handling the Multiphysics phenomena instantaneously is a very complicated matter, especially at the fracture-matrix interface. Conventional modelling techniques rely on one-way coupling between geomechanics and multiphase flows, which is often adequate depending on the application. However, in case of naturally fractured tight reservoirs which are filled with oil and are subjected to internal water injection and external stress loading, one-way coupling between geomechanics and multiphase flow results in inaccurate prediction regarding oil recovery. Thus, there is a need to develop an innovative numerical modelling approach that can fully couple both geomechanics and multiphase flow in naturally fractured tight reservoirs and should be able to accurately predict the complex Multiphysics phenomena at the fracture-matrix interface.

1.8 Research Aims

This study attempts to provide insight into the multiphase flow exchange that occurs at the fracture-matrix interface. This was carried out by modelling the underlying flow and geomechanical physics that controls flow dynamics in tight reservoir blocks in a manner that is both accurate and plausible. The foremost aims of this research study are mentioned below:

1) Evaluation of multiphase flow characteristics at the fracture-matrix interface in naturally fractured tight reservoirs.

2) Establishment of interdependency between external loading and multiphase flow at the fracture-matrix interface in tight reservoirs for accurate oil recovery predictions.

3) Development of a novel approach for accurate characterisation of geomechanics and multiphase flow in naturally fractured tight reservoirs.

1.9 Organization of Thesis

Chapter 2 presents an extensive literature review of the key hydraulic parameters in naturally fractured tight reservoirs. It also reviews the different types of coupling schemes of reservoir geomechanics and fluid flow in naturally fractured right reservoirs.

Chapter 3 documents the fundamental principles of Computational Fluid Dynamics and Finite Element Analysis. It includes the CFD modelling of multiphase flow, FEA of structural analysis, solver settings, and the appropriate boundary conditions specified to solve the stress-dependent multiphase flow parameters in naturally fractured tight reservoirs. The meshing technique used for the flow domain has been discussed.

Chapter 4 presents CFD based modelling techniques to model multiphase flow at the fracture-matrix interface in naturally fractured tight reservoirs. This chapter also provides the predicted numerical results and the validation of the models with the experimental data.

Chapter 5 presents one-way FEA-CFD coupled model of reservoir geomechanics and transient multiphase flow to investigate the effects of geomechanics on multiphase flow parameters at the fracture-matrix interface.

Chapter 6 presents a novel fully coupled model of reservoir geomechanics and transient multiphase flow to investigate the effect of geomechanics on multiphase flow parameters at the fracture-matrix interface in tight reservoirs.

Chapter 7 concludes the findings of this study its major achievements. The novel contributions of this study are also highlighted along with recommendations for future work.

Chapter 2
Literature Review

This chapter presents a detailed review of literature with the aim to identify knowledge gaps in the body of existing literature, relevant to the identified aims. Published studies regarding multiphase flow characterisation of naturally fractured tight reservoirs have been critically evaluated. The effects of geomechanical parameters on multiphase flow and the different strategies of coupling geomechanics with multiphase flows in numerical modelling of naturally fractured tight reservoirs have been presented. The research objectives of this study have been formulated in light of the knowledge gaps identified.

2.1 Multiphase Flow Characterisation in Naturally Fractured Tight Reservoirs

Based on aim 1 of this study regarding the multiphase flow characterisation in naturally fractured tight reservoirs, a critical review of published literature is presented in the following sections, focusing on the key hydraulic parameters identified in chapter 1.

2.1.1 Permeability

Numerous research studies have been conducted to examine how fractures affect multiphase flow. A number of analytical models have been developed in the published literature to estimate the permeability of arbitrary parallel sets of smooth fractures with zero matrix permeability (Chen et al., 2000; Snow, 1969), with obvious limitations. These limitations have been addressed by considering the matrix's fractures as a planar source that varies in length (Lee et al., 2001; Nakashima et al., 2000). These studies have helped improve the estimation of complex matrix permeability by introducing a new parameter, known as effective permeability, to accurately analyse the permeability of naturally fractured tight reservoirs (Teimoori et al., 2003).

The primary limitation of the aforementioned studies lies in representing the inherently complex fracture system as a simple geometrical feature. Fractures in naturally fractured tight reservoirs have varying aperture diameters and lengths, at varied intersecting angles and orientations. An accurate representation of the actual conditions is a network of fractures (de Hoop et al., 2022). A considerable improvement over earlier research was then made by explicitly introducing the naturally fractured rock, in which each fracture has its own permeability and dimensional characteristics. Another limitation that needs to be addressed is that the aforementioned research studies consider fluid flow only through connected fractures and overlook flow through matrix and isolated fractures. In later scientific investigations (Abdelazim and Rahman, 2016; Doonechaly et al., 2013; Huang et al., 2019), particular flow regions have been discretized, including matrix, fracture, and fracture-matrix interfaces, with suitable boundary conditions by linking boundary elements. The use of cubic law in fractures, Darcy's diffusivity for the flow in the matrix, and Poison's equation at the fracture-matrix interface has significantly improved understanding and estimation of different permeabilities involved in naturally fractured tight reservoirs.

2.1.2 Saturation and Wettability

Numerous investigations have been conducted in the last three decades focusing on saturation and wettability effects (Diomampo, 2001; Fourar et al., 1993). It has been reported that the relationship between relative permeability and fluid saturation is nonlinear however, these research studies investigated flow through fractures only and neglected the impact of a fracture-matrix interface. The estimation of relative permeability was further enhanced by analysing flow through a fracture-matrix system utilizing Berea Sandstone (Akin, 2001). In contrast, displacing (non-wetting) fluid relative permeability is more significant with a wider fracture aperture, resulting in a lower recovery factor, indicating that the relative permeability is exclusively dependent on the saturation and wettability of the naturally fractured rock (Rod et al., 2019). Since the media is hydrophilic, a water-wet system always has higher oil-relative permeability and vice versa. Naturally fractured tight reservoirs are neither entirely oil-wet nor water-wet.

2.1.3 Relative Permeability

Relative permeability is the most uncertain yet crucial parameter for determining saturation profiles of various phases, which can help assess a reservoir's production potential (Kazemi, H, Gilman, J R, and Eisharkawy, 1992; Oostrom et al., 2016; Shad and Gates, 2010). Based on Romm's constant aperture and glass plate tests, fracture permeability has traditionally been represented as a unit slope and linear saturation functions (Romm, 1966). The wetting phase saturations were dispersed at a value of 0.72 for practically the whole range of flow rates and fractional flows by Merrill (1975), who attempted to replicate Romm's studies. This pattern deviated when both the overall flow rate and the fractional flow were high. Merrill's investigations on pieces of Berea Sandstone that had been epoxy-sealed revealed the same phenomenon. The sole difference was that multiphase flow occurred at a wetting phase saturation value of around 0.62. The aperture distributions of natural systems can change (Keller, 1997; Pyrack-Nolte et al., 1987). Pyrak-Nolte et al. (1990) produced drainage relative permeability curves for a computationally generated, spatially correlated log-normal aperture distribution. It was observed that the relative permeability was a nonlinear function of saturation.

The displacement model was altered by Pyrak-Nolte et al. (1992) to represent invasion percolation with trapping, which was then applied to imbibition. The crossover point experienced a significant shift after trapping in favour of lower relative permeability values and lower wetting phase saturation. To determine the relative permeability within a single fracture, Keller (1997) also employed a percolation-type model. Simulating percolation on a log-normal aperture distribution was carried out by (Pruess and Tsang (1990). It has been reported that there is hardly any multiphase flow for short-range correlations. This finding is consistent with Wilkinson and Willemsen (1983). It has been demonstrated that it is topologically impossible to have continuous paths of two-phases across a two-dimensional media for random percolation models.

Pruess and Tsang (1990) observed that wetting phase relative permeability curves might be approximated as a power-law function of saturation for correlations significantly more robust in the flow direction. When a crucial grid block was filled, non-wetting phase relative permeability followed a similar Corey-like trajectory before falling to zero. Pruess and Tsang (1990) short correlation length aperture distribution was subjected to a practical medium approach. With minimal computational effort, it has been observed that relative permeability is almost equal to what is reported by Pruess and Tsang (1990). Rossen and Kumar (1992) then assessed the effects of gravity, wetting layer flow, and the variance of the fracture aperture distribution on relative permeability using effective medium technique.

Over time, methods for estimating the relative permeability of fractured reservoirs have changed. The linear X-curve method and Corey curves are frequently used for estimating relative permeability (Brooks and Corey, 1966; Romm, 1966). The

Corey technique uses exponents to account for this behaviour, which improves the findings compared to the linear method because it incorporates the effects of system-wide phase interaction. To estimate relative permeability in a fractured medium, Romm (1966) first performed laboratory displacement experiments using water and kerosene between two plates and concluded that it has a linear relationship with fluid saturation. However, these experiments disregarded gravity and capillary forces. In a recent advancement, Wang et al. (2021) carried out two-phase flow (water-nitrogen) experiments in a pair of fracture replicas, including a smooth replica and a plaster replica, to visualise flow structures. The fracture's aperture data are imported to the numerical model. The model replicates the flow structures in the investigation, and the numerically produced relative permeability likewise shares characteristics with the relative permeability determined experimentally (Wang et al., 2020; Yang et al., 2020).

The two-phase flow numerical model was then performed in two fractures with apertures distributed normally (Abdel Azim, 2022). The study demonstrate that the relative permeability follows the Corey model in both fractures. However, it is unclear whether the aperture distribution, particularly the relative permeability of the wetting phase, has any impact or not. Therefore, to accurately determine a system's relative permeability, it is necessary to collect precise data, which can only be done by considering all aspects of fluid flow in naturally fractured tight reservoirs.

2.1.4 Capillary Pressure

Capillary and gravitational forces regulate a variety of fluid flow phenomena occurring in naturally fractured tight reservoirs, such as the flow through capillary continuity between matrix blocks and infiltration (Fung, 1991). The multiphase flow is also influenced by the size and structure of the matrix, as demonstrated by studies on chalk and sandstone core samples involving water absorption (Torsaeter, O.; Silseth, 1985). Glass (1993) simulated gravity-driven fingers in fractured tight reservoirs using a modified invasion percolation model. The in-plane curvature was added to the ordinary invasion percolation in a way akin to what Lenormand and Zarcone (1984) referred to as a series of mechanisms, which depends on the number of nearby areas filled with non-wetting phases. This phenomenon was given the name capillary facilitation. The facilitation term was modified in a later study (Glass et al., 1998), and the model was used to treat horizontal fractures. The flow in wetting layers was not considered, and relative permeability was not presented. The general wetting behaviour was noticed independently of the aperture distribution when facilitation was not considered (invasion percolation).

When facilitation was considered, the wetting behaviour ranged from flat frontal advance for narrow distributions to thin fingers for broad aperture distributions. It has been reported by Reitsma and Kueper (1994) analysis of oil-water displacement in a naturally occurring fractured limestone that Brooks-Corey porous media type capillary pressure function can well depict the capillary pressure curves. Fernø (2008) focused on creating a consistent saturation for each rotational speed while measuring capillary pressure using a centrifuge. The significance of fracture capillary pressure in the water floods of fractured limestone rocks was shown through numerical replication of the experimental findings. The findings demonstrated that the formation of waterfronts during water injection strongly depended on the capillary pressure in the fracture and its distribution throughout the fracture network. Recently, Li et al. (2022) has developed a unique method for estimating foam capillary pressure and water saturation. Glass plates have been used to create both model fractures, having different hydraulic apertures. It has been reported that each model fracture has a different aperture, unlike microfluidics, which has a consistent etching depth. Foam is pre-generated and then injected into the fractures. Water saturation and capillary pressure are estimated by examining images in terms of fracture geometry. Both model fractures' drop in water saturation is accompanied by increased capillary pressure. However, details need to be provided regarding the capillary pressure of the multiphase flow at the fracture-matrix interface.

2.2 Effects of Geomechanical Parameters on Multiphase Flow in Naturally Fractured Tight Reservoirs

An accurate understanding of the physical interaction between multiphase flow properties (e.g., relative permeability and capillary pressure) and stress-dependent deformation of fractures is required to explain multiphase flow in fractured tight reservoirs, for applications such as oil and gas field recovery and geothermal reservoir recovery (Ahmed and Mckinney, 2004; Rahman et al., 2022), CO_2 subsurface sequestration and H_2 storage performance (Berre et al., 2019), and groundwater transport (Huo and Benson, 2016). Single-phase fluid transport has been the primary focus of most studies on flow in deformable fractures (Berre et al., 2019).

Despite fractures' crucial role in multiphase fluid transport in geological formations, the stress dependence of the multiphase flow characteristics in fractures has received severely limited attention. Evolving stress patterns can considerably affect matrix and fracture permeability in restricted zones, typically when fractures significantly contribute to production. As a result, there is a need to employ more than just the permeability based on initial reservoir conditions. For this purpose, numerical models can be employed to calculate permeability and porosity as a function of reservoir pressure and validating the numerical predictions against experimental data.

The effects of pressure variation on relative permeability in fractures must be considered. The numerical models need to adjust the relative permeability in several tight reservoir rocks to consider pressure variations. The fluid flow between the solid matrix and the fracture is quite intricate. To calculate the rates at which oil and gas will migrate from matrix to fracture, detailed distributions for pressure and saturation along the matrix/fracture contacts are required. The flow in a fracture cannot be compared to the flow in an open channel. At reservoir conditions, fracture apertures of a few microns are typical. When simulating fracture flow, relative permeability and capillary pressure are crucial. A few laboratory experiments have revealed inconsistent variations in the relative permeability of naturally fractured tight reservoir in response to increasing effective confining stress (Huo and Benson, 2016; Lian et al., 2012; McDonald et al., 1991). Complex physical causes and inconsistent results challenge our understanding of stress-dependent multiphase flow in deformable fractures.

2.2.1 Stress-dependent Fracture Aperture

Bai and Elsworth (1994) developed a model to analyse the effects of Hertzian contact between spherical grains and how responsive hydraulic conductivity is to stress loads. A planar opening with a constant equivalent thickness or aperture is a good approximation for the fractured rock, as each fracture is idealized as a single fracture in this network of equivalent fractures. The variation in hydraulic conductivity is governed by changes in fracture aperture brought on by variations in elastic deformation. Deformations caused by subsidence resulted from hydraulic conductivity changes brought on by mining in both intact and fractured media. The study considers fracture, idealized as a planar opening with a constant thickness or aperture, to conceptualize flow in a single fracture using parallel plate analogue.

Sanaee et al. (2013) used a back-calculation method based on the treatment of fracture as an equivalent porous media, which was implemented in a coupled Darcy law, Brinkman flow, and Navier-Stokes fluid flow formulation to investigate fracture aperture fluctuation under varying overburden stresses. Poroelasticity was used to accurately account for changes in the fracture aperture, caused by overburden stress loading. The same fluid flow equations were coupled to the obtained displacements. The fracture aperture has been reported to decrease with increase in stress loading. The study uses single-phase flow and thus, there is no multiphase flow information provided in fractured tight reservoirs.

Huo et al. (2014) measured the fracture aperture distribution using Computed Tomography (CT) scanning and single-phase flow under various stress situations. The statistics on the stress-dependent aperture distribution showed that as stress rises, the mean aperture decreases. The study has no information about the relative permeability of the multiphase flow fields within the fractured tight reservoir. Huo and Benson (2016) used X-ray and two-phase flow to simultaneously measure aperture and water saturation distributions in the fractured tight reservoir. The stress loads of 2.07 MPa and 5.52 MPa were applied to investigate the fracture aperture changes, as shown in Figure 2.1. The fracture apertures were expected to close as stress loading increased, and to depict channel-like flow pathways oriented from the top left to the lower right at both the stress levels. It is impossible to model these experiments with a variable aperture-based permeability parameterisation. Therefore, a direct numerical simulation of multiphase flow in the fracture is required to understand the observed behaviour.

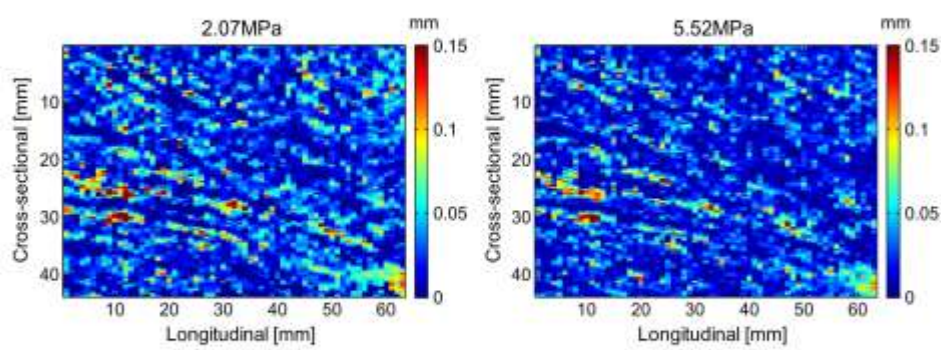

Figure 2.1. Aperture variations for stress loads of 2.07 MPa and 5.52 MPa (Huo and Benson, 2016)

2.2.2 Stress-dependent Porosity

Zhao and Liu (2012) conducted a three-dimensional stress-strain and single-phase flow analysis of porous rock under elastic and anisotropic stress conditions. The connection between stress-strain and single-phase flow uses Hooke's principles to describe deformation in specific pores based on natural strain and other pores based on engineered strain. The analysis of this unexpected association uses information from other uniaxial and triaxial tests reported in the literature. Figure 2.2 displays the porosity as a function of stress. According to the curve-fitting results, the porosity value for the sandstone samples ranges from 1.77 % to 2.04 %. The study only concerns isotropic rocks.

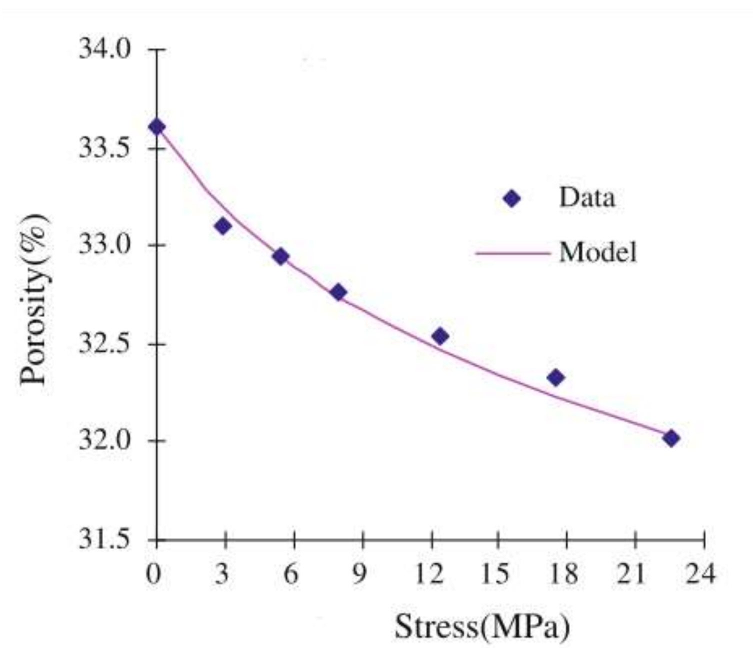

Figure 2.2. Variations of porosity under different stress loads (Zhao and Liu, 2012)

The porosity values of anhydride and carbonate rocks are examined concerning stress magnitude and history (Zivar et al., 2019). Twelve anhydride and carbonate core samples' porosity characteristics are assessed under stress loading and unloading circumstances. The hysteresis (gap) between stress loading and unloading is more pronounced at lower effective stress values. The findings also show that the anhydride core samples exhibit more pronounced hysteresis. The anhydride core samples exhibit three separate flow channel systems, whereas the carbonate core samples only exhibit one. For both anhydride and carbonate core samples, porosity measurements reveal that it is less sensitive to stress. The effects of poroelasticity are not considered in this study.

Ren et al. (2016) developed a novel hydraulic conductivity-void ratio relationship, based on Poiseuille's law, by utilising the concept of effective void ratio, as shown in Equation (2.1). The proposed equation is assessed and found to reasonably predict hydraulic conductivity for various soils, from coarse-grained to fine-grained.

$$\varphi = \frac{e}{1+e_i} = \frac{e_i-(1+e_i)\,\varepsilon_{vol}}{1+[e_i-(1+e_i)\,\varepsilon_{vol}]} \tag{2.1}$$

where φ is the porosity, ε_{vol} is the volumetric strain, e_i is the initial void ratio, e is the void ratio.

Cheng et al. (2022) proposed a model that considers the geomechanics deformation by pore pressure and stress-dependent porosity. The problem was solved using COMSOL Multiphysics. The reservoir depletion from the Dabei gas field in China provided proof that the numerical model was accurate. The findings indicate that the gas generation rate increases nonlinearly when porosity increases. Lower reservoir porosity will cause considerable near-wellbore pressure and more significant rock deformation. The reservoir rocks' enhanced potential for deformation will result in higher pore pressure close to the wellbore. The study focused on the matrix rather than the fractured reservoir rock.

2.2.3 Stress-dependent Matrix Permeability

Bai and Elsworth (1994) developed a model to explain how the Hertzian contact between spherical grains might make hydraulic conductivity sensitive to effective loads. An approximate representation of the fragmented rock is a network of equivalent fractures, where each fracture is idealized as a planar opening with a constant equivalent thickness or aperture. The relationship between strain and hydraulic conductivity is depicted using the model. Deformations caused by subsidence result from mining-related modifications to the hydraulic conductivity of both matrix and fractured rocks. The Hertzian contact theory was used by Gangi (1978) to develop an equation representing hydraulic conductivity as a function of stress conditions.

$$k_{mat} = k_{i-mat}\left\{1 \pm \frac{1}{2}\left[\frac{9(1-\nu^2)}{2}\left(\frac{\pi\,\Delta\sigma}{E}\right)^2\right]^{1/3}\right\}^2 \tag{2.2}$$

where k_{mat} is the matrix permeability (mD), k_{i_mat} is the initial matrix rock permeability, ν is the Poisson's ratio, $\Delta\sigma$ is the differential stress of the rock matrix (Pa), and E is the drained Young's modulus of the rock matrix (GPa). The positive sign refers to dilatational loading, and the negative signal corresponds to the compressional loading.

Bai et al. (1997) developed a numerical model based on the finite element scheme and embedded correlations of induced strain-modified permeability. The model is compared with analytical solutions and experimental results under steady-state conditions. Numerical investigations show that mechanical influences, if the media is naturally fractured, considerably change the physical parameters of the rock matrix, including permeability. No information regarding the permeability changes is provided under unsteady state conditions. Zhang et al. (2018) conducted an analytical and experimental study to investigate the effects on stress-dependent permeability under in-situ conditions. The findings suggest that changes in the stress state brought on by oil production and water injection may cause changes in rock permeability. Water injection may be advantageous despite stress-dependent permeability negatively impacting production rate and recovery volume. The effect of poroelasticity is however not considered in this study.

Haghi et al. (2018) developed a semi-analytical model to analyse the impact of stress-dependent spontaneous imbibition. The model investigates how stress-dependent effects affect the absolute permeability and oil recovery in both intact and naturally fractured carbonate reservoirs. Pure compliance poroelastic definitions and nonlinear joint normal stiffness equations are employed to evaluate the deformation of the rock matrix to represent the geomechanical interactions. The result of stress-dependent permeability is shown in Figure 2.3. Moreover, the absolute permeability is computed based on the matrix porosity.

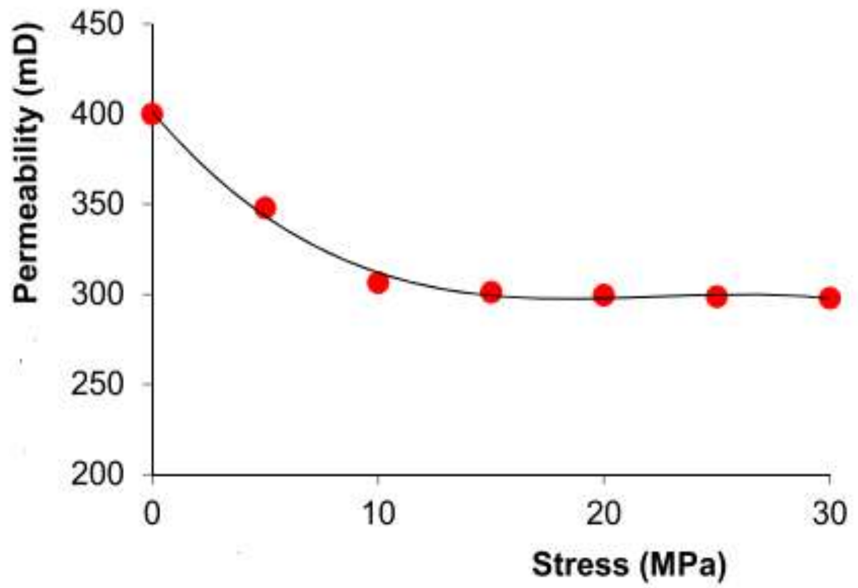

Figure 2.3. Variations in permeability w.r.t stress loading (Haghi et al., 2018)

2.2.4 Stress-dependent Fracture Permeability

Zhang et al. (2007) investigated fluid flow and permeability variations under uniaxial, biaxial, and triaxial stress-strain processes using concrete blocks with randomly distributed fractures and rock core samples. Experimental correlations between flow rate, permeability and fracture aperture are examined in the fractured media. Results reveal a cubic law relationship between flow rate and stress aperture for randomly spread fractures. The experimental findings are used to propose a permeability-aperture relationship. The suggested model indicates how stress redistributions affect permeability variations for an angled borehole dug in naturally fractured tight reservoir. The findings show that the permeability surrounding subsurface apertures is highly dependent on stress variations and the directions of the natural fractures. Zhang et al. (2007) developed a relationship between permeability and stress-induced fracture aperture change based on experimental data, as expressed below.

$$k_f = k_{i\_f}\left(1 + \frac{\Delta h}{h_i}\right)^3 \tag{2.3}$$

$$\Delta h = h - h_i \tag{2.4}$$

where Δh is the fracture aperture change (mm), h_i is the original fracture aperture before loading, h is the fracture aperture after loading, k_f is the fracture permeability and k_{i_f} is the initial fracture permeability.

Latham et al. (2013) used a unique modelling strategy, and the impact of in-situ stresses on flow dynamics in fractured rock is examined. The deformation of a fragmented rock mass is modelled using the combined finite-discrete element approach. The Complex Systems Modelling Platform (CSMP) examines the resulting changes in the rock mass's flow characteristics. Single-phase flow through fractures with variable aperture and a porous rock matrix is modelled using CSMP. The findings demonstrate that a change in the stress state can reactivate pre-existing fractures and channel flow in critically stressed fractures. Furthermore, natural fracture geometries are rarely linear, enabling dilating fracture segments.

Cao et al. (2019) conducted a quantitative model that manifests the controls on the permeability of fracture systems with different extents of fracture penetration. A theoretical stress-dependent permeability model is proposed, considering the degree of fracture penetration. The findings demonstrated that the closure of the fractures causes a significant reduction in the rock permeability of cores with fractures first. As effective stress increased, the permeability of the fractured core initially decreased significantly, as shown in Figure 2.4. As effective stress increases, the permeability steadily decreases. The effect of poroelasticity however is not taken into consideration.

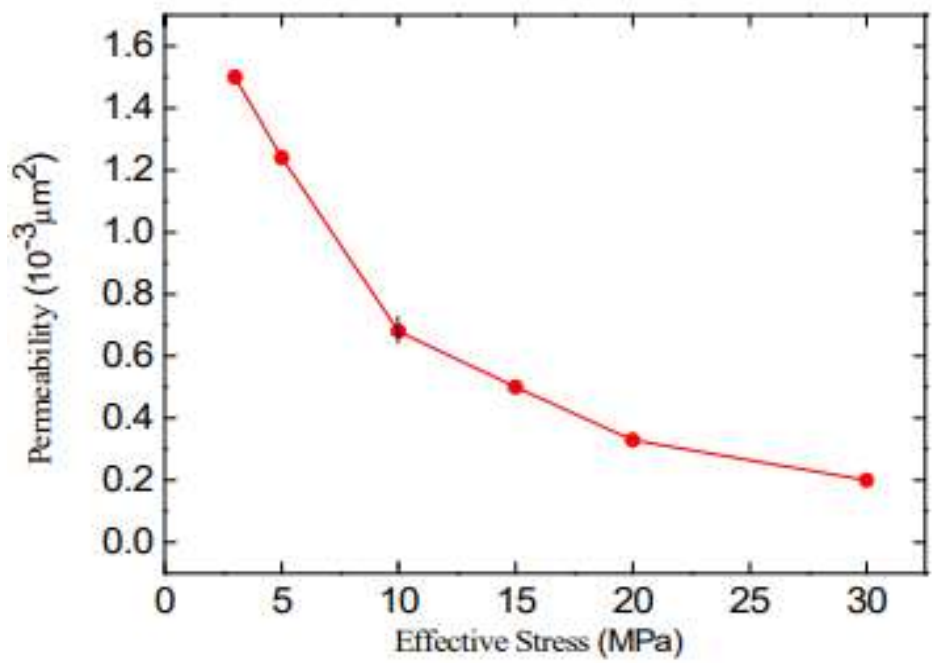

Figure 2.4. Numerical results of stress-dependent fracture permeability (Cao et al., 2019)

Li et al. (2021) used real-time X-ray imaging and Triaxial Direct-Shear (TDS) tests to quantify the stress-dependent fracture permeability of Western Texas and Marcellus shale under subsurface conditions. The importance of shale gas production was then examined using stress-dependent fracture permeability measurements in a formation-linear flow model. The Marcellus Shale Energy and Environment Laboratory serve as the model's primary case. The model's results show that fracture closure can be crucial for production within a limited stress-dependent permeability range. The effects of pore pressure on fracture permeability during the tests have not been reported.

2.2.5 Stress-dependent Relative Permeability

McDonald et al. (1991) conducted experimental work on stress-dependent relative permeability using nuclear magnetic resonance techniques. According to the experimental findings, increased stress loading causes the relative permeability curves to shift to the left while decreasing irreducible water saturation. Multiphase flow analysis at the fracture-matrix interface has not been carried out. Lian et al. (2012) performed research on the carbonate cores from the Kenkiyak oil field's oil/water relative permeability and compared the relative permeability curves of natural matrix cores against artificially fractured cores. The stress sensitivity properties of the relative permeability curves were also examined based on the research on naturally fractured cores. The findings show that the irreducible water saturation rises with increased stress loading, the residual oil saturation changes somewhat, and the equal permeability point shifts downward as shown in Figure 2.5. Investigation on multiphase flow at the fracture-matrix interface however have not been carried out.

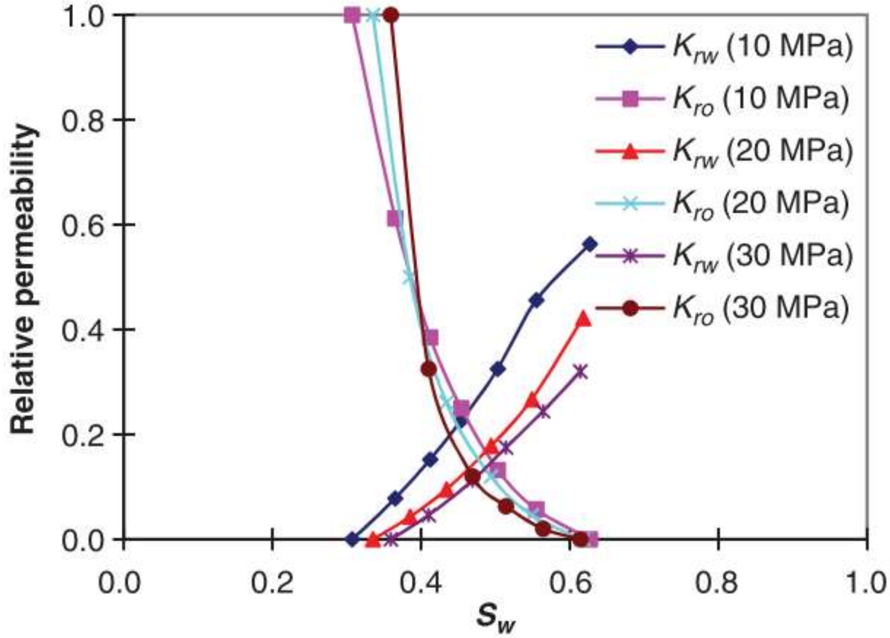

Figure 2.5. Stress sensitivity analysis of several relative permeability curves (Lian et al., 2012)

Huo and Benson (2016) carried out laboratory core flooding experiments to assess the relative permeability of nitrogen-water mixes in fractured rock under various stress-loading conditions. The stress dependency is tested under 2.07 MPa and 5.52 MPa effective stress loading. The observations for both stress conditions demonstrate that relative gas permeability is very low until a critical saturation is reached. Additionally, when the experiments run at the same flow rate, the results show that increasing stress decreases the end-point non-wetting phase relative permeability and the irreducible water saturation. Although the experiments are limited to the flow through fractures and neglect the fracture-matrix interface, it has been observed that there exists a nonlinear relationship between relative permeability and fluid saturation (Diomampo, 2001; Fourar et al., 1993). By examining the flow through a fracture-matrix system utilizing Berea Sandstone

(Akin, 2001), the impact of stress loading and fracture dimensions on relative permeability (Lian et al., 2012) and the estimation of relative permeability has been enhanced. It has been further noticed that a rise in stress loading has little to no impact on residual oil saturation while decreasing the irreducible water saturation. On the other hand, the relative permeability of displacing (non-wetting) fluid is exclusively reliant on the wettability of the porous medium. The multiphase flow is also influenced by the size and structure of the matrix, as demonstrated by studies on chalk and sandstone core samples involving water absorption (Jacob et al., 2021). As a result, obtaining accurate data is necessary to determine a system's relative permeability in naturally fractured tight reservoir. This data can only be obtained by considering all aspects of fluid flow in naturally fractured tight reservoirs.

2.2.6 Stress-dependent Capillary Pressure

Bertels et al. (2001) developed an experimental technique that uses CT scanning to provide high-resolution measurements of aperture distribution and capillary pressure for the same rough-walled fracture. This technique is performed on an induced fracture in a cylindrical basalt core, undergoing water drainage. The capillary pressure initially increased and then decreased with increased stress loading. Although this capillary behaviour is atypical for unsaturated flows, the sizes of the gas-filled apertures are consistent with the measured capillary pressure.

Huo et al. (2014) used a CT scan and numerical models to conduct tests on fracture aperture distributions under various stress loading. The statistics on the stress-dependent aperture distribution show that as the stress rises, the fracture aperture will contract. The plateau area of the capillary pressure curve tends to become steeper as the variation of aperture distribution increases with stress, showing that capillary behaviour shifts more in the fracture rather than the rock matrix. Moreover, the effect of poroelasticity is ignored. Furthermore, no information regarding the capillary pressure at the fracture-matrix interface has been provided.

Lima et al. (2019) developed two aperture-based capillary pressure models to numerically simulate the injection of supercritical CO_2 into single fractures, saturated with brine, under various stress levels. Using photogrammetry, naturally fractured tight reservoirs were scanned to be input in the numerical simulations, and a contact mechanics model was applied to create aperture fields for different stresses. The Young-Laplace equation is used directly to get the capillary pressure and is compared to the van Genuchten equation. The findings demonstrate that the stress exerted on the rock formation substantially impacts multiphase flow in fractured rock, as shown in Figure 2.6. For instance, the aperture deviation tends to decrease as the stress increases because the subsurface reservoir is being depleted. The effects of poroelasticity are not considered in this study.

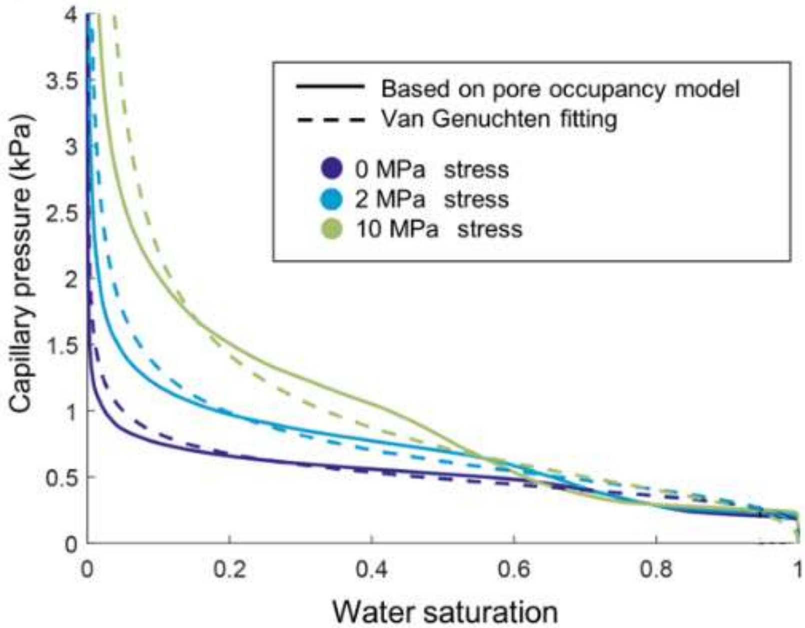

Figure 2.6. Capillary pressure saturation (Lima et al., 2019)

It has been noticed that in all the published studies regarding the effects of geomechanical properties on multiphase flow through naturally fractured tight reservoirs, the effect of stress loading on multiphase flow is ignored at the fracture-matrix interface in naturally fractured tight reservoirs. Accurate modelling is required to model stress-dependent multiphase flow exchange at the fracture-matrix interface.

2.3 Strategies of Coupling Geomechanics and Multiphase Flow in Naturally Fractured Tight Reservoirs

The dynamic coupling of geomechanical properties of naturally fractured tight reservoirs and associated multiphase fluid flow is of particular interest (Minkoff et al., 2003). Coupling geomechanics and multiphase fluid flow has received much attention in civil and geotechnical engineering for many years (Majorana et al., 2015; McCartney et al., 2016). As a result of the shrinkage and extension of structural deformation, coupled structural mechanics and heat flow has also been investigated in structural science and mechanical engineering (Baran et al., 2017). In the petroleum engineering discipline, coupled multiphase fluid flow and geomechanical interactions can play a significant role in dictating fluid flow behaviour in natural fractures and tight rock reservoirs. The characterisation of reservoir geomechanics can play a critical role in enhanced oil recovery (Chiaramonte et al., 2011; Guy et al., 2012), subsidence, stability of wells (Fjær et al., 2008), stress-dependent porosity, the permeability of rock matrix and stress-dependent fracture aperture change (Cao et al., 2019; Mohiuddin et al., 2000; Sanaee et al., 2012) in fractured and unconventional reservoirs. Wellbore stability problems have been the subject of several studies due to the vicinity changes of the stress and strain around the wellbore (Zoback, 2007). Reservoir compaction may lead to severe damage in the wellbore during surface subsidence due to reservoir pressure depletion but can also increase oil recovery and the slow decline in reservoir pressure while production takes place (Muggeridge et al., 2014; Pettersen, 2010).

Several coupling strategies have been used to model geomechanics and multiphase fluid flow interactions (Ahmed and Al-Jawad, 2020; Curnow and Tutuncu, 2015; Doster and Nordbotten, 2015; Jing, 2003; Kim et al., 2013; Lavrov, 2017; Longuemare et al., 2002; Rutqvist and Stephansson, 2003; Sanaee et al., 2013; Weishaupt et al., 2019; Xiong et al., 2011; Zhao et al., 2017). Coupling methods are generally divided into two different categories i.e. i) volume coupling, and ii) coupling through flow properties (Settari and Mourits, 1998).

Volume coupling requires the same pore volume changes in reservoir geomechanics and flow models, which are functions of stress, pressure and temperature (Lee and Schechter 2015). In the coupling through flow properties, permeability and relative permeability are varied due to changes in stress and displacements (Settari and Mourits, 1998). Furthermore, methods of coupling through flow properties between geomechanics (solid deformation) and reservoir flow, in mathematical terms, are generally categorized into four types i.e. i) one-way coupling, ii) two-way coupling, iii) iterative coupling, and iv) full coupling (Tran et al., 2004).

2.3.1 One-way Coupling

In one-way coupling scheme, two separate essential sets of equations are solved independently for fluid flow and geomechanical deformation over the same time period (Minkoff et al., 2003). This type of coupling is also called explicit coupling because the data is merely conveyed in a one direction, from fluid flow solver to the geomechanical model. This means that changes in pore pressure lead to changes in stress, strains, and displacements, but changes in stress and strain do not impact pore pressure changes (Tran et al., 2004). Although there is a weak link between geomechanical deformation and fluid flow (Tran et al., 2004), one-way coupling has provided valuable insight into physical scenarios, and it is desirable for fluid flow modelling where the mechanical conditions are essential (Minkoff et al., 2003). For instance, a one-way coupling experiment successfully employed 200 fluid flow simulations to predict well failure rates in the Belridge Field, California (Fredrich et al., 2000, 1996). Although numerical modelling using one-way coupling is simple and does not require extensive or complicated modelling techniques for field scale, one-way coupling is less desirable from the physical point of view compared to the other types of couplings (Fredrich et al., 2000). Moreover, utilizing the traditional formulation of the dual-porosity dual-permeability model and one-way coupling method, commercial codes like Imex-CMG and Schlumberger's-Visage mimic the hydromechanical behaviour of fractures (Mejia et al., 2022).

2.3.2 Two-way Coupling

Two-way coupling is an extension of one-way coupling and is sometimes called loose coupling or pseudo-coupling (Chin et al., 2002; Tran et al., 2004). In two-way coupling, reservoir geomechanics and fluid flow solvers run sequentially (Jin et al., 2000) based on two distinct sets of equations that are solved independently, and the information is conveyed in both directions between the two solvers (Minkoff et al., 2003). Two-way coupling is relatively simple with the main advantage that it captures nonlinear physics between geomechanical and reservoir flow solvers (Dubinya et al., 2015; Kim et al., 2012). The primary drawback of explicit coupling schemes (both one-way and two-way coupling) is that the explicit nature of coupling can enforce time step restrictions on numerical runs because of concerns regarding stability and accuracy (Dean et al., 2006).

2.3.3 Iterative Coupling

In this type of coupling, geomechanical variables are solved first and the reservoir flow variables are solved subsequently, at each time step (Lee and Schechter

2015; Tran, Settari, and Nghiem 2004). A coupled system of equations decomposes the governing equations of geomechanical and multiphase flow solvers. While the reservoir flow simulator and geomechanics model solve governing subsystems of equations separately, the equations are solved iteratively using data variables between both subsystems, as shown in Figure 2.7, through a data exchange interface (Chin et al., 2002). The main advantage of iterative coupling is that it is easy to implement between an existing reservoir flow simulator and geomechanics model through a data exchange interface (Mikelić et al., 2014). The primary shortcoming of the iterative coupling scheme is the use of first-order convergence in nonlinear calculations, which may require a significant number of iterations for complex problems like naturally fractured tight reservoirs (Cervera et al., 1996; Dean et al., 2006).

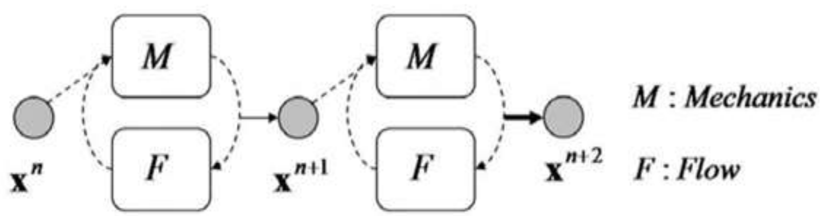

Figure 2.7. Iterative coupling scheme (Kim, 2010)

2.3.4 Full Coupling

The governing equations of reservoir flow variables (such as saturation, pressure, and temperature) and the geomechanical response (such as displacements) are solved simultaneously in fully coupled numerical scheme (Charoenwongsa et al., 2010; Giani et al., 2018; Mejia et al., 2022; Pan et al., 2007; Settari and Walters, 2001; Stone et al., 2000). This coupling scheme is sometimes called implicit coupling because the whole system is solved simultaneously and can be discretized on a single grid domain (Tran et al., 2004), as depicted in Figure 2.8.

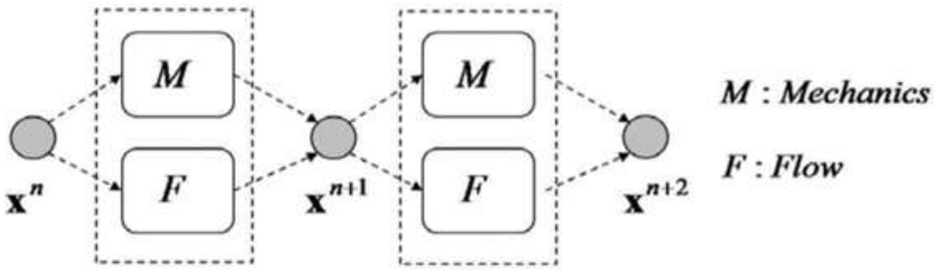

Figure 2.8. Full coupling scheme (Kim, 2010)

The main advantage of a fully coupled scheme is the internal consistency and the accuracy of the solution (Giani et al., 2018; Gudala and Govindarajan, 2021). Another advantage of the fully coupled scheme is the stability and conservation of the second-order convergence for nonlinear iterations. However, the coupling of multiphase fluid flow and geomechanics conservative relations is complicated and is considerably difficult for inelastic mechanical deformation (Minkoff et al., 2003; Osorio and Chen, 1999; Zhu et al., 2021). Moreover, the fully coupled scheme requires code development, becomes more expensive than other schemes, and utilizes iterative methods in some situations (Rocca, 2009). Figure 2.9 depicts how distinct numerical coupling schemes work.

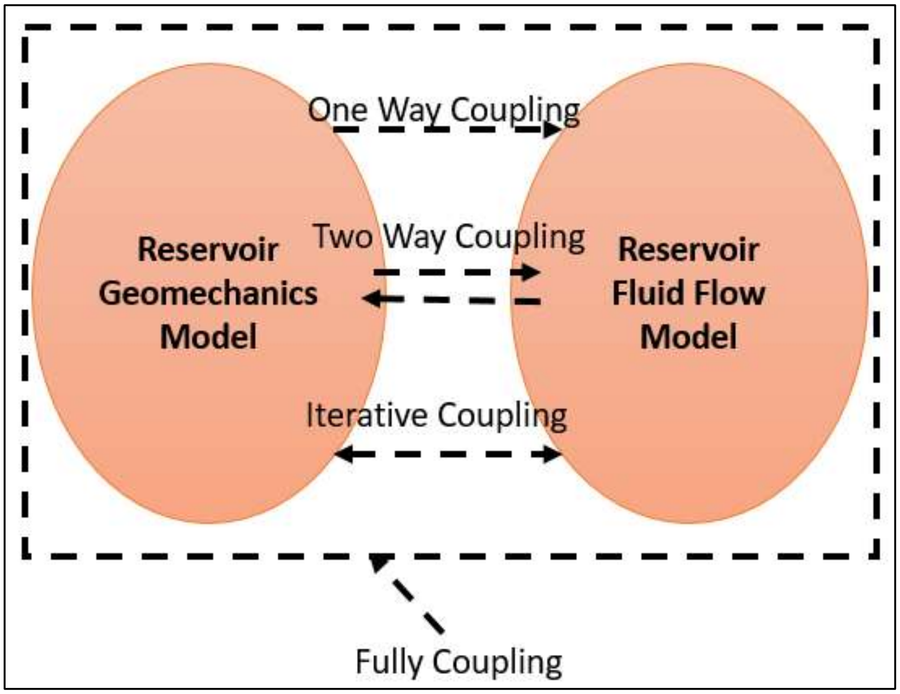

Figure 2.9. Geomechanics and fluid flow coupling schemes

2.4 Research Gaps in Knowledge

Based on the literature review presented in this chapter, it can be concluded that the published literature is severely limited in terms of the multiphase flow modelling (flow velocities, pressure drop, concentration of the fracture aperture) and detailed analysis of the multiphase flow properties at the fracture-matrix interface. This is especially true for multiphase flow modelling in naturally fractured tight reservoirs. Hence, a better understanding of the multiphase flow behaviour at the fracture-matrix interface within naturally fractured tight reservoirs is required.

It has also been observed that several research studies are available that investigate coupled geomechanics and single-phase fluid flow in naturally fractured rocks. However, the published literature severely lacks in coupled geomechanics and multiphase flow in tight reservoirs. Commercial codes like TOUGH2 and Eclipse mimic fluid flow behaviour in fractured porous media by using conventional formulation of dual-porosity dual-permeability, which cannot provide an accurate description of multiphase flow exchange at the fracture-matrix interface. Thus, there is a need to carry out detailed numerical investigations on naturally fractured tight reservoirs and employing coupled geomechanics and multiphase models for accurate predications at the fracture-matrix interface.

Numerical modelling techniques have been widely used in the published literature for modelling naturally fractured tight reservoir because of their cost-effectiveness and simplicity to carry out numerical experiments. A potential reason identified is the use of one-way coupling scheme between geomechanics and fluid flow. There is a need to develop a novel and robust numerical modelling technique that can accurately predict multiphase flow characteristics at the fracture-matrix interface, when the rock is subjected to external stress loading.

2.5 Research Objectives

Based on the knowledge gaps identified after conducted a thorough review of the published literature, a number of research objectives for this study have been formulated. The research objectives of this study are:

1. Comparative analysis of numerically modelling natural fracture in tight reservoirs as a duct and as a porous medium, leading to the identification of the most appropriate modelling technique.

2. Transient multiphase flow diagnostics at the fracture-matrix interface of naturally fractured tight reservoirs through the introduction of a novel source terms in the momentum governing equations.
3. Implementation of one-way coupling scheme on the geomechanical and multiphase flow parameters for realistic estimation of oil recovery from naturally fractured tight reservoirs.
4. Numerical investigations on the effects of geomechanical parameters on multiphase flow characteristics at the fracture-matrix interface of naturally fractured tight reservoirs.
5. Development of a novel fully coupled scheme for enhanced oil recovery predictions from naturally fractured tight reservoirs.
6. Comparative analysis of one-way and novel fully coupled schemes for the estimation of oil recovery from naturally fractured tight reservoirs.

Chapter 3
Numerical Modelling of Naturally Fractured Tight Reservoirs

Based on the research objectives identified in the previous chapter, a number of different methodologies need to be employed in order to achieve the aims of this study. These methodologies include i) Computational Fluid Dynamics to analyse the multiphase flow in tight reservoirs, ii) Finite Element Analysis to analyse geomechanical behaviour of tight reservoirs, and iii) Coupling of fluid dynamics and geomechanical behaviour of tight reservoirs. These methodologies have been discussed in detail in this chapter, along with the identification of the scope of work for each methodology

3.1 Computational Fluid Dynamics of Tight Reservoirs

Computational Fluid Dynamics (CFD) is a modern technique to analyse fluid flow systems based on conservation equations for mass, momentum and energy (Versteeg, H K Malalasekera, 2007). The literature review carried out in the previous chapter clearly shows the advantages of using CFD in analysing multiphase flow through tight reservoirs. In this section, the details of CFD modelling in the current context is presented.

3.1.1 Governing Equations of Fluid Flow in Tight Reservoirs

The governing equations of fluid flow in tight reservoirs are solved here using the Finite Volume Method (FVM). In this method, the flow parameters are considered to be conserved in infinitesimally small volumes of the flow domain. In the current context, the primary conservation equations are i) mass conservation, and ii) momentum conservation. The mass conservation equations (also known as the Continuity equation), in 3D can be written as (Versteeg, H K Malalasekera, 2007):

Rate of increase of mass in a fluid element = Net rate of flow of mass into the fluid element

Or, in mathematical form as:

In X direction: $$\frac{\partial \rho}{\partial t} + div\ (\rho u) = 0 \tag{3.1}$$

In Y direction: $$\frac{\partial \rho}{\partial t} + div\ (\rho v) = 0 \tag{3.2}$$

In Z direction: $$\frac{\partial \rho}{\partial t} + div\,(\rho w) = 0 \tag{3.3}$$

where ρ is the density of the fluid (kg/m^3), t is time (s) and u, v and w are flow velocities (m/s) in x, y and z direction, respectively.

The momentum conservation equations (also known Navier-Stokes equations, or simply NS equations), in 3D can be written as (Versteeg, H K Malalasekera, 2007):

Rate of increase of momentum of a fluid particle = Sum of forces applied on a fluid particle

Or, in mathematical form as:

In X direction: $$\rho \frac{Du}{Dt} = -\frac{\partial P}{\partial x} + div(\mu\ grad\ u) + \Psi_x \tag{3.4}$$

In Y direction: $$\rho \frac{Dv}{Dt} = -\frac{\partial P}{\partial y} + div(\mu\ grad\ v) + \Psi_y \tag{3.5}$$

In Z direction: $$\rho \frac{Dw}{Dt} = -\frac{\partial P}{\partial z} + div(\mu\ grad\ w) + \Psi_z \tag{3.6}$$

where Ψ_x, Ψ_y and Ψ_z are the source terms in x, y and z direction respectively. $\rho \frac{Du}{Dt}, \rho \frac{Dv}{Dt}$, and $\rho \frac{Dw}{Dt}$ are the rate of change of x, y, and z momentum per unit volume of a fluid particle, respectively.

In order to solve these conservation equations, CFD solvers employ iterative techniques.

3.1.2 Stages in CFD

There are three main stages in any CFD analysis. These are:

1. Pre-processing: this stage is further divided into two main sub-stages. The first sub-stage is the development of the numerical model i.e. geometrical modelling of the flow domain. The second sub-stage is the spatial discretisation of the flow domain i.e. meshing.
2. Solver Execution: this stage is further divided into various sub-stages, depending on the complexity of the problem under consideration. However, some common sub-stages are solver settings, boundary conditions, material properties, flow modelling techniques etc.
3. Post-processing: this stage comprises of data analysis, both qualitative and quantitative.

The details of stages 1 and 2 are presented in this chapter, while post-processed results are presented in chapter 4. The CFD solver used in the present study is ANSYS® FLUENT 19.2. All the numerical simulations have been carried out on Intel® Core™ i5-6500 3.2 GHz processor on 2 cores and 32 GB RAM.

3.1.3 Geometry of Fractured Tight Reservoir

The geometric scale of tight reservoirs is in kilometres, modelling which is computationally prohibitive and thus, a representative sample of a tight reservoir has been modelled in the present study. The 3D geometric model of the sample tight reservoir is shown in Figure 3.1. The geometric design of this sample is based on Berea Core Sandstone sample (Kazemi and Merrill, 1979), as shown in the

Appendix A (Table A1). It can be seen that the reservoir sample comprises of two distinct parts i.e. the outer cylindrical core region and the inner rectangular fracture. The diameter of the core (*D*) is 2.54 cm, while its length (*L*) is 7.62 cm. The aperture (*h*) of the fracture is 0.03 cm.

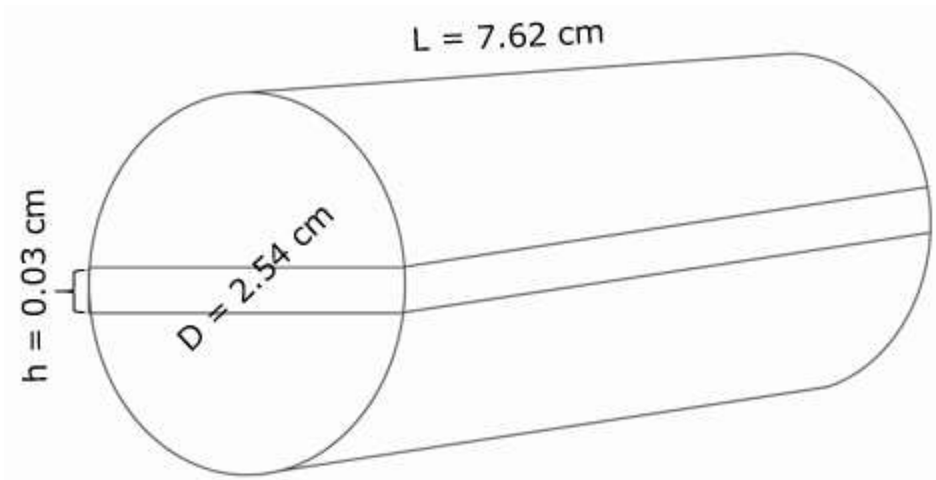

Figure 3.1. Geometric model of the tight reservoir

3.1.4 Meshing of Fractured Tight Reservoir

Two different mesh strategies have been employed in the present study, based on similar studies in the published literature. In the first strategy, a butterfly mesh has been generated in the flow domain, as shown in Figure 3.2(a). In the second strategy, an O-ring type mesh has been generated in the flow domain, as shown in Figure 3.2(b) (Hernandez-Perez et al., 2011). The reason for generating two different meshes in the flow domain is to compare the results obtained from them and then choose the better mesh strategy for carrying out further analysis.

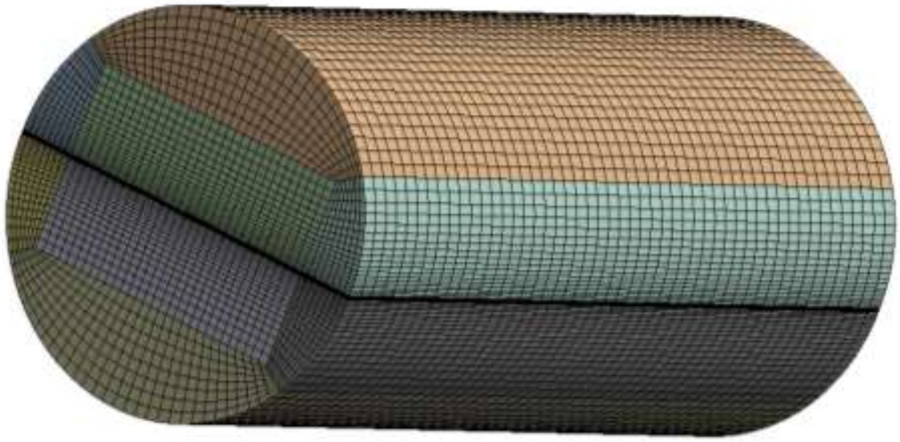

(a)

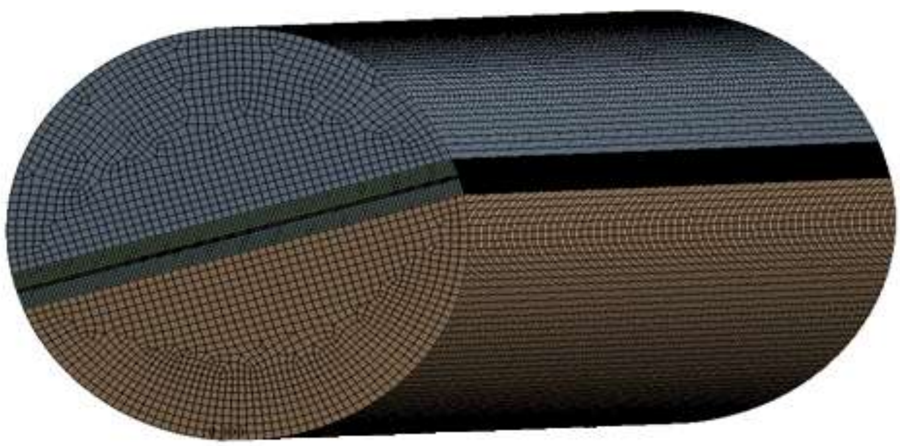

(b)

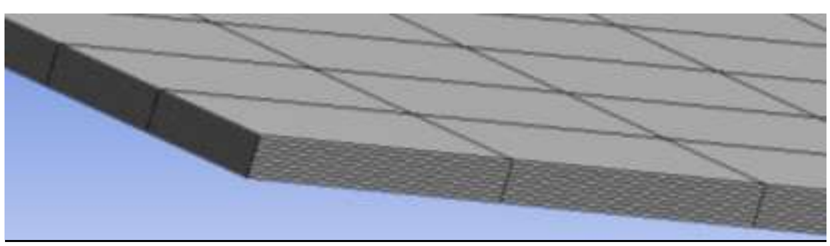

(c)

Figure 3.2. Meshing of the flow domain (a) butterfly mesh (b) O-ring mesh (c) close-up view of the mesh in the fracture region

The meshing in the fracture region comprises of 10 hexahedral element layers and hence, the mesh density is significantly higher compared to the core region. The mesh density has been kept the same in both the meshing strategies for accurately capturing complex flow characteristics in the fracture region.

Numerically predicted results should be independent of the mesh size used (Kim et al., 2022). Thus, four different butterfly meshes and four different O-ring meshes have been created in order to performance comparative analysis to ascertain mesh independence (which is presented in the next chapter). The details of mesh elements in the flow domain are summarised in table 3.1.

Table 3.1 CFD Mesh details

Mesh	Total Number of Elements
Butterfly 1	1.4×10^5
Butterfly 2	1.1×10^5
Butterfly 3	9.8×10^4
Butterfly 4	7.6×10^4
O-ring 1	1.4×10^5
O-ring 2	1.2×10^5
O-ring 3	9.9×10^4
O-ring 4	8.9×10^4

3.1.5 Solver Settings

The two flowing fluids being considered in the present study, based on Berea Sandstone Core Flooding experiments, are oil and water. The modelling approach used in the present study considers that the tight reservoir is initially full of oil. Then water is injected through the fracture aperture in order to extract oil out of the reservoir. Thus, in order to identify the appropriate solver settings to be used, Reynolds Number (*Re*) based on water injection is computed as:

$$Re = \frac{\rho\, U\, L}{\mu} = \frac{1000 \times\ (3.9 \times 10^{-5}) \times\ 0.0762}{0.001} = 2.97$$

where *U* is the flow velocity (m/s) and *μ* is the dynamic viscosity of the fluid (Pa.s).

Thus, the flow is laminar, and the laminar flow model has been employed. This also indicates that the flow is incompressible and thus, the incompressible solver has been used. As discussed before, the thermal effects have been neglected i.e. isothermal flow conditions are considered. Moreover, the solver employed to carry out numerical calculations in this study is transient.

As the flow governing equations in the reservoir are discretised, a pressure-velocity coupling relationship is needed to calculate accurate pressure distribution in the flow domain. Thus, Pressure Implicit with Splitting of Operators (PISO) algorithm has been used for pressure-velocity coupling since it is the preferred choice to carry out transient simulations (Soulaine et al., 2015). Another coupling is required between the momentum and pressure-based continuity equations when they are solved simultaneously, because of large time steps (Xiao et al., 2017). The momentum equations' pressure gradient terms and the face mass flux are implicitly discretized in order to accomplish this.

At the cell centres, the CFD solver stores discrete scalar values. Convection terms, on the other hand, necessitate face values, which must be interpolated from cell centre values. Upwind spatial discretization is used to achieve this. When the face value is up-winding, it signifies that it is generated from data in the cell that is upstream (in the direction of the average flow velocity). Second-order upwind scheme has been used in the current study to model pressure, momentum, and volume fraction, in order to enhance calculation accuracy (Barth and Jespersen, 1989; Issa, 1986).

3.1.6 Fluid Properties and Multiphase Flow Modelling

The densities of oil and water (ρ_o and ρ_w) considered in the present study are 846 kg/m^3 and 1000 kg/m^3, respectively. Similarly, the dynamic viscosities of oil and water (μ_o and μ_w) are 0.0046 Pa.s and 0.001 Pa.s, respectively. The multiphase flow has been modelled using the Volume of Fluid (VOF) approach, which can model two or more immiscible fluids by a single set of momentum equations. The VOF model is a free-surface modelling tool for locating and tracking fluid-fluid interface. In VOF model, the saturation (S), which is essentially the volume fraction, of each fluid is calculated in the control volumes while simulating the flow of two or more immiscible fluids. The saturation of all the fluid phases present in the control volumes is equal to 1. When a control volume is completely filled with oil, the saturation of oil in that control volume is 1 (i.e. S_o=1), while the saturation of water in that control volume is 0 (i.e. S_w=0). Similarly, if a control volume contains both oil and water, then both S_o and S_w are between 0 and 1 (i.e. $S_m \neq 0$).

3.1.7 Core and Fracture Properties

The core region has been considered as a porous medium in the present study, having porosity (φ) of 18.5 % and permeability (k) of 97 mD (9.573 x 10^{-14} m^2). Furthermore, the pore size distribution index (λ_p) in the core region is taken as 0.674, and the entry capillary pressure (Pc) is 345 Pa.

The fracture within the core region has been modelled using two separate techniques, based on the published literature (Kazemi and Merrill, 1979). In the first technique, the fracture region has been modelled as a duct, while in the second technique, it has been modelled as a porous medium (like the core region). In the second case (porous medium), the porosity and permeability of the fracture region are 100 % and 10000 mD (9.869 x 10^{-12} m^2), respectively. Thus, there are two numerical models generated and analysed in this study; model 1 where the fracture is modelled as a duct and model 2 where the fracture has been modelled as a porous medium. Detailed flow modelling in these two models is discussed in the section below.

3.1.8 Multiphase Flow Modelling in Model 1

In model 1, the core region has been modelled as a porous medium while the fracture region has been modelled as a duct, as shown in Figure 3.3.

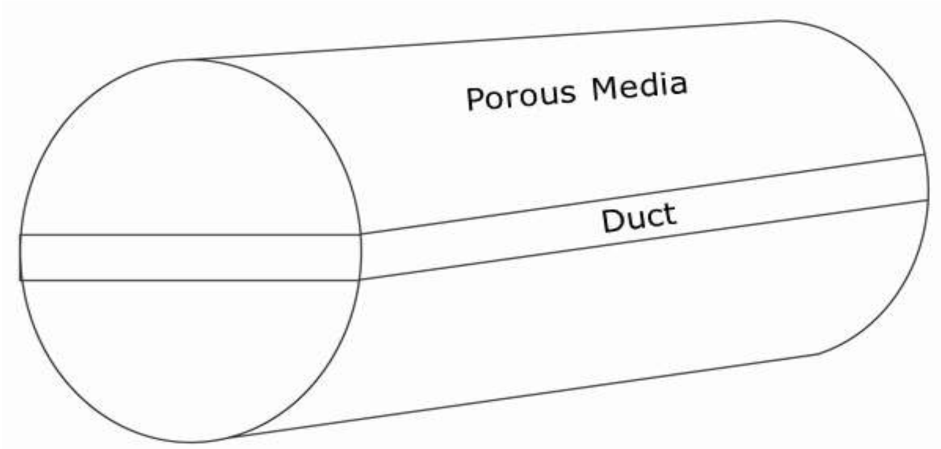

Figure 3.3. Flow Modelling in Model 1

- *Core Region*

The core region is modelled as a porous medium in this study. In real-world, a porous medium comprises of several torturous paths (or pores), where the flow velocity vector is different in different paths. When a porous medium is modelled numerically, no such paths exist in the model. The flow is controlled through the application of porosity and permeability. However, the flow velocity vectors need to be adjusted accordingly in order to accurately represent them. For this purpose, the superficial velocity vectors are being considered in the present study while modelling the porous media. The relationship between the superficial flow velocity vector and the physical (real-world) flow velocity vector is given as:

$$\vec{U}_{superficial} = \varphi\, \vec{U}_{physical} \tag{3.7}$$

where φ is the porosity of the core region. Hence, the mass conservation (continuity) equation can be written as (Whitaker, 1969):

$$\frac{\partial}{\partial_t}\left(\varphi\, S_\beta\, \rho_\beta\right) + \nabla.\left(\varphi\, S_\beta\, \rho_\beta\, \overrightarrow{U_\beta}\right) + \Psi_\beta = 0 \tag{3.8}$$

where β means the phase (*o* for oil and *w* for water). The term Ψ in the mass conservation equation is the source term originating from the additional viscous losses offered by the core region (porous media), based on Darcy's law. This viscous loss source term can be written as (Jackson and James, 1986):

$$\Psi_\beta = \frac{\mu}{k}\,\overrightarrow{\eta_\beta} \tag{3.9}$$

where k is the permeability of the core region and η is the Darcy velocity (m/s).

Similarly, when modelling momentum conservation in the core region, the same viscous loss source term is added to the momentum conservation equations (NS equations) given in equations 3.4 – 3.6.

➢ *Fracture Region*

The mass conservation equation in the fracture region can be written as (Hirt and Nichols, 1981):

$$\frac{1}{\rho_\beta}\left[\frac{\partial\left(S_\beta\, \rho_\beta\right)}{\partial_t} + \nabla.\left(S_\beta\, \rho_\beta\, \overrightarrow{U_\beta}\right)\right] = 0 \tag{3.10}$$

When the flow domain is fully saturated with only one particular phase, the fluid properties mentioned in section 3.1.6 are used in the control volumes. However, when the control volumes contain both the phases (oil and water), the fluid properties need to be adjusted accordingly. Thus, the mixture density can be expressed as (Hirt and Nichols, 1981):

$$\rho_m = S_w \, \rho_w + (1 - S_w) \, \rho_o \tag{3.11}$$

where subscript *m* represents mixture. The mixture dynamic viscosity is given as (Hogg et al., 2006):

$$\mu_m = S_w \, \mu_w + (1 - S_w) \, \mu_o \tag{3.12}$$

3.1.9 Multiphase Flow Modelling in Model 2

In model 2, both the core and fracture regions are modelled as porous media, as shown in Figure 3.4.

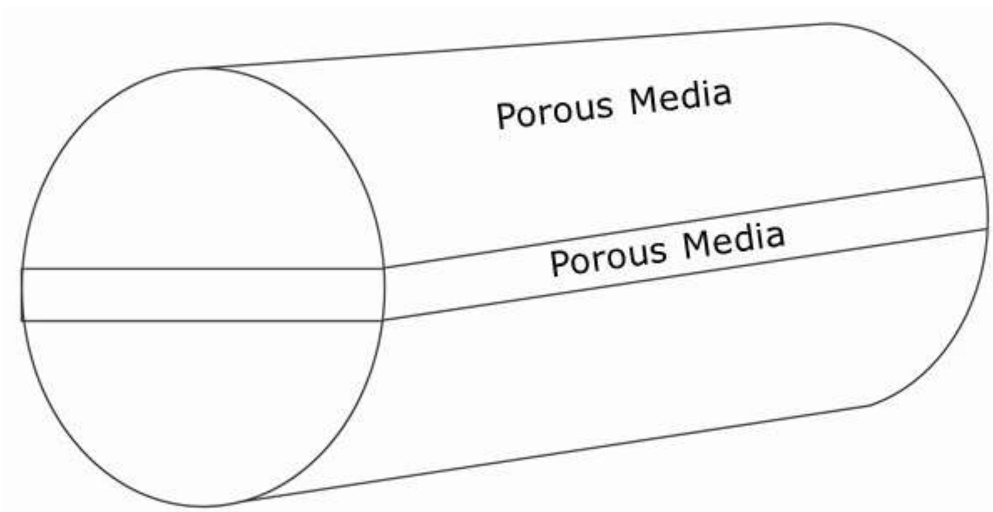

Figure 3.4. Flow Modelling in Model 2

Thus, equations 3.7 - 3.9, and equations 3.11 – 3.12, are applicable in both these regions.

3.1.10 Modelling the Interface between the Core and Fracture

The interface between the core and fracture regions, in both the models, has been modelled based on Brooks and Corey method (Brooks and Corey, 1966). The saturation (*S*), capillary pressure (*Pc*) and the relative permeability (*Kr*) can be expressed as:

Oil Saturation: $$S_o = \frac{(S_{oi} - S_{ro})}{(1 - S_{ro} - S_{rw})} \tag{3.13}$$

Water Saturation: $$S_w = \frac{(S_{wi} - S_{rw})}{(1 - S_{ro} - S_{rw})} \tag{3.14}$$

where the subscripts *i* and *r* represent initial and residual respectively.

$$Pc = Pec\, {S_w}^{-1/\lambda_p} \tag{3.15}$$

where *Pec* is the entry capillary pressure and λ_p is the pore size distribution index.

$$Kr_w = {S_w}^{(3+2/\lambda_p)} \tag{3.16}$$

$$Kr_o = (1 - S_w)^2 \left(1 - {S_w}^{(1+2/\lambda_p)}\right) \tag{3.17}$$

3.1.11 Boundary Conditions

The boundary conditions specified in the numerical solver are based on Berea Sandstone Core Flooding experiments (Kazemi and Merrill, 1979). The fracture inlet has been modelled as velocity inlet, with a water injection velocity (*U*) of 0.000039 m/s. The outlet of the fracture region has been modelled as pressure outlet, with atmospheric pressure conditions specified (1 atm). The rest of the flow boundaries have been modelled as stationary walls, as shown in Figure 3.5.

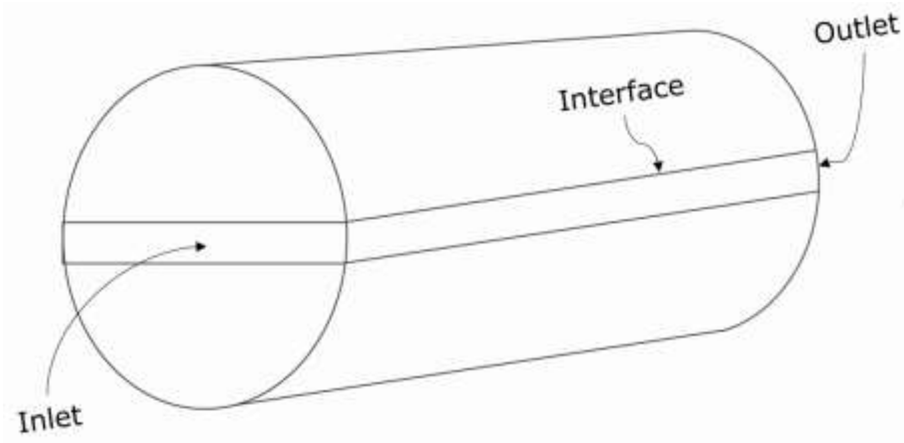

Figure 3.5. Boundary conditions specified

3.1.12 Initial Conditions and Solution Strategy

As discussed in section 3.1.5, the solver is initialised with S_o=1 within the flow domain. This means that both the core and fracture regions are completely filled with oil before the start of the solution. It is noteworthy that the porosity of the core region is 18.5 %, based on Berea Sandstone core flooding experimental data, while the porosity of the fracture region (model 2 only) is 100 %, as expected in real-world situations. The boundary condition at the inlet is a constant water injection velocity, as discussed earlier. The time-dependent solution strategy adopted in the present study is based on the volume of water being injected from the inlet. Based on fracture's geometric dimensions and the water injection velocity, the volumetric flow rate is computed. Based on this, for specific time intervals, the total volume of water being injected (V_w) in the flow domain is calculated. The time step size used in the present study is 0.1s while the solution data is saved when the injected volume of water is equal to 10 % of the pore volume (i.e. 10 % of the volume of all the pores together). This is then repeated for 20 %, 30 %, 40 %, 50 %, 60 % and 70 %.

3.2 Finite Element Analysis of Tight Reservoirs

In order to characterise the geomechanical properties of the tight reservoir, Finite Element Analysis (FEA) has been carried out. It is however noteworthy that FEA has not been carried out on its own, rather FEA-CFD coupling has been employed. This section presents the detailed FEA modelling carried out in the present study.

3.2.1 Introduction to FEA

The Finite Element Analysis (FEA) is a numerical technique where computer-based analyses are carried out to quantify the structural behaviour of mechanical systems, like tight reservoirs. FEA is based on Finite Element Method (FEM) in which, the differential equations governing the structural behaviour are replaced by a set of *n* algebraic equations. Simultaneous solution of these algebraic equations results in the structural parameter values at discrete points. In this way, sufficiently accurate approximate solutions can be obtained. Similar to CFD, there are three stages of FEA i.e. pre-processing (geometry and meshing), solver execution (solver settings, boundary conditions, constraints etc), and post-processing (analysis of results). The pre-processing and solver execution stages of FEA for tight reservoirs are discussed in the following sections, while the data analysis (for FEA-CFD coupling) is presented in chapters 5 and 6. The FEA solver used in the present study is ANSYS® Static Structural 19.2.

3.2.2 Geometry and Meshing of Fractured Tight Reservoir

The 3D geometric model of the sample tight reservoir is shown in Figure 3.6. The geometric design of this sample is based on Clashach's Core Flood laboratory experiments (Stalker et al., 2009), as shown in the Appendix A (Table A2). The diameter of the core (*D*) is 3.79 cm, while its length (*L*) is 7.54 cm. The aperture (*h*) of the fracture is 130 μm. Note that as opposed to CFD analysis where the flow domains are modelled, and thus fracture region was modelled as a distinct body, FEA is based on physical (real-world) geometric features and thus, the fracture region is not modelled in Figure 3.6.

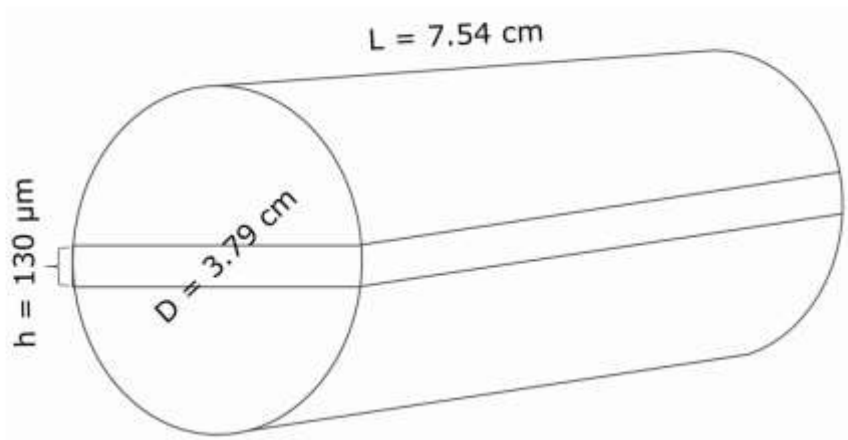

Figure 3.6. Geometry of the tight reservoir

Five different meshes have been generated in the geometry of the tight reservoir, for mesh independence study. The sizes of mesh elements specified are summarised in table 3.2. Mesh 4 is shown in Figure 3.7. It can be seen that mesh refinement has been carried out on the edges of the fracture.

Table 3.2. FEA Mesh details

Mesh	Size of Elements (mm)	Total Number of Elements
Mesh 1	5	1.2×10^4
Mesh 2	3.5	2.7×10^4
Mesh 3	2.8	3.7×10^4
Mesh 4	2	7.4×10^4
Mesh 5	1.8	9.5×10^4

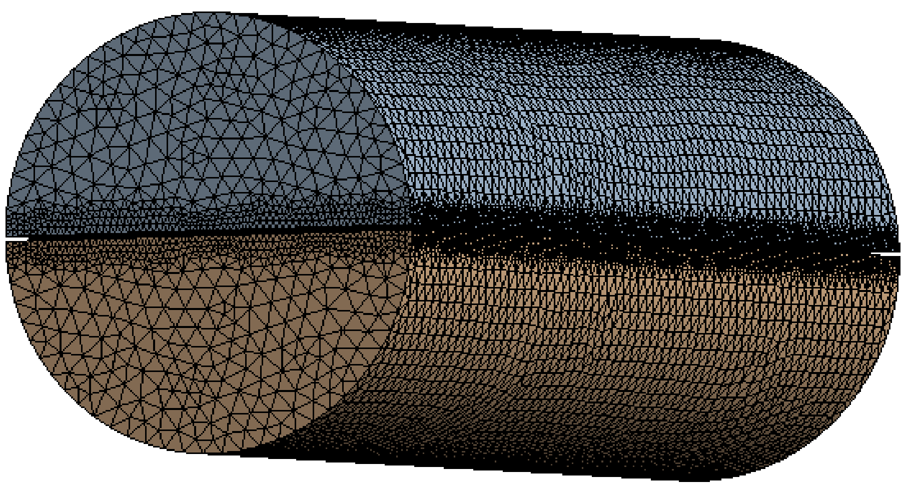

Figure 3.7. Mesh 4

3.2.3 Geomechanical Characterisation of Tight Reservoir

Geomechanics of tight reservoirs involve the quantification of rock's mechanical properties when subjected to compressive forces. The rock remains relatively rigid with minimal volumetric deformation while the empty regions (like fractures) undergo geometric changes. The rock deformation can be described accurately using the stress-strain relationship i.e. Hooke's law, as:

$$\Delta\sigma^{el} = C\ \Delta\varepsilon^{el} \tag{3.18}$$

where σ^{el} is the elastic stress tensor, ε^{el} is the elastic strain tensor and C is the linearized elastic stiffness tensor, provided by bulk and shear modulus as (Cai and Sun, 2017):

$$C = K_b\ I + 2\ R\ I_{dev} \tag{3.19}$$

where K_b is the bulk modulus (MPa), I is the second-order identity tensor, R is the shear modulus (MPa), and I_{dev} is the fourth-order deviatoric projection tensor. Moreover, the change in pore spaces is proportional to the logarithmic pressure (Tachibana et al., 2020) when the rock is subjected to elastic stress loading, which can be expressed as:

$$\Delta e^{el} = -X\ \Delta(ln\ p) \tag{3.20}$$

where e^{el} is the elastic pore space (or void ratio), X is the swell index of rock material and *p* is the pressure or the mean effective stress (MPa). It is noteworthy that the fluid pore pressure is neglected here (for one-way coupling scheme only). Similarly, the relationship of the elastic void ratio to the logarithmic pore pressure is:

$$\Delta e^{el} = -X\ \Delta\left(ln\left(p + p_t^{el}\right)\right) \tag{3.21}$$

where p_t^{el} is the elastic limit of tensile strength (MPa).

Void spaces cause non-linear behaviour in the porous medium, resulting in changes in the void ratio, therefore, the void spaces' dimensions change during stress loading (Alymann, 2010; Dazel and Dauchez, 2009). Hence, a non-linear elastic model, called the Porous Elastic Model, is employed in the present study (Lewis and Schrefler, 1999). The relationship between elastic void ratio and the elastic volumetric strain is given as (Federico and Grillo, 2012; Simo et al., 1985):

$$\varepsilon_{vol}^{el} = ln\left(\frac{1+e^{el}}{1+e_i}\right) \tag{3.22}$$

where ε_{vol}^{el} is the elastic volumetric strain and e_i is the initial void ratio. Substituting the porous elasticity relationship (3.21) into (3.22) gives the pressure as a function of the elastic volumetric strain, as:

$$p = -p_t^{el} + \left(p_i + p_t^{el}\right) exp\left(\frac{1+e_i}{X}\left(1 - exp\left(\varepsilon_{vol}^{el}\right)\right)\right) \tag{3.23}$$

where p_i is the initial mean pressure (MPa). The bulk modulus (K_b) is also based on the stress and elastic volumetric strain (Simulia, 2011), and can be expressed as:

$$K_b = \left(p + p_t^{el}\right)\left(\frac{1+e_i}{X} exp\left(\varepsilon_{vol}^{el}\right)\right) \tag{3.24}$$

The shear modulus (R) also depends on the void ratio and pressure indirectly because the Poisson's ratio (ν) is a constant (Lay and Wallace, 1995; Saxena et al., 2018), and can be expressed as:

$$R = \frac{3\,K_b\,(1-2\nu)}{2(1+\nu)} \tag{3.25}$$

➢ *Stress-dependant Porosity*

Porosity is conventionally obtained through physical testing such as a saturation tests (Ma and Wang, 2016). As the core undergoes compaction, its porosity (φ) changes due to the volumetric strain (ε_{vol}), resulting in geometric variations in the pore spaces, while the solid regions remain intact. The porosity of the sample can be obtained through constitutive models, such as (Ren et al., 2016):

$$\varphi = \frac{e}{1+e_i} = \frac{e_i-(1+e_i)\,\varepsilon_{vol}}{1+[e_i-(1+e_i)\,\varepsilon_{vol}]} \tag{3.26}$$

➢ *Stress-dependant Permeability*

As the rock undergoes compression, the ability of multiphase flow through it changes. The permeability of the rock matrix (k_{mat}) can be expressed as (Sanaee et al., 2013):

$$k_{mat} = k_{i-mat}\left\{1 \pm \frac{1}{2}\left[\frac{9(1-\nu^2)}{2}\left(\frac{\pi\,\Delta\sigma}{E}\right)^2\right]^{1/3}\right\}^2 \tag{3.27}$$

where k_{i-mat} is the initial rock matrix permeability (mD), σ is the stress applied (MPa), E is the Young's modulus (GPa) of the rock matrix. The positive sign refers to dilatational loading, and the negative signal corresponds to the compressional loading (Bai and Elsworth, 1994).

Under stress loading, the permeability of the fracture region also changes (Bogdanov et al., 2003). (Zhang et al., 2007) provide a relationship between the fracture permeability (k_f) and stress-induced fracture aperture change, which can be expressed as:

$$k_f = k_{i-f}\left(1 + \frac{\Delta h}{h_i}\right)^3 \tag{3.28}$$

where $k_{i\text{-}f}$ is the initial fracture permeability (mD) and Δh is the change in the fracture aperture after the application of stress loading i.e. $\Delta h = hi - h$.

3.2.4 Material Properties and Boundary Conditions

The rock sample has a density of 2500 kg/m^3 and has a porosity of 15.4 %. The Poisson's ratio specified in the present study is 0.14 and the Young's Modulus is 40 GPa. The swell index is 0.0072. The boundary conditions specified in the numerical solver are based on Clashach's Core Flood laboratory experiments (Stalker et al., 2009). The dry core sample is initially subjected to 6.9 MPa stress loading, while all the edges of the core region are constrained in all 6DOF to keep the fracture open during the initial flooding stage. Figure 3.8. shows the application of the stress loading and the constraints used in the numerical model of the rock sample.

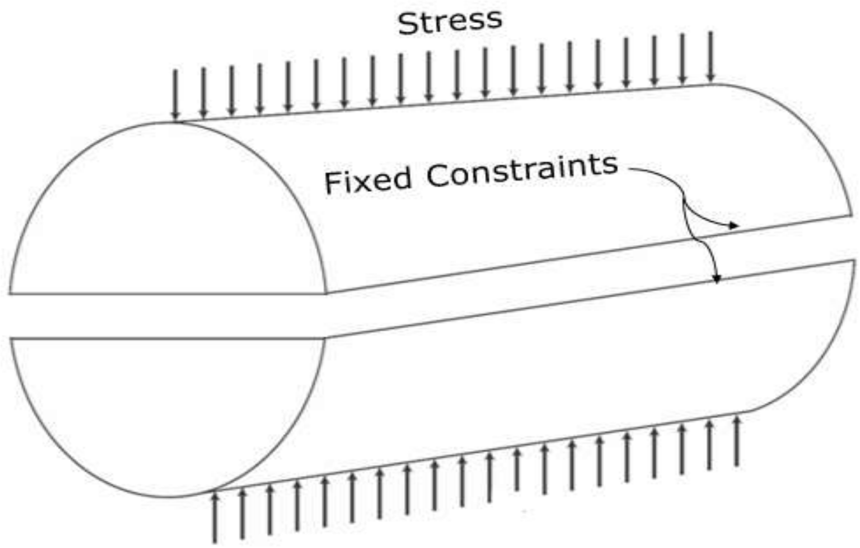

Figure 3.8. Stress loading on the rock sample

3.3 Coupling of FEA and CFD for Fractured Tight Reservoirs

The inter-relationship between stress loading and multiphase flow in tight reservoirs is a well-known fact (Jacob et al., 2021; Liu et al., 2020). This indicates that the numerical modelling of geomechanical properties (FEA) and fluid flow (CFD analysis) should be inter-linked in order to obtain accurate results. This inter-linking of FEA and CFD is realised through the use of different FEA-CFD coupling schemes, as discussed in chapter 2. In the present study, the one-way coupling and fully coupled schemes have been employed to investigate stress-dependant multiphase flow characteristics in tight reservoirs. The details regarding the implementation of both these coupling schemes has been discussed in the following sections.

3.3.1 One-way Coupling Scheme

While carrying out CFD analysis of tight reservoirs, the porosity and permeability in the rock matrix need to be known (i.e. input parameters). In order to obtain these parameters, FEA needs to be carried out. Thus, in one-way coupling scheme, FEA is conducted to obtain stress-dependant porosity and permeability values. These are then input into the CFD model of the tight reservoir, and the multiphase flow analysis is carried out. Once multiphase flow analysis is conducted, Brooks and Corey method is implemented to obtain the saturation, capillary pressure and the relative permeability for both oil and water at the core-fracture interface (Brooks and Corey, 1966). The schematic diagram of one-way coupling is shown in Figure 3.9.

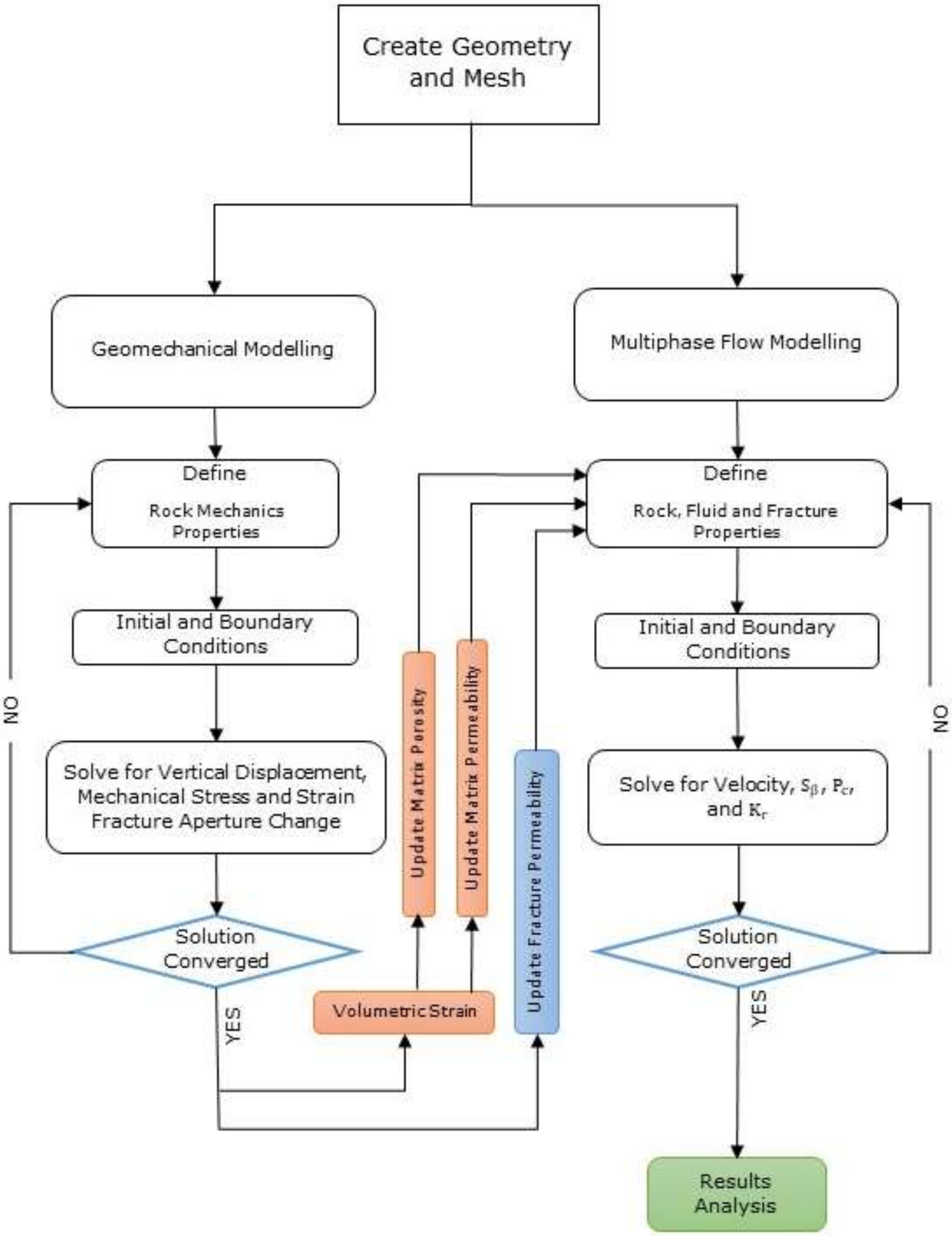

Figure 3.9. One-way coupling scheme

3.3.2 Fully Coupled Scheme

The computational expense required in one-way coupling is reasonably small and thus, is widely adopted for coupled FEA-CFD analyses. However, this leads to inaccuracies in the predicted results due to unidirectional flow of information (i.e. from FEA to CFD only). These inaccuracies in the predicted results are minimised through the use of fully coupled scheme in which both geomechanical and multiphase flow governing equations are solved simultaneously at each time step. Expectedly, the implementation of fully coupled scheme to solve a three-dimensional model is computationally very expensive compared to one-way coupling scheme and is often prohibitive. It is a well-known fact that three-dimensional modelling is more accurate than two-dimensional modelling while solving for turbulent flows. This is because the inherent flow characteristics in turbulent flows are three-dimensional in nature (e.g. vorticity). In all practical purposes, the multiphase flow in tight reservoirs is laminar in nature, and the model can be sufficiently resolved in two dimensions. Thus, in the present study, while implementing the fully coupled scheme, a two-dimensional model of the tight reservoir is considered. This significantly reduces the computational expense, while still providing accurate results. The two-dimensional model details are presented in chapter 6, while the flow chart representing the implementation of the fully coupled scheme is shown in Figure 3.10.

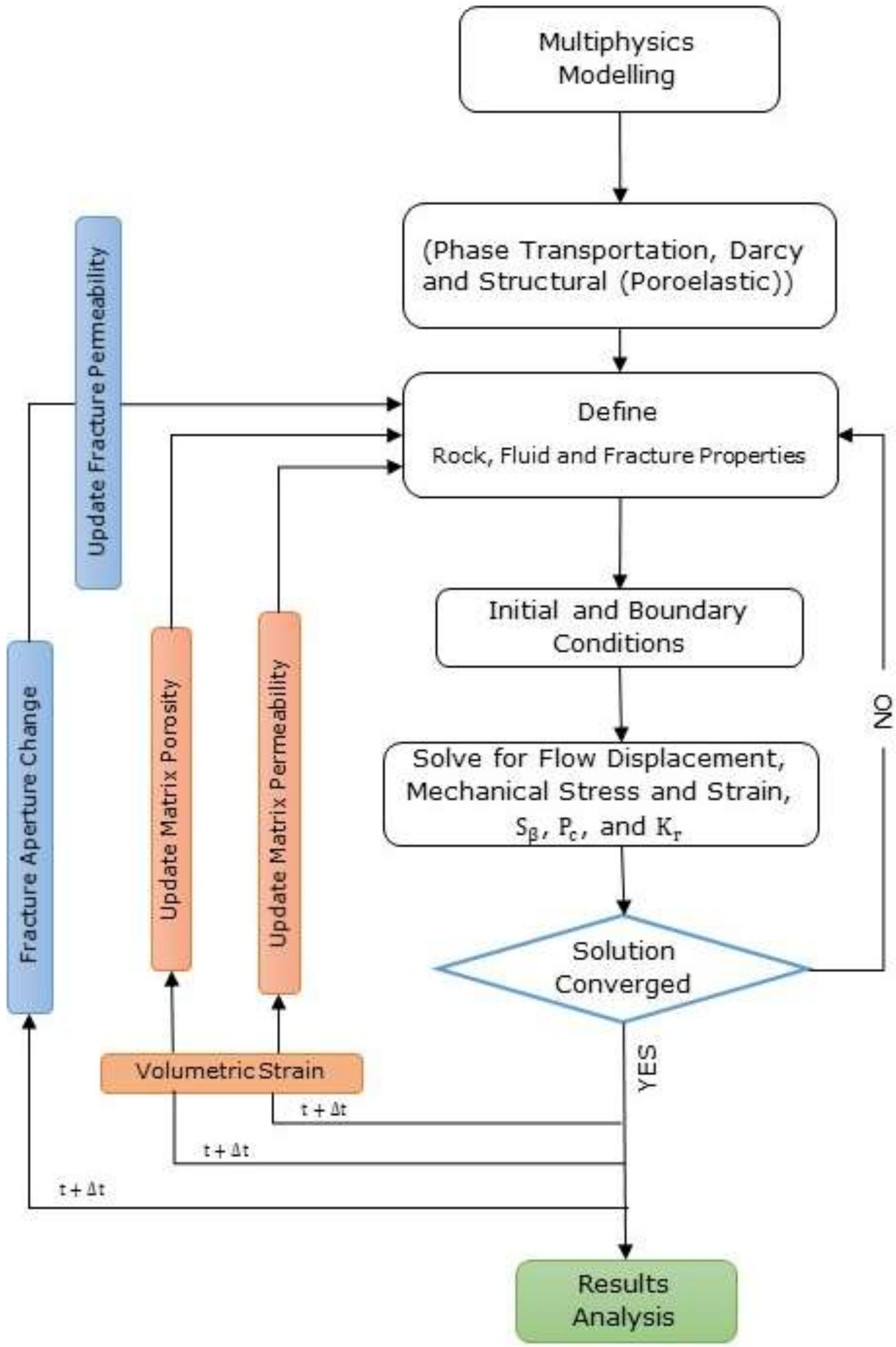

Figure 3.10. Fully coupled scheme

➢ *Modified Multiphase Flow and Geomechanical Governing Equations*

While solving mass and momentum conservation equations in a fully coupled manner, some modifications to these equations are required. In case of mass conservation equation, because the core region has been modelled as a porous medium, in fully coupled scheme, Darcy velocity is used instead of superficial velocity. Moreover, the viscous loss term is replaced by a source term. The modified mass conservation equation can be written as:

$$\frac{\partial}{\partial t}\left(\phi\, S_\beta\, \rho_\beta\right) + \nabla.\left(\rho_\beta\, \eta_\beta\right) + \Psi_\beta = 0 \tag{3.29}$$

where β represents phase, η is the Darcy velocity (m/s) and Ψ is the source term. The Darcy velocity can be expressed as:

$$\eta_\beta = -\frac{k_a\, Kr_\beta}{\mu_\beta}\left(\nabla P_\beta - \rho_\beta\, g\, \nabla D\right) \tag{3.30}$$

where k_a is the absolute permeability (mD), *P* is the pressure (Pa) and *D* is the diameter of the core region (m). Similarly, the source term (ζ) can be written as:

$$\Psi_\beta = \rho_\beta\, \alpha_B\left(\frac{\partial \varepsilon_{vol}}{\partial t}\right) \tag{3.31}$$

where α_B is Biot modulus and ε_{vol} is the volumetric strain. In the present study, the effects of gravity are ignored and thus, the pressure gradient acts as the only driving force for the transport of oil within the core and fracture regions. The storage model (*M*) and the Biot modulus (α_B) can be written as:

$$\frac{\partial}{\partial t}\left(\varphi\, S_\beta\, \rho_\beta\right) = \frac{1}{M}\frac{\partial\left(S_\beta\, \rho_\beta\, p_\beta\right)}{\partial t} \tag{3.32}$$

$$\frac{1}{M} = \frac{\varphi}{k_f} + (\alpha_B - \varphi)\frac{1-\varphi}{K_d} \tag{3.33}$$

where K_d is drained bulk modulus (MPa). Substituting equations 3.30 – 3.33 into equation 3.29, the governing mass conservation equation suitable for the fully coupled scheme can be expressed as:

$$\left(\frac{\varphi}{k_f} + (\alpha_B - \varphi)\frac{1-\varphi}{K_d}\right)\frac{\partial(S_\beta \rho_\beta p_\beta)}{\partial t} - \nabla.\left(-\frac{k_a Kr_\beta\, \rho_\beta}{\mu_\beta}\left(\nabla P_\beta - \rho_\beta g \nabla D\right)\right) = \rho_\beta \alpha_B \left(\frac{\partial \varepsilon_{vol}}{\partial t}\right) \tag{3.34}$$

The saturation (S), capillary pressure (Pc) and the relative permeability (Kr) at the fracture-matrix interface is then calculated based on Brooks and Corey method, presented in section 3.1.10.

Based on the modified multiphase flow governing equations presented here, the poroelastic relationship between stress, strain and pore pressure needs to be modified. This relationship can be written as:

$$\sigma = \sigma' - \alpha_B\, P_\beta\, I \tag{3.35}$$

where σ and σ' are total and effective stress (MPa) respectively, and I is the second-order identity tensor. The volumetric strain in equation (3.34) can then be expressed as:

$$\varepsilon_{vol} = \frac{1}{2}\left[(\nabla d)^2 + \nabla d\right]\, \varepsilon_{ij} = \frac{1}{2}\left(\frac{\partial d_i}{\partial x_j} + \frac{\partial d_j}{\partial x_i}\right) \tag{3.36}$$

where d is the displacement (cm). The force equilibrium (or solid deformation) can be represented by:

$$\nabla.\sigma + \left(\rho_\beta\, \varphi + \rho_\beta\right) g = 0 \tag{3.37}$$

The stress-dependant porosity and permeability in the core and fracture regions are calculated based on the equations provided in section 3.2.3.

Chapter 4
Characterisation of Multiphase Flow in Naturally Fractured Tight Reservoirs

This chapter presents the results on the multiphase flow characteristics of tight reservoirs. Mesh sensitivity analysis and validation of the numerical modelling have been carried out. Qualitative and quantitative analyses of models 1 and 2 are presented for the identified key multiphase flow parameters, i.e., oil saturation, capillary pressure and relative permeability at the fracture-matrix interface. A summary of the key findings has been presented at the end of the chapter.

4.1 Mesh Sensitivity Analysis

Mesh sensitivity analysis has been carried out for two mesh types, i.e., butterfly and O-ring, to verify the accuracy of the numerical solutions. The results of the mesh sensitivity analysis are shown in Figure 4.1. Numerically predicted recovered oil volume (V_o) for various injected water volume (V_w) values have been obtained for four different configurations of butterfly (B1, B2, B3, and B4) and O-ring (O1, O2, O3, and O4) meshes, along with the Berea Sandstone core flooding experimental data. Injected water volume has been defined here in terms of the water volume available in the flow domain; 18.5 % in the matrix region and 100 % in the fracture region. Injected water volume values for equivalent pore volume have been used in the present study. Thus, V_w = 0.1 represent that water volume equivalent to 10 % of the pore volume has been injected into the flow domain via the fracture inlet, while V_w = 0.7 represents 70 % equivalent water volume has been injected.

It can be seen that for all the mesh configurations, as V_w increases, V_o also increases. Comparative analysis between butterfly and O-ring meshes clearly shows that predicted V_o at individual V_w values from all eight mesh configurations is very close to each other, with the highest difference of less than 5 % amongst all of them (at V_w = 0.4). Thus, there is a negligible difference in numerically predicted butterfly and O-ring mesh results.

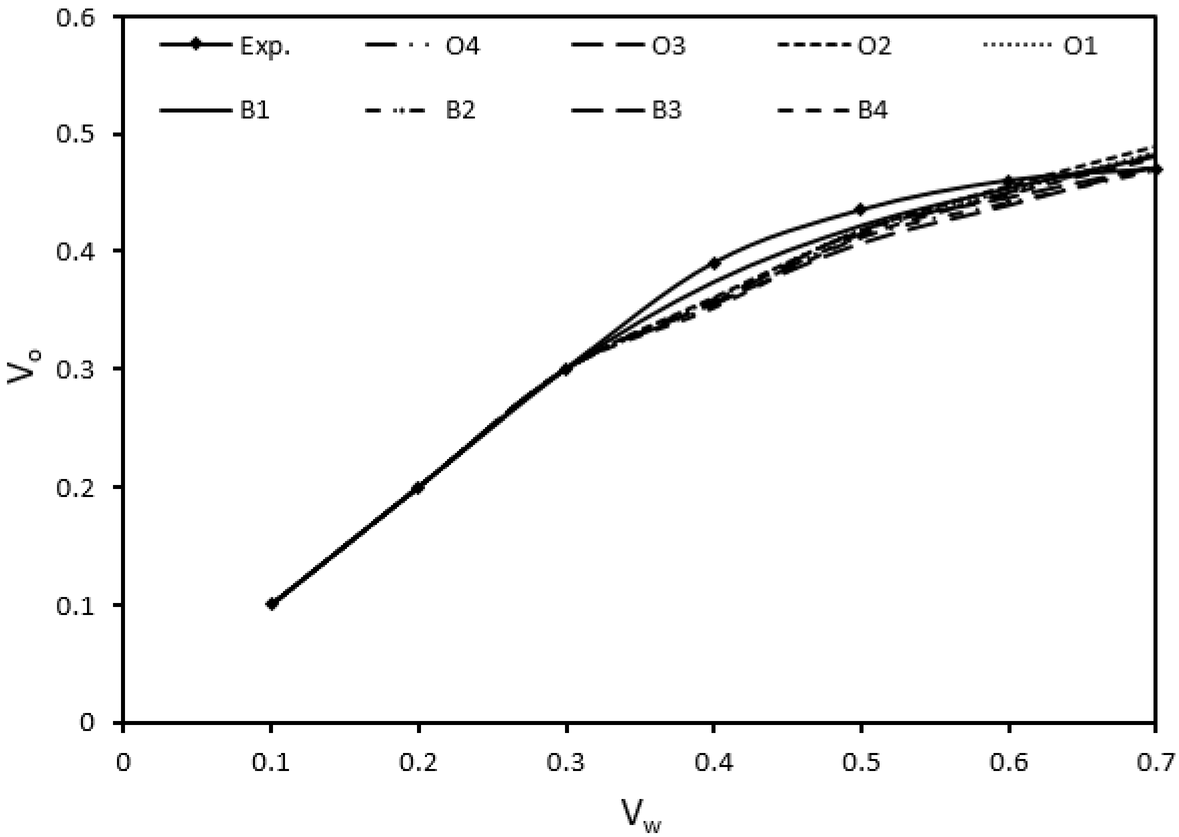

Figure 4.1. Mesh sensitivity results for four different configurations of butterfly (B1, B2, B3, and B4) and O-ring (O1, O2, O3, and O4) meshes

The validation of models 1 and 2 (discussed in Chapter 3) has been presented in section 4.4.4. During the mesh sensitivity testing, it has been observed that the maximum average difference between experimental and numerical results is 4.62 % (for O4 mesh), while the minimum average difference is 2.57 % for B4 mesh. For more clarity, comparison of V_o between experimental and B4 mesh is summarised in Table 4.1, which clearly indicates that the maximum difference between the two at any given V_w does not exceed 5 %. This clearly indicates the accuracy of the numerical modelling carried out and thus, B4 mesh has been chosen for conducting further analysis in this study.

Table 4.1. Comparative analysis between B4 mesh and the experimental data

Experimental Data		B4 Mesh	
Injected V_w	Experimental V_o	Numerical V_o	Difference w.r.t Experimental V_o %
0.1	0.1	0.1	0.0
0.2	0.2	0.2	0.0
0.3	0.3	0.3	0.0
0.4	0.390	0.374	4.10
0.5	0.435	0.424	2.53
0.6	0.460	0.453	1.52
0.7	0.470	0.480	-2.13
Average difference %			2.57

4.2 Multiphase Flow Characterisation of Model 1

As discussed in detail in Chapter 3, two different models have been considered in the present study for multiphase flow characterisation in tight reservoirs. The first numerical model is based on porous media modelling for the matrix region and duct flow modelling in the fracture region. The key multiphase flow characterisation parameters analysed here have been identified in Chapter 1. The focus of multiphase flow characterisation is on the fracture-matrix interface, as identified in Chapter 2. The key characterisation parameters at the fracture-matrix interface thus are:

1. Oil saturation (S_o)
2. Capillary pressure (Pc)
3. Relative permeability (Kr)

Quantitative analysis has been carried out on all the above parameters, while oil saturation has been analysed qualitatively as well. The quantitative analysis is based on the area-weighted average at the fracture-matrix interface, while the local/spatial qualitative analysis has been carried out on the plane that defines the boundary of matrix and fracture regions, identified as the fracture-matrix interface in Figure 4.2.

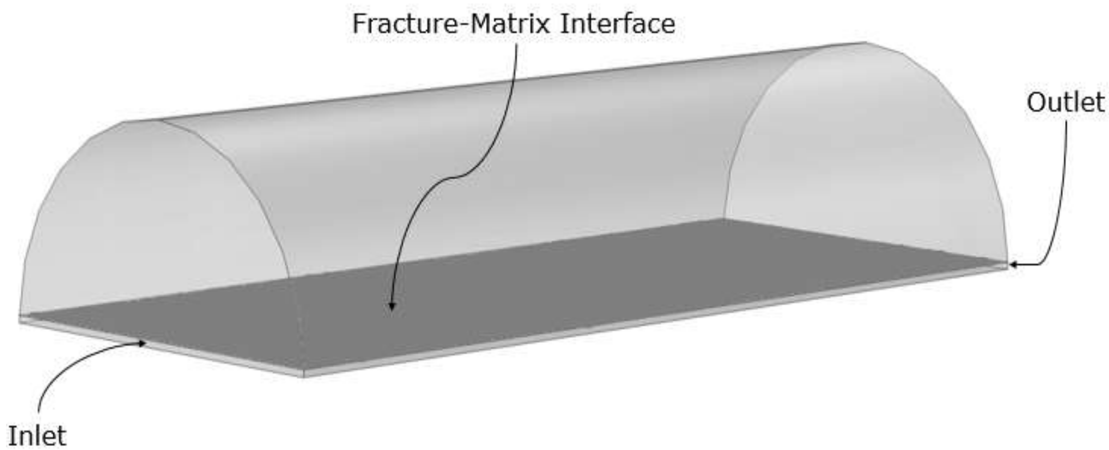

Figure 4.2. Plane for qualitative analysis

4.2.1 Oil Saturation at the Fracture-Matrix Interface

Figure 4.3 depicts the variations in oil saturation (S_o) at the fracture-matrix interface of the tight reservoir model at different V_w values considered in the present study. Note that the direction of flow is from left to right in the figure, i.e., the inlet is on the left, and the outlet is on the right. Moreover, for better comparative analysis, a common scale of variations has been used. It can be clearly seen that as more and more water is being injected into the fracture region, oil is being pushed out of the flow domain (through the outlet boundary). As the fracture region has been modelled as a duct in model 1, the oil volume fraction variations represent a classical duct flow behaviour, i.e., at the cross-section of the water-oil boundary, water pushes itself along the walls of the fracture-matrix interface while the oil remains in the middle. Further injection of water pushes the oil out from the middle while water penetration along the wall increases further.

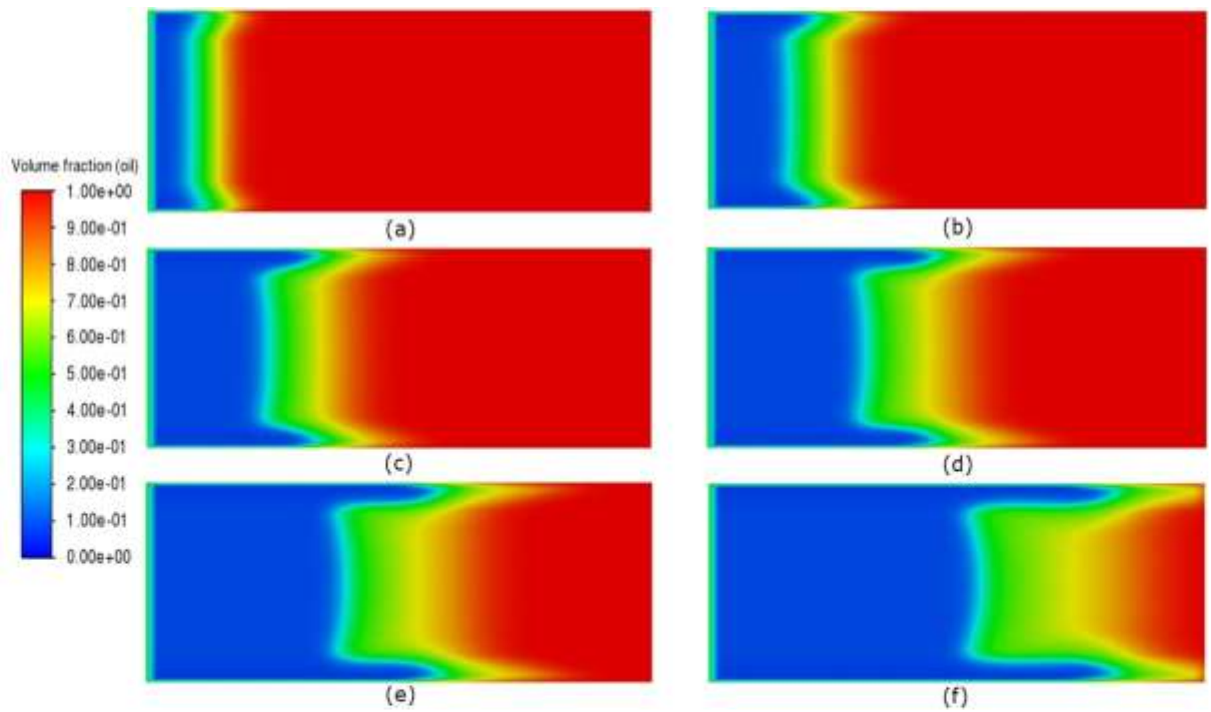

Figure 4.3. Variations in oil saturation at the fracture-matrix interface for injected water volume of (a) 10 % (b) 20 % (c) 30 % (d) 40 % (e) 50 % (f) 70 %

Table 4.2 summarizes the oil saturation at the fracture-matrix interface for different V_w values considered. It can be seen that when 10 % of pore volume equivalent water volume is being injected into the flow domain, the oil saturation decreases from 100 % to 94 %. Further increasing V_w to 20 % reduces oil saturation to 89 %, a decrease of 5.3 %. With a further increase in V_w to 30 %, the oil saturation reduces to 84 % (a further 5.6 % decrease). Increasing V_w to 40

%, 50 %, 60 % and 70 % reduces oil saturation by 5.9 %, 6.3 %, 6.8 %, and 7.0 %, respectively. Hence, when 70 % pore volume equivalent water volume is injected into the flow domain compared to the initial condition (S_o=1), the oil saturation decreases by 32 %. This reduction of oil saturation shows that a high amount of oil remains at the fracture-matrix interface and does not match real-world oil recovery in naturally fractured tight reservoirs.

Table 4.2. Oil saturation at different V_w

V_w	S_o
0.1	0.94
0.2	0.89
0.3	0.84
0.4	0.79
0.5	0.74
0.6	0.69
0.7	0.64

4.2.2 Capillary Pressure at the Fracture-Matrix Interface

Figure 4.4 depicts the variations in capillary pressure (kPa) for different V_w values at the fracture-matrix interface. As stated in Chapter 3, Brooks and Corey method has been used to compute the capillary pressure values at the fracture-matrix interface (eq. 3.15). It can be seen that as the injected V_w increases (from 10 % to 70 %), the capillary pressure decreases non-linearly. The capillary pressure is

21 kPa at injected V_w of 10 %. Increasing the injected V_w to 20 %, it can be seen that the capillary pressure decreases to 9 kPa, a decrease of 57 %. Further increasing the injected V_w to 30 %, the capillary pressure decreases to 5.5 kPa, a further 39 % decrease. This decrease in the capillary pressure is due to an increase in the wetting phase (water) volume fraction at the fracture-matrix interface. It can be further noticed that as V_w increases from 40 % to 70 %, the decrease in the capillary pressure is just 1.9 kPa. Thus, the slope of the *Pc* curve keeps on decreasing from V_w=0.1 to V_w=0.7 because of the increasing wetting (water) phase at the fracture-matrix interface.

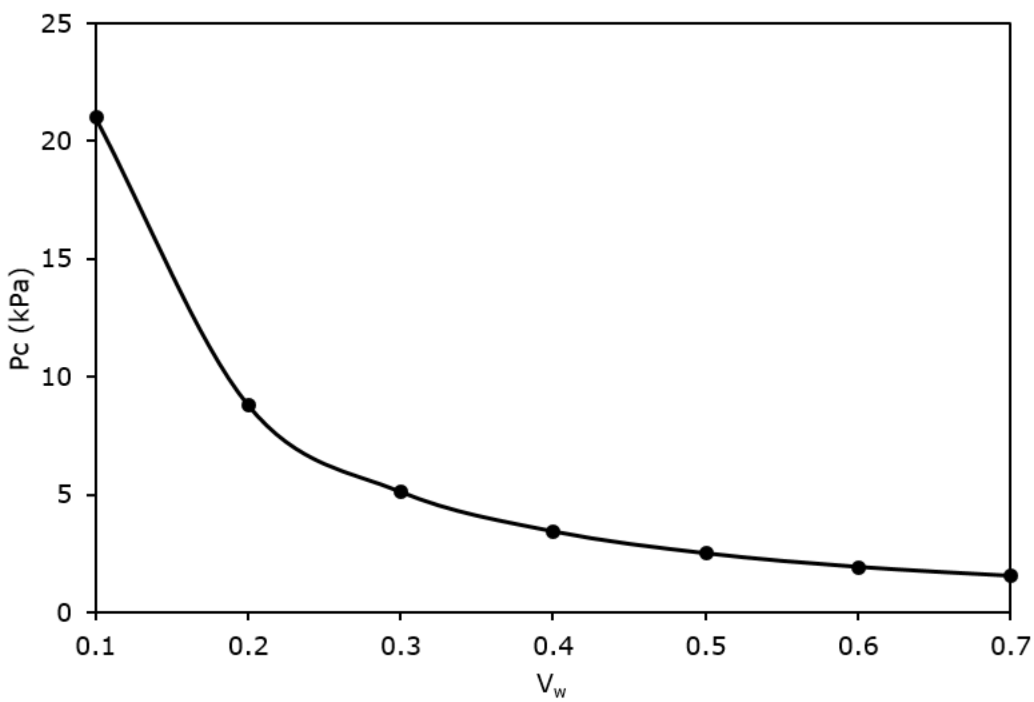

Figure 4.4. Capillary pressure variations w.r.t injected water volume

4.2.3 Relative Permeability at the Fracture-Matrix Interface

The relative permeabilities of water (Kr_w) and oil (Kr_o) at the fracture-matrix interface have been calculated using Brooks and Corey's method (Brooks and Corey, 1966), for different injected V_w values considered. The relative permeabilities are often compared against water saturation (S_w), rather than V_w, in the literature (Abdel Azim, 2022; S. Cheng et al., 2022; Jahanbakhsh et al., 2020). Water saturation values for corresponding V_w values are summarized in table 4.3. It can be seen that as V_w increases, S_w also increases.

Table 4.3. Water saturation at different V_w

V_w	S_w
0.1	0.063
0.2	0.113
0.3	0.162
0.4	0.212
0.5	0.261
0.6	0.311
0.7	0.359

Figure 4.5 depicts the variations in the relative permeabilities of oil and water for water saturation values presented in table 4.3, at the fracture-matrix interface. It can be seen that as water saturation increases, oil relative permeability decreases linearly. The oil relative permeability is 0.88 when S_w is 6 %. Increasing the water

saturation to 11 %, the oil relative permeability decreases to 0.79, a decrease of 10 %. Further increasing the S_w to 16 %, the oil relative permeability decreases to 0.7, a further 11 % decrease. The oil relative permeability reduces continuously as the injected water volume increases. The oil relative permeability reduces by 11.6 %, 12.4 %, 13.5 %, and 14.2 % due to increase in S_w values from 21 %, 26 %, 31 %, to 36 % at the fracture-matrix interface, respectively. Hence, when the water saturation is 36 % at the fracture-matrix interface compared to the initial condition (S_w=0.06), the oil relative permeability decreases by 54 %. The reason behind the decrease in oil relative permeability is the non-proportionality between V_w and S_w as evident from table 4.3.

As far as water relative permeability is concerned, it does increase but the values are very small (6.6×10^{-8} at S_w=0.06 and 2.2×10^{-3} at S_w=0.36) because water volume injection does not penetrate the fracture-matrix interface toward the rock matrix region. Increasing the water saturation to 11 %, oil relative permeability increases to 2.18×10^{-6}. Further increasing the water saturation to 16 %, the water relative permeability further increases to 1.92×10^{-5}.

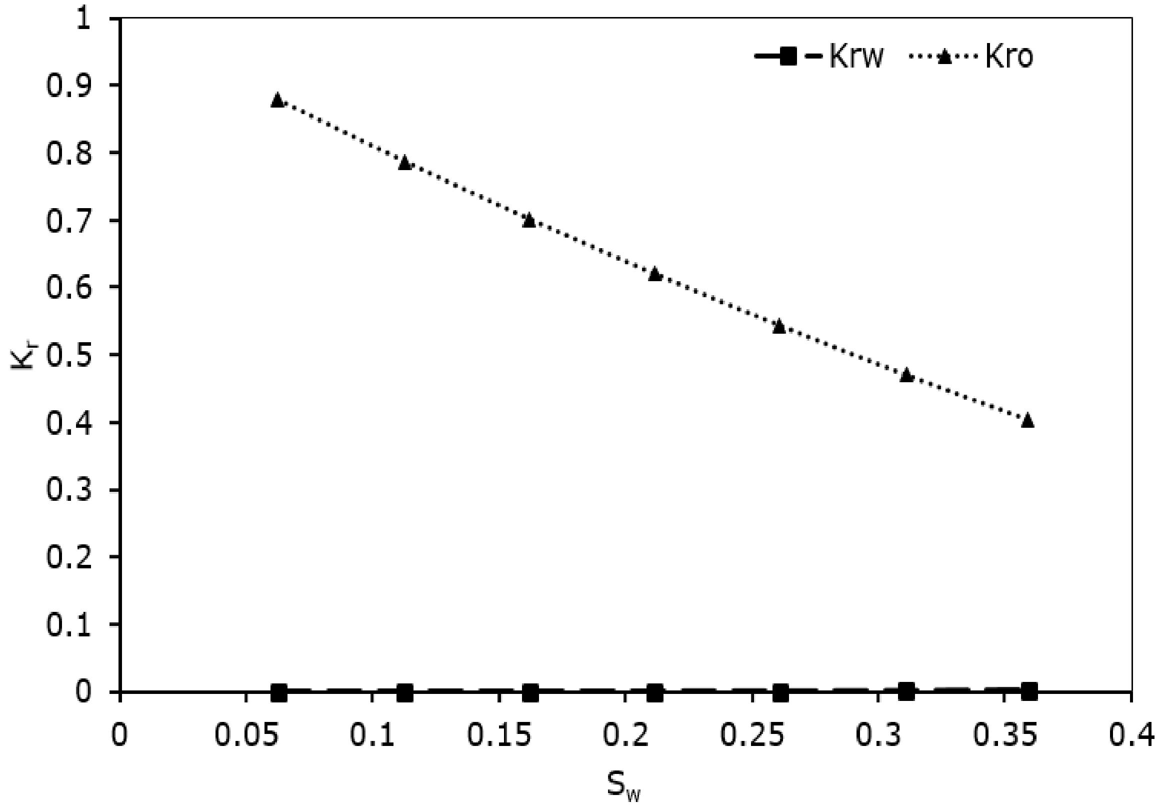

Figure 4.5. Relative permeability variations w.r.t water saturation

4.2.4 Recovered Oil Volume

Figure 4.6 presents the comparison between the numerical results and Berea Sandstone core flooding experimental data (Kazemi and Merrill, 1979). The recovered oil volume (V_o) is being calculated at different injected water volumes (V_w). It can be seen that numerically predicted oil volume increases linearly with injected water volume till V_w=0.2. Increasing V_w further increases V_o almost linearly, but the slope of the curve is significantly smaller than for V_w=0-0.2. In comparison, the Berea Sandstone core flooding experimental data, as shown in the Appendix A (Figure A1), indicates that recovered oil volume increases linearly with injected water volume till V_w=0.4. With further increase in V_w, V_o increases almost linearly, but the slope of the curve is considerably smaller than for V_w=0-0.4. The recovered oil volume from the Berea Sandstone core flooding experimental data and numerical predictions matches well for V_w=0-0.2. Increasing the injected V_w to 0.3, the numerically predicted V_o is 0.24, while the experimental V_o is 0.3, a difference of 20 %. From V_w=0.4-0.7, the difference between the numerical and experimental V_o remains almost constant, i.e., an average difference of 33 % between the two. The reason behind this significant difference between the experimental and numerical results is due to the way the fracture region has been modelled i.e. as a duct, which offers less resistance to the flow than measured in real-world.

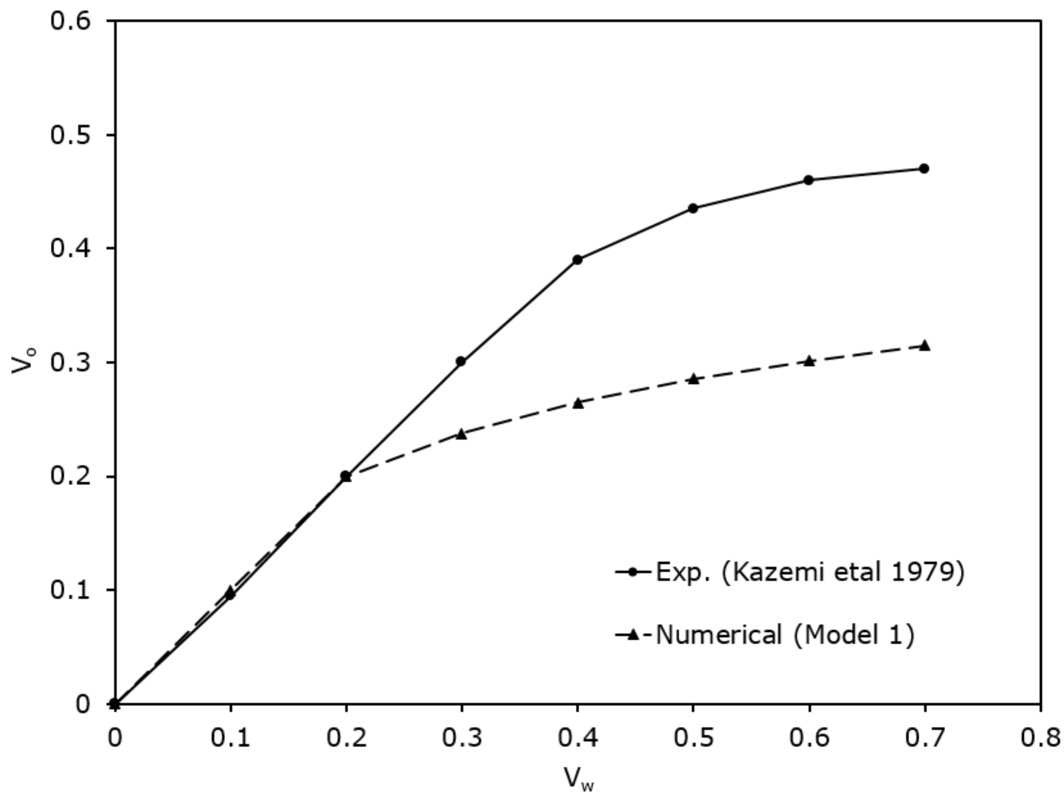

Figure 4.6. Comparison of Model 1 numerical results and Berea Sandstone core flooding experimental data

4.3 Multiphase Flow Characterisation of Model 2

As discussed in detail in Chapter 3, the second numerical model is based on porous media modelling for the matrix and the fracture regions. The analysis of the key multiphase flow characterisation parameters is presented below.

4.3.1 Oil Saturation at the Fracture-Matrix Interface

Figure 4.7 depicts the variations in oil saturation (S_o) at the fracture-matrix interface of the tight reservoir model for different injected V_w values. It can be seen that the oil saturation increases as the injected V_w increases. Till V_w of 20 %, the oil is being pushed out of the fracture-matrix interface by water, which resembles piston-like displacement. However, as V_w increases further, the boundary between the oil and water starts to get affected, i.e., water starts penetrating into oil, leaving residual streaks of oil behind. This is commonly referred to as viscous fingering in the literature (Berge et al., 2019; Fanchi, 2018; Gudala and Govindarajan, 2021).

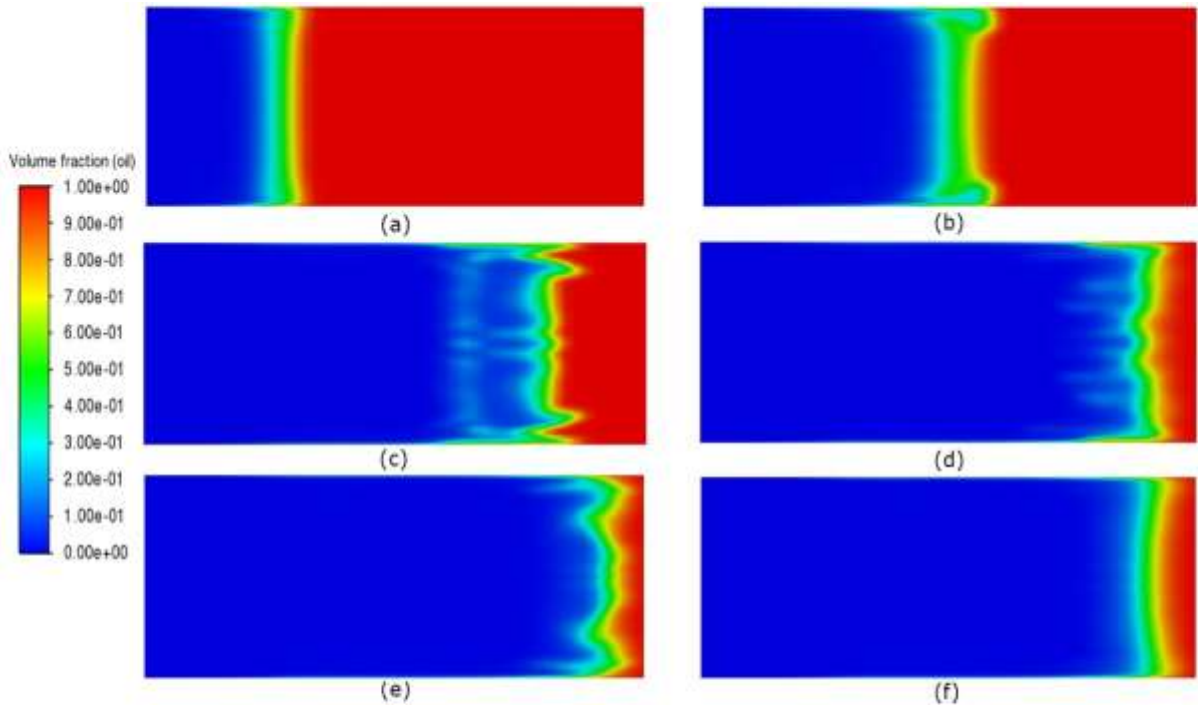

Figure 4.7. Variations in oil saturation at the fracture-matrix interface for injected water volume of (a) 10 % (b) 20 % (c) 30 % (d) 40 % MPa (e) 50 % (f) 70 %

Table 4.4 summarizes the oil saturation at the fracture-matrix interface for the various V_w values. When 10 % of the pore volume equivalent water volume (V_w) is added into the flow domain, the oil saturation drops from 100 % to 76 %. Increasing V_w to 20 % reduces oil saturation to 53 %, a 45 % reduction. With a further increase in V_w to 30 %, the oil saturation drops to 18 % (a 44.8 % reduction). By increasing V_w to 40 %, 50 %, 60 %, and 70 %, oil saturation is reduced by 37.9 %, 14.2 %, 6.0 %, and 5.2 %, respectively. As a result, injecting 70 % pore volume equivalent water volume into the flow domain reduces oil saturation by 81.5 %.

Table 4.4. Oil saturation at different V_w

V_w	S_o
0.1	0.76
0.2	0.53
0.3	0.30
0.4	0.18
0.5	0.16
0.6	0.15
0.7	0.14

4.3.2 Capillary Pressure at the Fracture-Matrix Interface

Figure 4.8 shows the variations in capillary pressure (kPa) for injected water volume (V_w) at the fracture-matrix interface. As the injected V_w increases (from 10 % to 70 %), the capillary pressure reduces nonlinearly. The capillary pressure is 2.8 kPa at injected V_w of 10 %. Increasing the injected V_w to 20 %, the capillary pressure decreases to 1.07 kPa, a decrease of 39 %. Further increasing the injected V_w to 30 %, the capillary pressure decreases to 0.58 kPa, a further 29 % decrease. This decrease in the capillary pressure is due to an increase in the wetting phase (water) volume fraction at the fracture-matrix interface. From V_w=0.4-0.7, the capillary pressure remains almost constant (0.44 kPa), due to the fracture-matrix region fully saturated with the wetting phase (water), resulting in minimum residual oil being left behind.

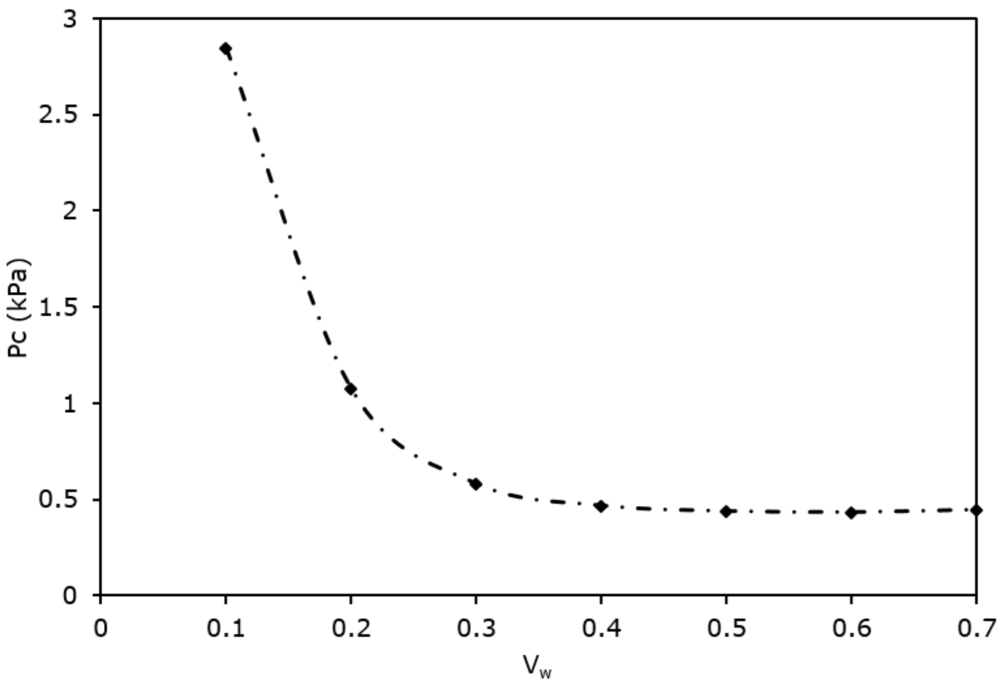

Figure 4.8. Capillary pressure variations w.r.t injected water volume

4.3.3 Relative Permeability at the Fracture-Matrix Interface

The relative permeabilities of water (Kr_w) and oil (Kr_o) at the fracture-matrix interface have been calculated using Brooks and Corey's method, for different injected V_w values considered. Water saturation values for corresponding V_w values are summarized in table 4.5. It can be seen that as V_w increases, S_w also increases.

Table 4.5. Water saturation at different V_w

V_w	S_w
0.1	0.241
0.2	0.466
0.3	0.705
0.4	0.817
0.5	0.852
0.6	0.860
0.7	0.843

Figure 4.9 depicts the variations in the relative permeabilities of oil and water for water saturation values presented in table 4.5, at the fracture-matrix interface. It can be clearly seen that the water relative permeability increases as the water saturation increases. In contrast, the oil relative permeability decreases as water saturation increases.

The oil relative permeability is 0.57 when S_w is 24 %. The oil relative permeability decreases to 0.27 due to increase in S_w to 46 %, a decrease of 52 %. Increasing the water saturation value to 70 %, the oil relative permeability reduces to 0.07, a further reduction of 76 %. The oil relative permeability continuously decreases due to increasing S_w values at the fracture-matrix interface. The oil relative permeability reduction is 72 %, 45 %, 37 %, and 14 % due to the increased S_w from 82 %, 84 %, 85 %, and to 86 %, respectively, due to non-proportionality in the increase of S_w as V_w increases.

The water relative permeability increases as S_w increases at the fracture-matrix interface. The water relative permeability is 2.1 x 10^{-4} when S_w is 24 %. The water relative permeability increases to 1.04 x 10^{-2} at S_w of 46 %, an increase of 98 %. With a further increase in S_w to 70 %, the water relative permeability increases to 1.24 x 10^{-1}, a further increase of 92 %. At higher S_w (82 %, 84 %, 85 % and 86 %), water relative permeability increases (by 58 %, 22 %, 13 %, and 5 % respectively) because water volume injection does not penetrate the fracture-matrix interface toward the rock matrix region. Hussain et al. (2021) have reported similar trends in the relative permeability while comparing fractured and unfractured tight reservoirs.

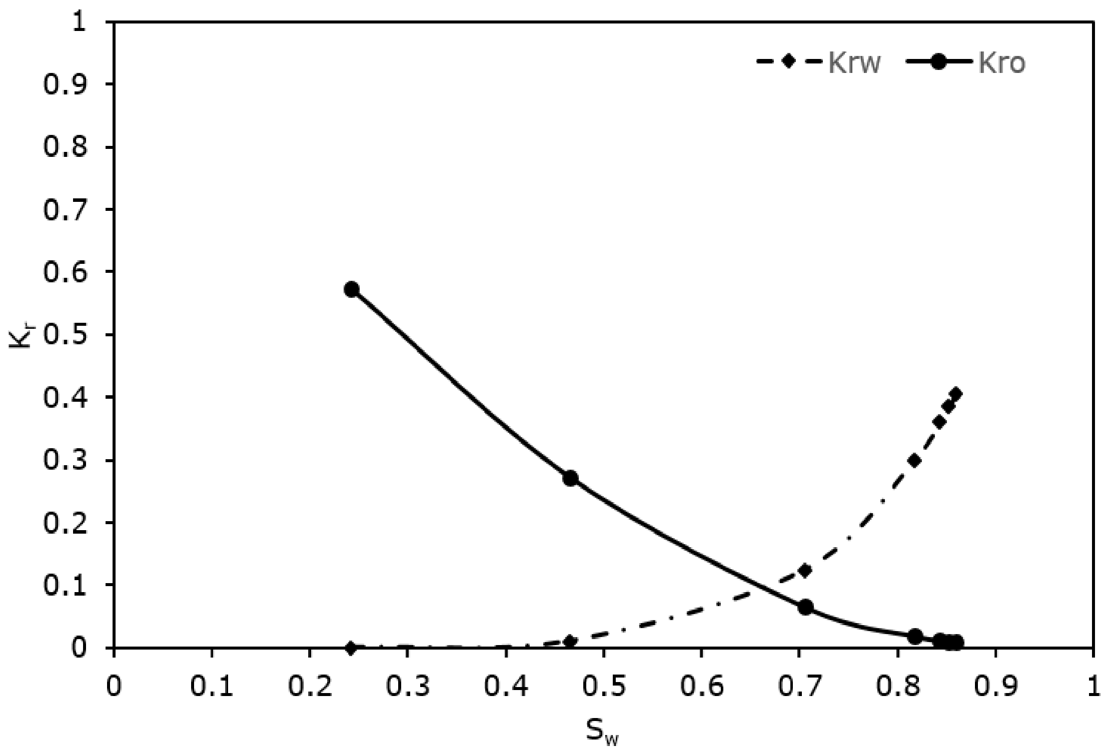

Figure 4.9. Relative permeability variations w.r.t water saturation

4.3.4 Recovered Oil Volume

The comparison of numerical results and Berea Sandstone core flooding experimental data is shown in Figure 4.10 (Kazemi and Merrill, 1979). At various injected water volume (V_w) values, the recovered oil volume (V_o) is computed. It can be seen that numerically predicted oil volume increases linearly with injected water volume till V_w=0.3. Increasing V_w further increases V_o almost linearly, but the slope of the curve is significantly smaller than for V_w=0-0.3. In comparison, the Berea Sandstone core flooding data indicates that the recovered oil volume increases linearly with injected water volume till V_w=0.4. With a further increase in V_w, V_o increases almost linearly, but the curve's slope is considerably smaller than for V_w=0-0.4. The recovered oil volume from the Berea sandstone experimental data and numerical predictions matches well for V_w=0-0.3. The numerical V_o is under-predicted on average by 2.9 % compared to the experimental V_o for V_w=0.4-0.6. The numerical V_o is over-predicted compared to the experimental V_o by 2.2 % at V_w=0.7. Thus, modelling of the fracture region as a porous medium results in highly accurate prediction of oil recovery from naturally fractured tight reservoirs as this modelling approach represents the real-world scenario more closely.

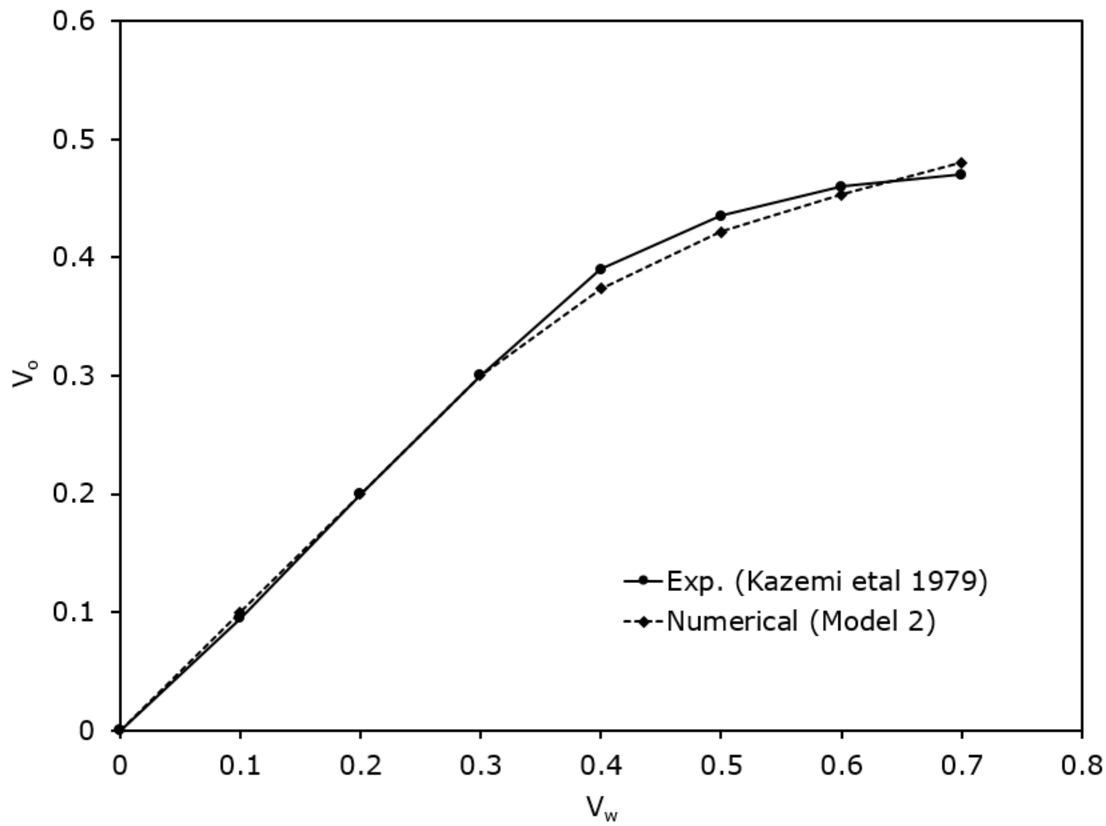

Figure 4.10. Comparison of the numerical results and the Berea Sandstone core flooding experimental data

4.4 Comparison between Model 1 and Model 2

A detailed comparative analysis between Model 1 and Model 2 is presented here.

4.4.1 Oil Saturation at the Fracture-Matrix Interface

Table 4.6 presents the comparison of oil saturation values between Model 1 (S_{o-1}) and Model 2 (S_{o-2}) at the fracture-matrix interface for the various injected V_w values considered. At V_w of 10 %, the oil saturation predicted by Model 2 is 19 % less than Model 1. The numerically predicted oil saturation from Model 2 is 40 % less than Model 1 at V_w of 20 %. The numerically predicted oil saturation from

Model 2 is 64 % less than Model 1 at V_w of 30 %. Thus, with increase in V_w, the difference in the oil saturation between the two models keeps on increasing, with Model 2 depicting lower oil saturation. The difference in oil saturation values between Model 1 and Model 2 remains almost constant (78 %) for V_w=0.4-0.7. Overall, the oil recovery predicted by Model 2 is significantly higher than predicted by Model 1. Note that higher oil saturation inside the tight reservoir means lower oil recovery at the outlet of the reservoir.

Table 4.6. Comparison in oil saturation between Model 1 and Model 2

V_w	S_{o-1}	S_{o-2}	Difference w.r.t. S_{o-1}, %
0.1	0.94	0.76	19
0.2	0.89	0.53	40
0.3	0.84	0.30	64
0.4	0.79	0.18	77
0.5	0.74	0.16	78
0.6	0.69	0.15	78
0.7	0.64	0.14	78

4.4.2 Capillary Pressure at the Fracture-Matrix Interface

Figure 4.11 presents the comparison of the capillary pressure (*Pc*) values between Model 1 and Model 2 as V_w increases from 10 % to 70 % at the fracture-matrix interface. For both models, the capillary pressure reduces non-linearly as V_w increases. The numerically predicted capillary pressure from Model 2 is 86 % less than Model 1 at a V_w of 10 %. The difference in capillary pressure values between Model 1 and Model 2 remains almost constant, i.e., an average difference of 88 % for V_w=0.2-0.4. The numerically predicted capillary pressure from Model 2 is 83 %, 78 %, and 72 % less than Model 1 at V_w of 50 %, 60 %, and 70 %. Thus, the capillary pressure reduction considerably affects the oil saturation minimizations at the fracture-matrix interface for Model 2. The significant reduction of capillary pressure for Model 2 is the increased water saturation at the fracture-matrix interface.

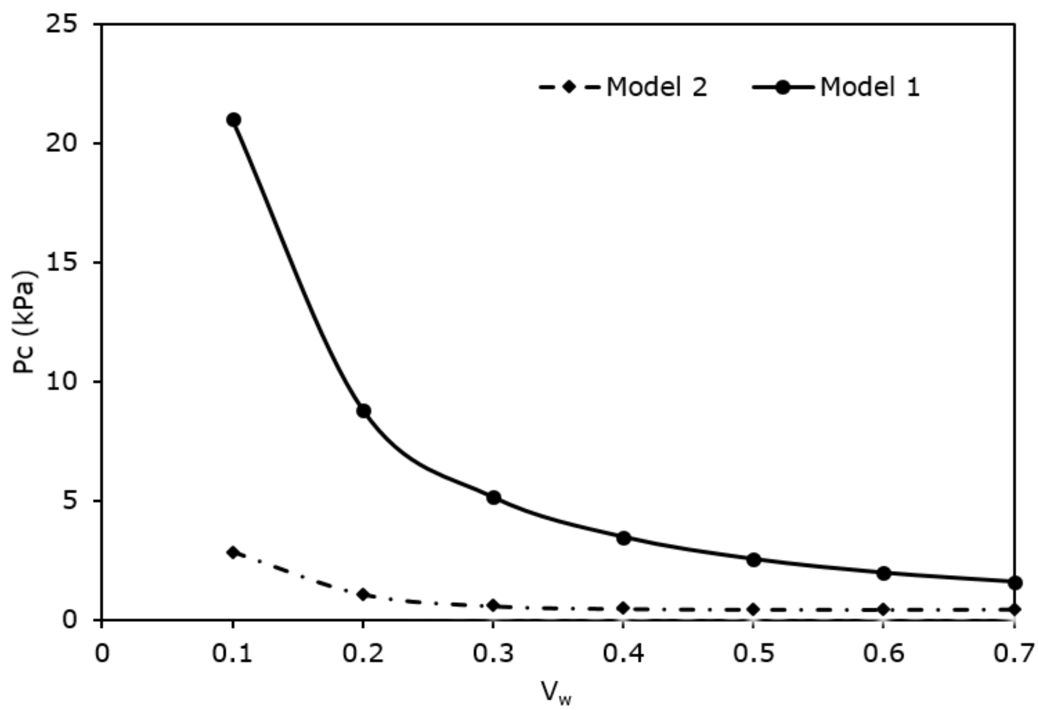

Figure 4.11. Comparison of the capillary pressure for Models 1 and 2

4.4.3 Relative Permeability at the Fracture-Matrix Interface

Figure 4.12 presents the comparison of the relative permeability w.r.t water saturation (S_w) at the fracture-matrix interface for Models 1 and 2. The relative permeability changes linearly w.r.t water saturation for Model 1, while the relative permeability changes non-linearly for Model 2 at the fracture-matrix interface, as discussed in sections 4.2.3 and 4.3.3. It can be seen that the oil relative permeability is 0.58 for both the Models at S_w=0.26. This does not mean that at similar conditions, the oil relative permeability predicted by both the models is the same. As shown in table 4.3 for Model 1, S_w=0.26 when V_w=0.5, while in table 4.5 for Model 2, S_w=0.26 when V_w=0.1. Thus, the operating conditions are completely different for the same S_w values in both the models. Similarly, at S_w=0.36, the oil relative permeability is 0.4 for both the models however, S_w of 0.36 corresponds to 70 % V_w injection for Model 1 while almost 20 % for Model 2.

In case of water relative permeability, both the models depict Kr_o of 2.1 x10^{-4} at S_w=0.24, and Kr_o of 2.1 x10^{-3} at S_w=0.36. Thus, the relative permeability values show that a considerable amount of oil has been retained at the fracture-matrix interface of Model 1. In contrast, the minimum residual oil is trapped at the fracture-matrix interface in Model 2 due to considering the fracture region as a porous medium and adding the tendency of the fluid flow.

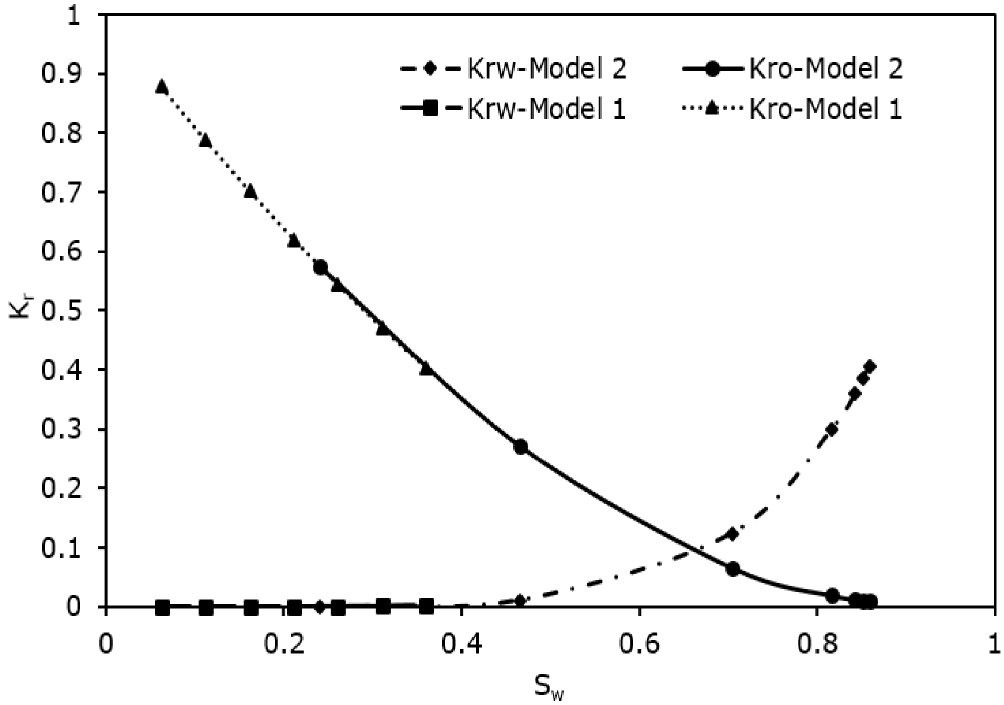

Figure 4.12. Relative permeability comparison w.r.t water saturation for Models 1 and 2

4.4.4 Validation of the Numerical Models

Figure 4.13 depicts the comparison of numerically recovered oil volume (V_o) from Models 1 and 2 at different V_w values. In order to validate the numerical results, Berea Sandstone core flooding experimental data (Kazemi and Merrill, 1979) has also been plotted in the figure. It can be clearly seen that the recovered oil volume from Model 2 matches reasonably accurately with the experimental data, while Model 1 severely under-predicts oil recovery, especially after V_w=0.2. At V_w=0.3, the numerically predicted V_o from Model 1 is 21% less compared to the experimental V_o. For V_w=0.4-0.7, the numerically predicted V_o from Model 1 is, on average, 34 % less compared to the experimental results. Thus, the results obtained clearly indicate that Model 2 is far superior to Model 1 in accurately predicting oil recovery from tight reservoirs and hence, Model 2 approach (i.e. fracture region as a porous medium and inclusion of viscous loss source term in the momentum equations) has been used for geomechanical characterisation of tight reservoirs in the next chapter.

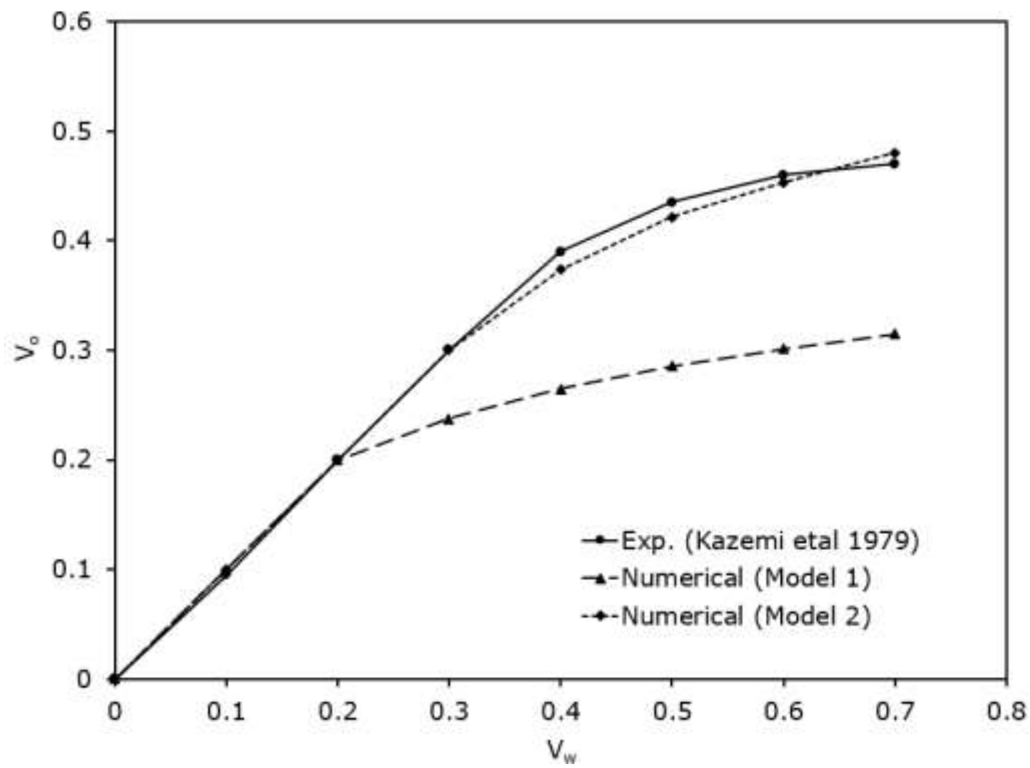

Figure 4.13. Comparison of the recovered oil volume of Model 1 and Model 2 with the Berea Sandstone core flooding experimental data

4.5 Summary of key findings

A detailed analysis of the multiphase flow characteristics at the fracture-matrix interface of tight reservoirs has been carried out in this chapter. The key results obtained can be summarized as follows:

- As water is injected into the flow domain, oil saturation decreases at the fracture-matrix interface. When the fracture region is modelled as a porous medium rather than a duct, numerically predicted oil saturation is 19 (min) – 78 (max) % less (see figures 4.3 and 4.7, and tables 4.1 and 4.3).

- Increasing the injected water volume, capillary pressure decreases significantly at the fracture-matrix interface. When the fracture region is modelled as a porous medium rather than a duct, numerically predicted capillary pressure is 72 (min) – 86 (max) % less (see figures 4.4, 4.8, and 4.11).

- Increasing the injected water volume, relative permeability slightly changes for numerical Model 1, while the relative permeability significantly changes for numerical Model 2 (see figures 4.5, 4.9, and 4.12).

  - Modelling the fracture region as a porous media (Model 2) results in accurate multiphase flow characteristics compared to when it is modelled as a duct (Model 1) (see figures 4.6, 4.10, and 4.13).

Chapter 5
Coupled Geomechanical and Multiphase Flow Characterisation in Naturally Fractured Tight Reservoirs

This chapter presents the results of one-way coupling between the geomechanical parameters and multiphase flow in tight reservoirs. Mesh sensitivity analysis and validation of the numerical model have been carried out. A detailed qualitative and quantitative analysis of the geomechanical effects on multiphase flow parameters at the fracture-matrix interface is presented. The key findings are summarized at the end of the chapter.

5.1 Numerical Methodology

One-way FEA-CFD coupling between the geomechanical parameters and transient multiphase fluid flow has been carried out using ANSYS® Static Structural (for FEA modelling) and ANSYS® Fluent (for transient multiphase flow modelling), in naturally fractured tight reservoirs. Geomechanical numerical modelling of the matrix and fracture regions is carried out by adding a poroelastic mathematical formulation and assuming constant pore pressure, as discussed in chapter 3 (section 3.2.3). The petrophysical properties of the tight reservoir, such as porosity, matrix permeability, fracture permeability and change in fracture aperture are computed under different stress loading conditions. These parameters are then input into the multiphase flow model with the aim to analyse stress-dependent key hydraulic parameters of the tight reservoir.

It is noteworthy that the numerical modelling carried out in this chapter, both FEA and CFD, employs different geometrical dimensions compared to the numerical models in chapter 4. The reason for this is the unavailability of appropriate experimental data. In chapter 4, the numerical models have been validated against Berea Sandstone core flooding experimental data (Kazemi and Merrill, 1979), which considers multiphase flow in tight reservoirs, but doesn't take geomechanical parameters into consideration. In this chapter, for geomechanical behaviour estimation, Clashach Core flooding experimental data (Stalker et al., 2009) has been used for numerical model validation purposes (in section 5.3). This experimental data takes into account the geomechanical parameters of tight reservoirs however, instead of multiphase flow, it considers single-phase flow.

Thus, the boundary conditions used for model validation is based on Clashach Core flooding experimental data however, for geomechanics based multiphase flow modelling carried out uses the same boundary conditions as in chapter 3. Moreover, the modelling approach used in chapter 3 is repeated here i.e. both matrix and fracture are modelled as porous media, and the fluid properties also remain the same.

The three-dimensional numerical model of the tight reservoir is shown in Figure 5.1. It can be seen that the diameter (*D*) and length (*L*) of the model are 3.79 cm and 7.54 cm respectively, while the aperture of the fracture (*h*) is 130 μm. Another important difference to highlight here is that water enters the flow domain from both the fracture inlet and the matrix inlets, as shown in the figure, where the inlet flow velocity remains the same as previously i.e. 0.000039 m/s. The range of stress loading (σ) applied on the rock matrix is based on Clashach Core flooding experiment i.e. 6.9 MPa to 17.2 MPa, as shown in the Appendix B (Table B2). In terms of time duration, each numerical simulation took five days to provide a reasonably converged solution.

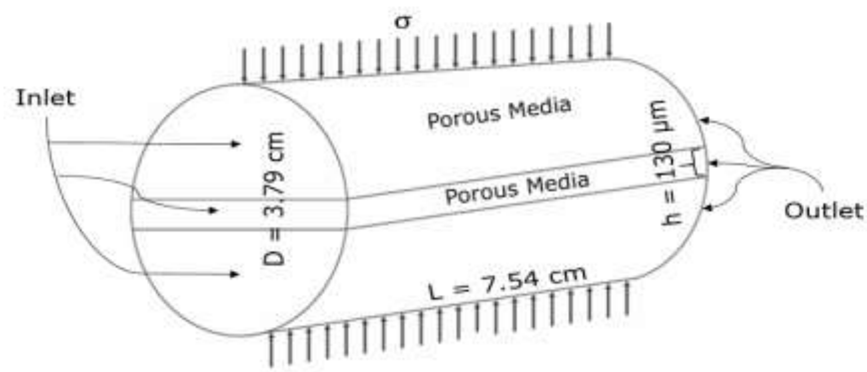

Figure 5.1. 3D model of fractured tight reservoir

5.2 Mesh Sensitivity Analysis

Figure 5.2 depicts the mesh sensitivity results for the finite element analysis (CFD mesh sensitivity is already presented in chapter 4). The unstructured meshes are chosen with element sizes of 0.005 m, 0.0035 m, 0.0028 m, 0.002 m, and 0.0018 m, while the corresponding number of mesh elements are 1.27×10^4 (M1), 2.7×10^4 (M2), 3.7×10^4 (M3), 7.4×10^4 (M4), and 9.5×10^4 (M5), respectively. The core matrix edge is refined with a growth ratio of 2 to account for the fracture-matrix interface. It can be seen that with an increase in the number of mesh elements from M1 to M3, the stress variations ($\Delta\sigma$) and the total displacement (d) increases. Further increasing the number of mesh elements from M3 to M5, there is negligible change in both these parameters. Thus, mesh M3, with element sizing of 0.0028 m and total number of elements equal to 3.67×10^4 is adequate to accurately predict the geomechanical behaviour of fractured tight reservoirs and thus, has been chosen to conduct further FEA based analyses in this chapter.

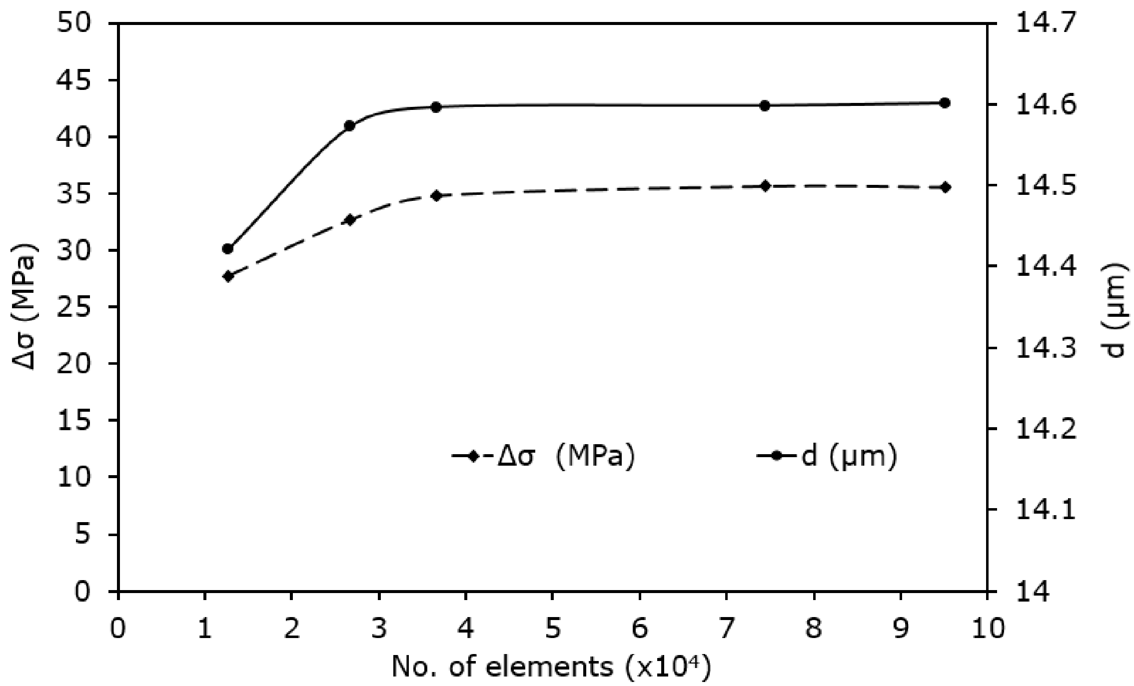

Figure 5.2. Mesh sensitivity analysis results

5.3 Numerical Model Validation

The FEA-CFD one-way coupling based numerical model has been validated against the Clashach Core flooding experimental data (Stalker et al., 2009) for single-phase flow of oil in the fractured tight reservoir. The experimental data on the cumulative outflow of oil (*Qc*) is based on the differential pressure (*ΔP*) applied across the sample reservoir, while the core sample is subjected to 21.4 MPa of stress loading. Boundary conditions used in the numerical model for validation purposes are in accordance with the experimental data, as shown in the Appendix B (Table B1). The results of numerical model validation are shown in Figure 5.3. It can be seen that both the numerically predicted *Qc* and the experimental *Qc* increase with increasing differential pressure, and the two are in agreement with each other, with an average deviation of < 9 %. Thus, the numerical model used here is reasonably accurate in representing the geomechanics based multiphase flow through tight reservoirs.

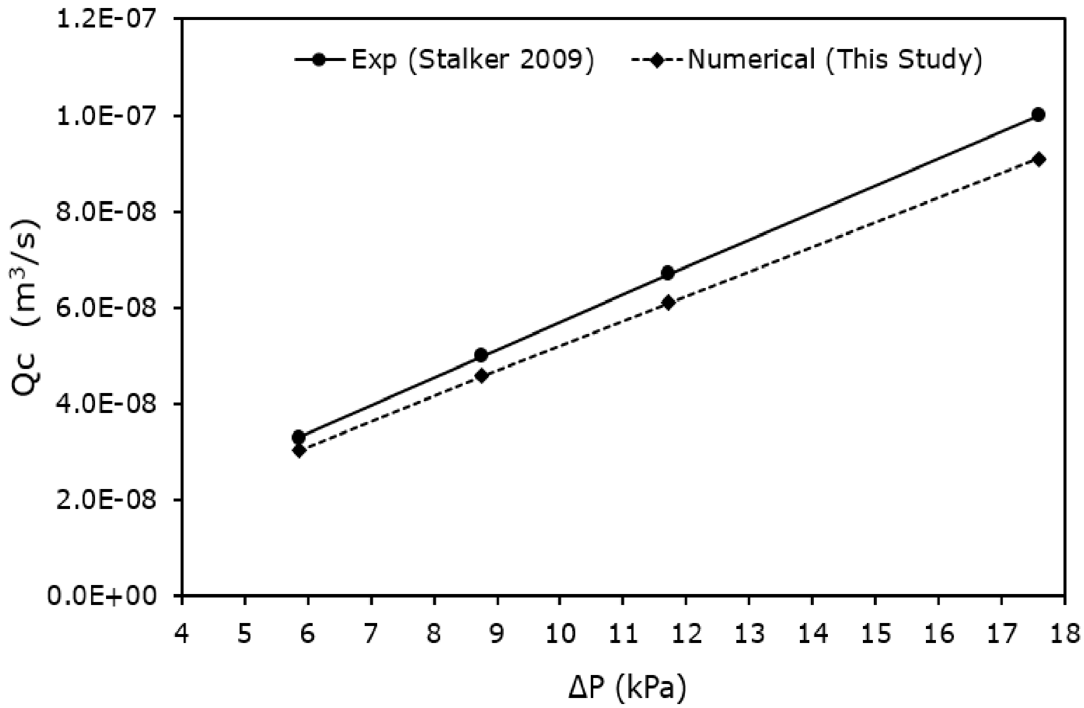

Figure 5.3. Numerical and experimental cumulative outflow w.r.t. differential pressure

5.4 Stress-dependent Matrix Porosity

Figure 5.4 depicts the stress-dependent porosity (φ) variations for stress loading (σ), where the pore fluid compression (or expansion) is neglected. The porosity decreases almost linearly as the stress loading increases. The same trend has been observed in the literature as well (Zhao and Liu, 2012) (Figure 2.2). The porosity is 15.38 % at a stress loading of 6.9 MPa. Increasing the stress loading to 9 MPa, the porosity decreases by 0.025 % to 15.378 %. Further increasing the stress loading to 11 MPa, the porosity decreases to 15.368 %. The porosity decreases by

0.019 %, 0.017 %, and 0.015 % when stress loading increases to 13.1 MPa, 15.2 MPa, and 17.2 MPa, respectively. This slight decrease in the matrix porosity is due to the rigidity of the core region. The core sample deformation changes the pore volume (porosity) and the pore network.

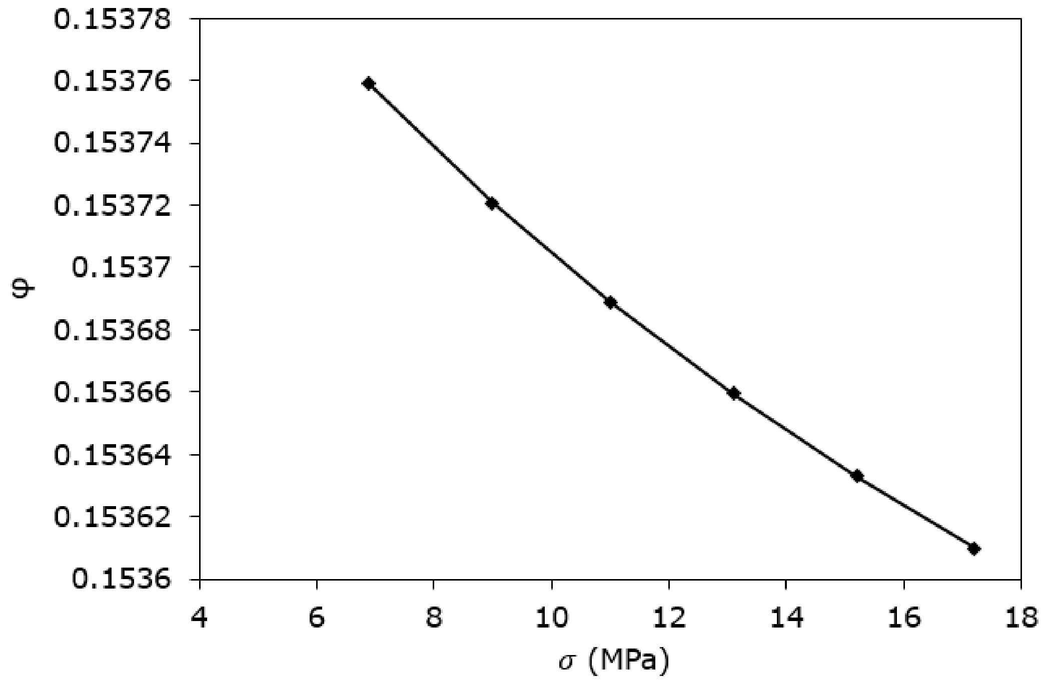

Figure 5.4. Porosity variations w.r.t. stress loading

5.5 Stress-dependent Matrix Permeability

Figure 5.5 shows the variations in rock matrix permeability (k_{mat}) for stress loading (σ). The permeability of the rock matrix was measured using equation (2.2). The matrix permeability reduces almost linearly as the stress loading increases, which has been observed by Haghi et al. (2018) as well in Figure 2.3. The matrix permeability is 308.4 mD at a stress loading of 6.9 MPa. Increasing the stress loading to 9 MPa, the matrix permeability decreases to 307.1 mD, a decrease of

0.41 %. As stress loading increases to 11 MPa, the matrix permeability decreases to 306 MPa, a further reduction of 0.36 %. The magnitude of matrix permeability is reduced by 0.35 %, 0.34 %, and 0.31 % due to increase in stress loading from 13.1 MPa, 15.2Mpa, to 17.2 MPa, respectively. The decrease in matrix permeability is directly related to reduction in matrix porosity i.e. the ability for flow to take place reduces.

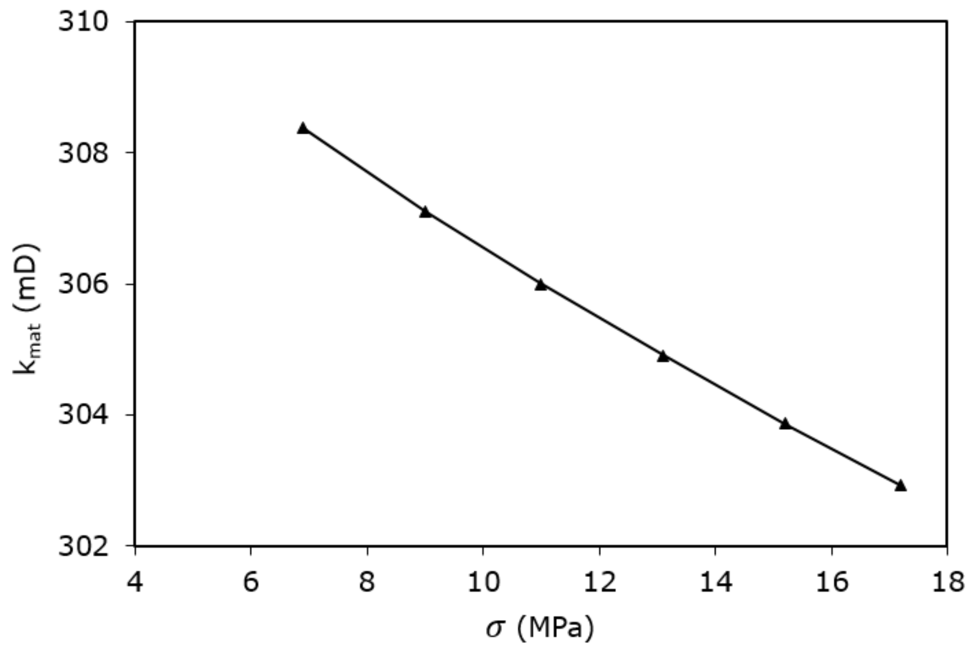

Figure 5.5. Matrix Permeability variations w.r.t. stress loading

5.6 Stress-dependent Fracture Aperture

It is a well-known fact that the fracture aperture changes under stress loading. These changes are a result of vertical displacement of the fracture aperture. The vertical displacement of the fracture aperture varies spatially along the core radius. The vertical displacement is minimum at the outer surface of the core and is maximum in the centre of the core. These spatial variations in the vertical displacement (δ) along the core radius are shown in Figure 5.6, where x/X=0 represent core's outer surface, while x/X=1 represents the centre of the core. It can be seen that while going from outside towards the centre of the core, the vertical displacement of the fracture aperture increases. The reason for this is the fact that fixed edge constraint has been applied at the core edges.

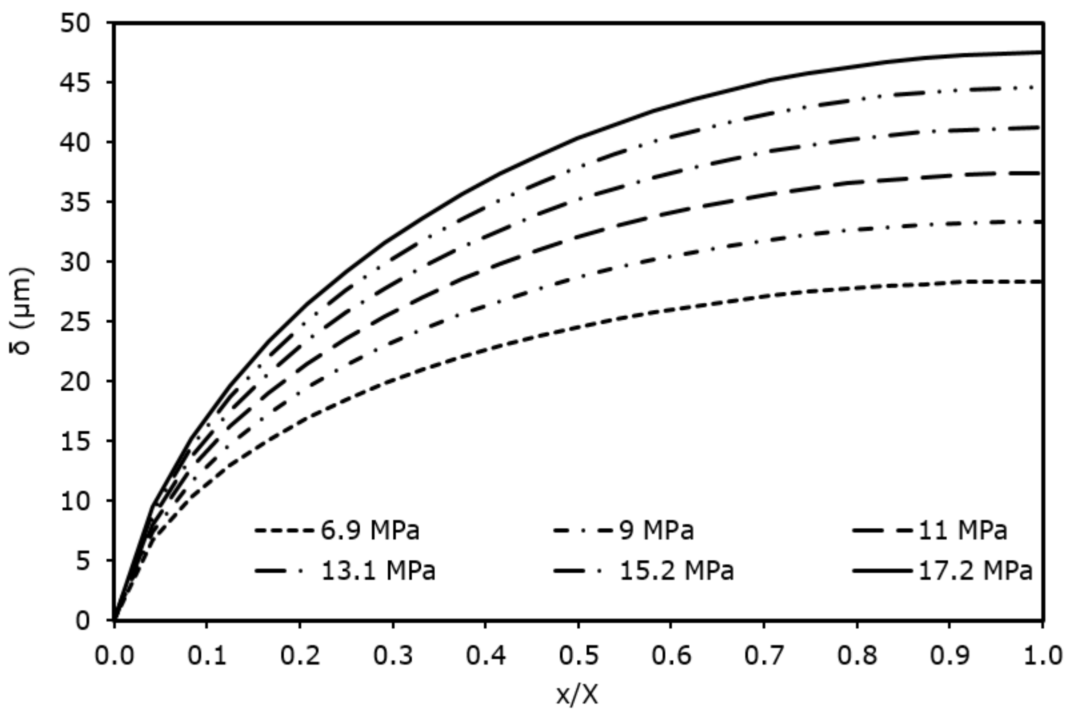

Figure 5.6. Variations in the vertical displacement of the fracture aperture along the core radius for different stress loadings

This trend has been observed for all the different stress loading conditions considered here. Quantitatively, the average δ is 21.54 µm at a stress loading of 6.9 MPa. Increasing the stress loading to 9 MPa, the average δ increases to 25.12 µm, an increase of 17 %. With a further increase in stress loading of 11 MPa, the average δ increases to 28.05 µm, a further increase of 12 %. The average δ increases to 30.74 µm (10 %), 33.14 µm (8 %), and 35.19 µm (6 %) as the stress loading increases to 13.1 MPa, 15.2 MPa, and 17.2 MPa, respectively. Thus, the variations in average δ are also nonlinear for the stress loading. Figure 5.7 depicts the variations in the maximum δ (at the core centre) as the stress loading increases. It can be clearly seen that as stress loading increases, the maximum δ experienced by the fracture aperture also increases however, the rate of this increase is not constant.

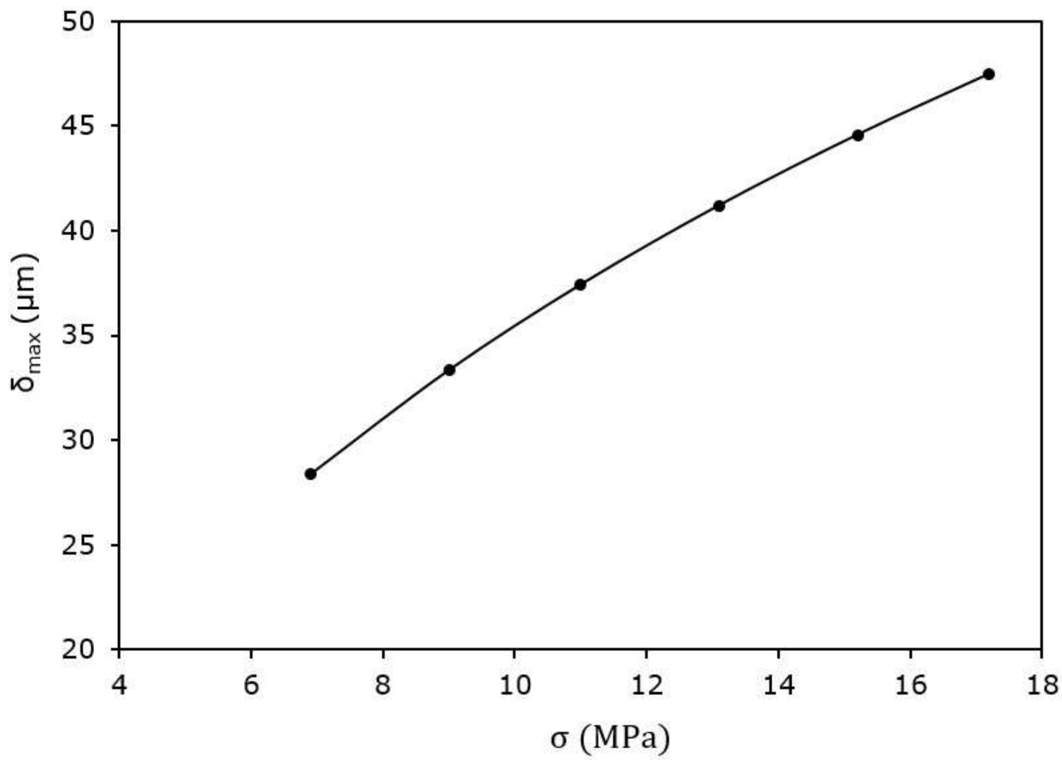

Figure 5.7. Variations in the maximum vertical displacement of the fracture aperture w.r.t. stress loading

Figure 5.8 shows the variations in fracture aperture (h) for stress loading (σ). Equation (2.3) is used to compute the fracture aperture. The fracture aperture decreases almost linearly as stress loading increases, due to the vertical displacement of the fracture, till the fracture is completely closed. The fracture aperture decreases from 130 μm (under no-load condition) to 108.46 μm, a 6.9 MPa of stress is being applied. The fracture aperture reduces to 104.88 μm (3.3 % decrease) as the stress loading increases to 9 MPa. With a further increase in stress loading to 11 MPa, the fracture aperture decreases to 101.95 μm, a further decrease of 2.8 %. Increasing the stress loading to 13.1 MPa, 15.2 MPa, and 17.2 MPa reduces fracture aperture by 2.6 %, 2.4 %, and 2.1, respectively.

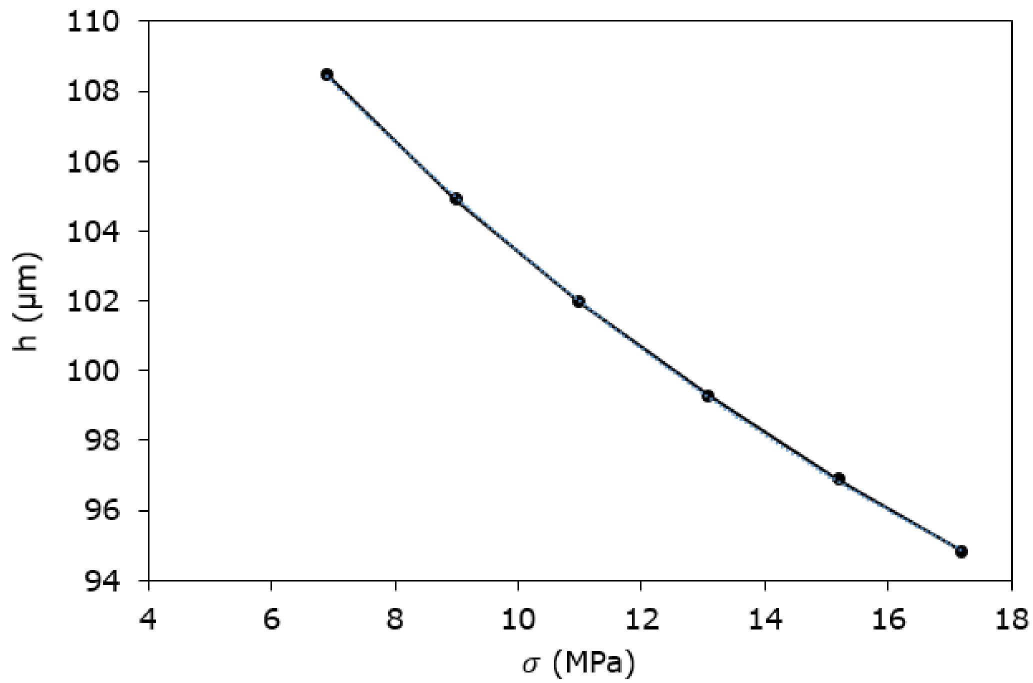

Figure 5.8. Variations in fracture aperture w.r.t. stress loading

5.7 Stress-dependent Fracture Permeability

Figure 5.9 depicts fracture permeability (k_f) variations for stress loading (σ). Equation (2.4) has been used to compute the fracture permeability under different stress loading conditions. It can be seen that the fracture permeability reduces nonlinearly as stress loading increases due to the rock's stiffness, as also observed by Cao et al. (2019) (Figure 2.4). This is due to the fact that as external stress loading increases, the fracture aperture decreases, and thus, the ability of fluid to flow in the fracture region also decreases. At a stress loading of 6.9 MPa, the fracture permeability is 180 D. The fractured permeability decreases to 163 D as the stress loading increases to 9 MPa (9.6 % decrease). Further increasing the stress loading to 11 MPa, the fracture permeability reduces to 150 D, a further reduction of 8.1 %. Increasing the stress loading to 13.1 MPa, 15.2 MPa, and 17.2 MPa reduces the fracture permeability by 7.7 %, 7.1 %, and 6.2 %, respectively.

Comparing the variations in K_f with K_{mat} (in Figure 5.5), it is evident that the fracture permeability is significantly higher than the matrix permeability, as expected. Moreover, under the same stress loading, the reduction in fracture permeability is significantly higher than reduction in matrix permeability.

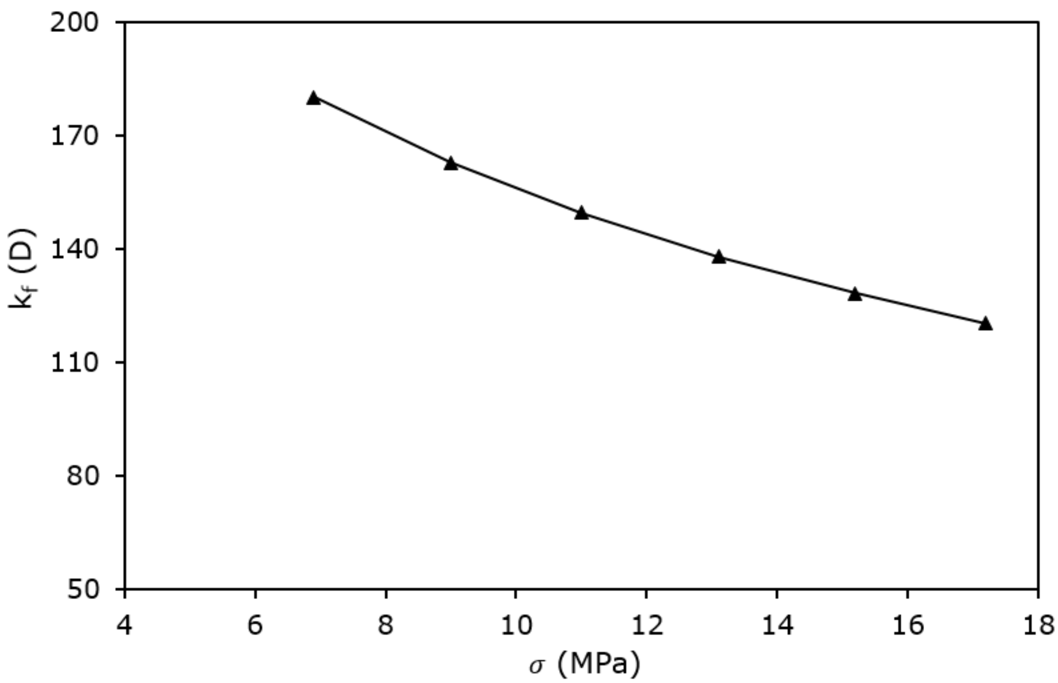

Figure 5.9. Fracture permeability variations w.r.t. stress loading

5.8 Stress-dependent Water and Oil Saturation

Figure 5.10 shows the stress-dependent water saturation (S_w) variations at the fracture-matrix interface for different injected water volume (V_w) under different stress loading conditions considered here. It can be seen that for all stress loadings, as V_w increases, S_w also increases, linearly till V_w=0.5. With a further increase in V_w, S_w increases however, the rate of increase is reduced. For V_w=0.1 (10 %), S_w=0.155 at stress loading of 6.9 MPa. Increase in water saturation as V_w increases is understandable as more and more water is injected into the fracture-matrix region.

As the stress loading increases to 9 MPa, 11 MPa, 13.1 MPa, 15.2 MPa, and 17.2 MPa, S_w increases to 0.166, 0.178, 0.191, 0.211, and 0.234, respectively. Similarly, for V_w=0.7, S_w=0.79 at stress loading of 6.9 MPa. As the stress loading increases to 9 MPa, 11 MPa, 13.1 MPa, 15.2 MPa, and 17.2 MPa, S_w increases to 0.83, 0,87, 0.9, 0.93, and 0.961, respectively. It is worth mentioning that as S_w approaches 1 for any given V_w value, the rate of increase in it decreases significantly as the rock matrix becomes more water-logged.

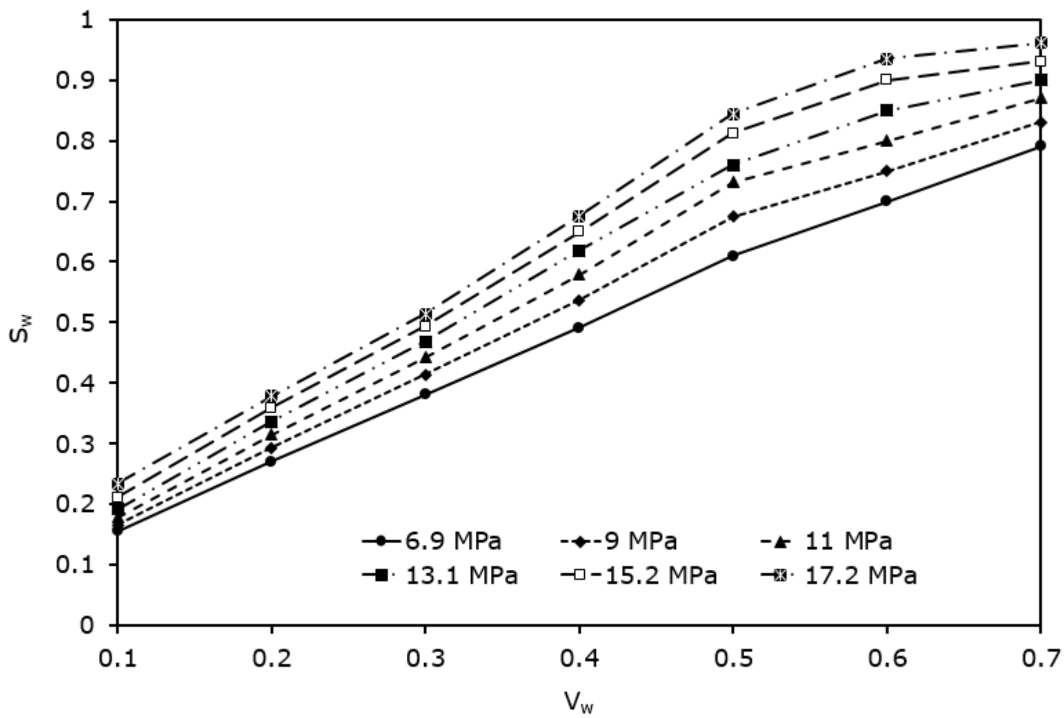

Figure 5.10. Variations in water saturation at the fracture-matrix interface for different water volume injection and stress loading

Figure 5.11 depicts the spatial variations in oil saturation at the fracture-matrix interface under different stress loading conditions and at injected water volume of 10 %. Note that the flow direction is from left to right in the figure, i.e., the inlet is on the left, and the outlet is on the right. Moreover, the same scale of variations has been used for better comparative analysis. It can be seen that as the stress loading on the core sample increases, more oil is being displaced by water at the fracture-matrix interface, resulting in higher recovery of oil at the exit of the reservoir. This is due to the reduction in the fracture aperture as the stress loading increases, decreasing the overall volume of the fracture region and thus, oil is being pushed out of the reservoir.

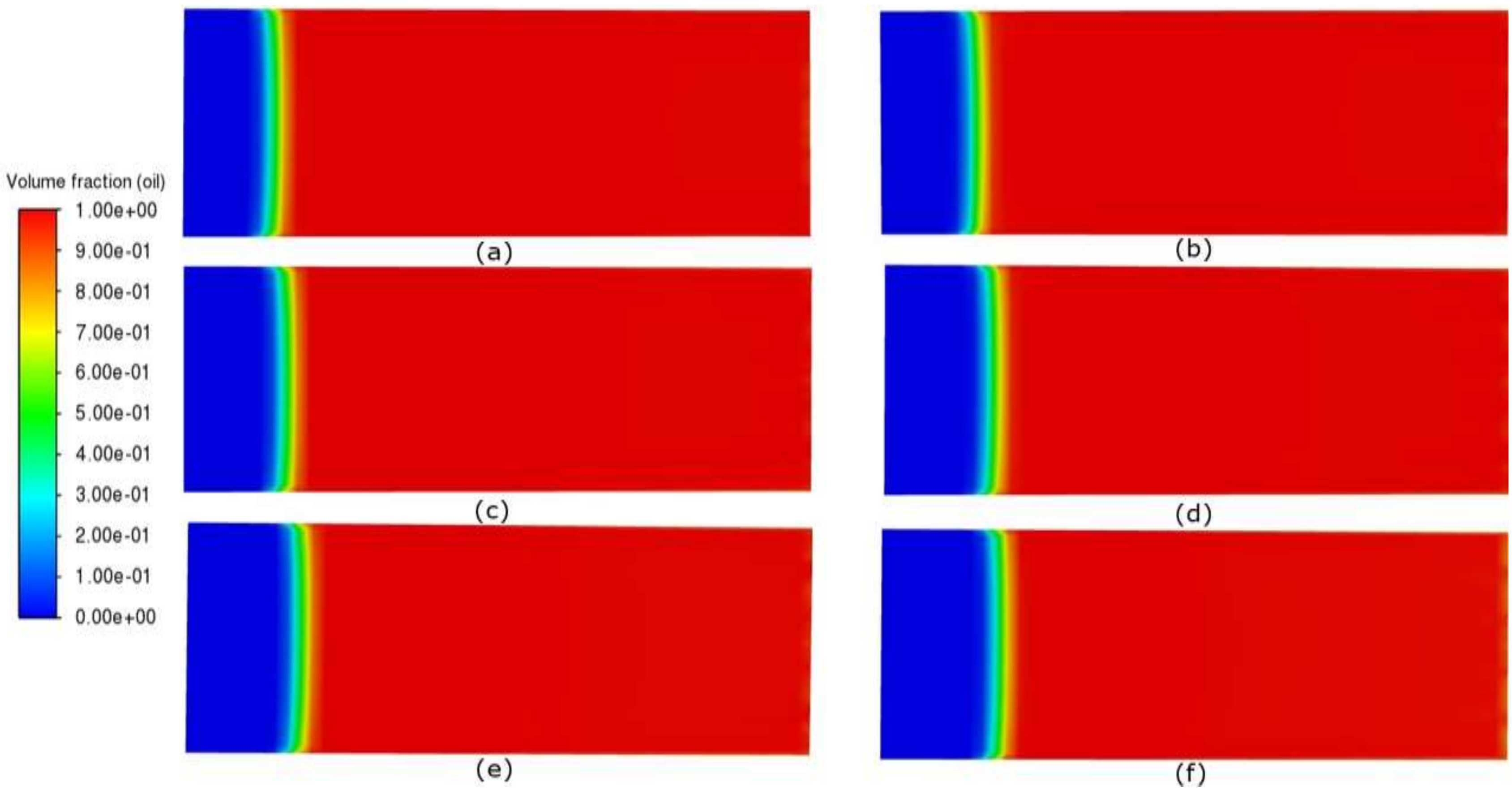

Figure 5.11. Variations in oil saturation at the fracture-matrix interface for 10 % of injected water volume and stress loading of (a) 6.9 MPa (b) 9 MPa (c) 11 MPa (d) 13.1 MPa (e) 15.2 MPa (f) 17.2 MPa

Figure 5.12 shows variations in oil saturation at the fracture-matrix interface for 40 % of the injected water volume and stress loading of 6.9 MPa, 9 MPa, 11 MPa, 13.1 MPa, 15.2 MPa, and 17.2 MPa, respectively. It can be seen that at V_w of 40 %, the boundary between the oil and water starts to get affected, i.e., water starts penetrating into the oil, leaving residual streaks of oil behind. This phenomenon is known as viscous fingering in the literature (Berge et al., 2019; Fanchi, 2018; Gudala and Govindarajan, 2021). Moreover, as the stress loading increases, due to reduction in the fracture aperture, more oil is being pushed out of the reservoir and thus, the oil recovery increases.

Figure 5.13 depicts variations in oil saturation at the fracture-matrix interface for 70 % of the injected water volume and different stress loadings. It can be seen that the oil saturation decreases due to increase in stress loading. As the injected water is very high (70 % of the total pore volume), almost all of the oil is being pushed out of the reservoir. This phenomenon is amplified with the application of stress loading on the core sample, facilitating the recovery of oil from the reservoir.

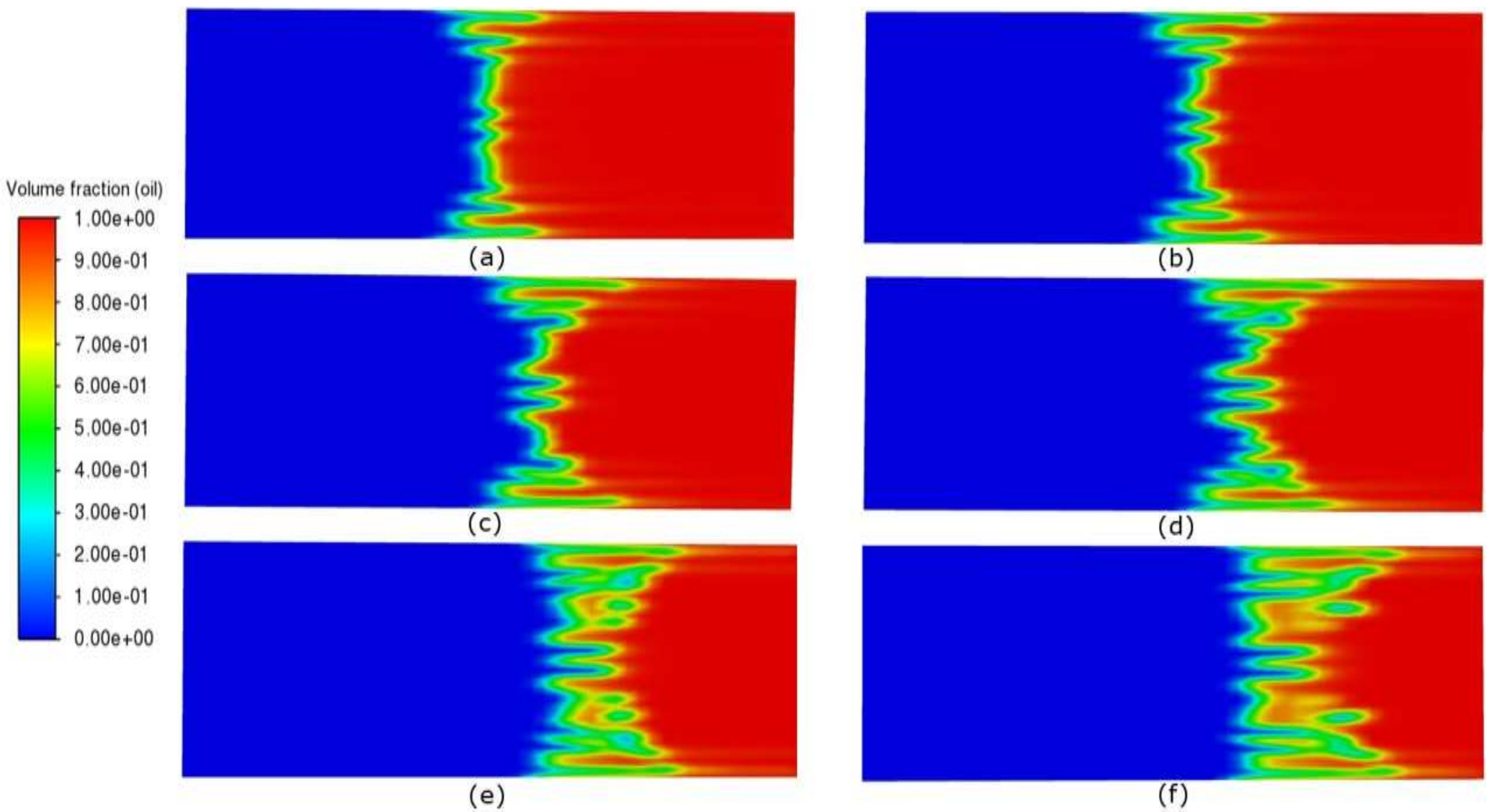

Figure 5.12 Variations in oil saturation at the fracture-matrix interface for 40 % of injected water volume and stress loading of (a) 6.9 MPa (b) 9 MPa (c) 11 MPa (d) 13.1 MPa (e) 15.2 MPa (f) 17.2 MPa

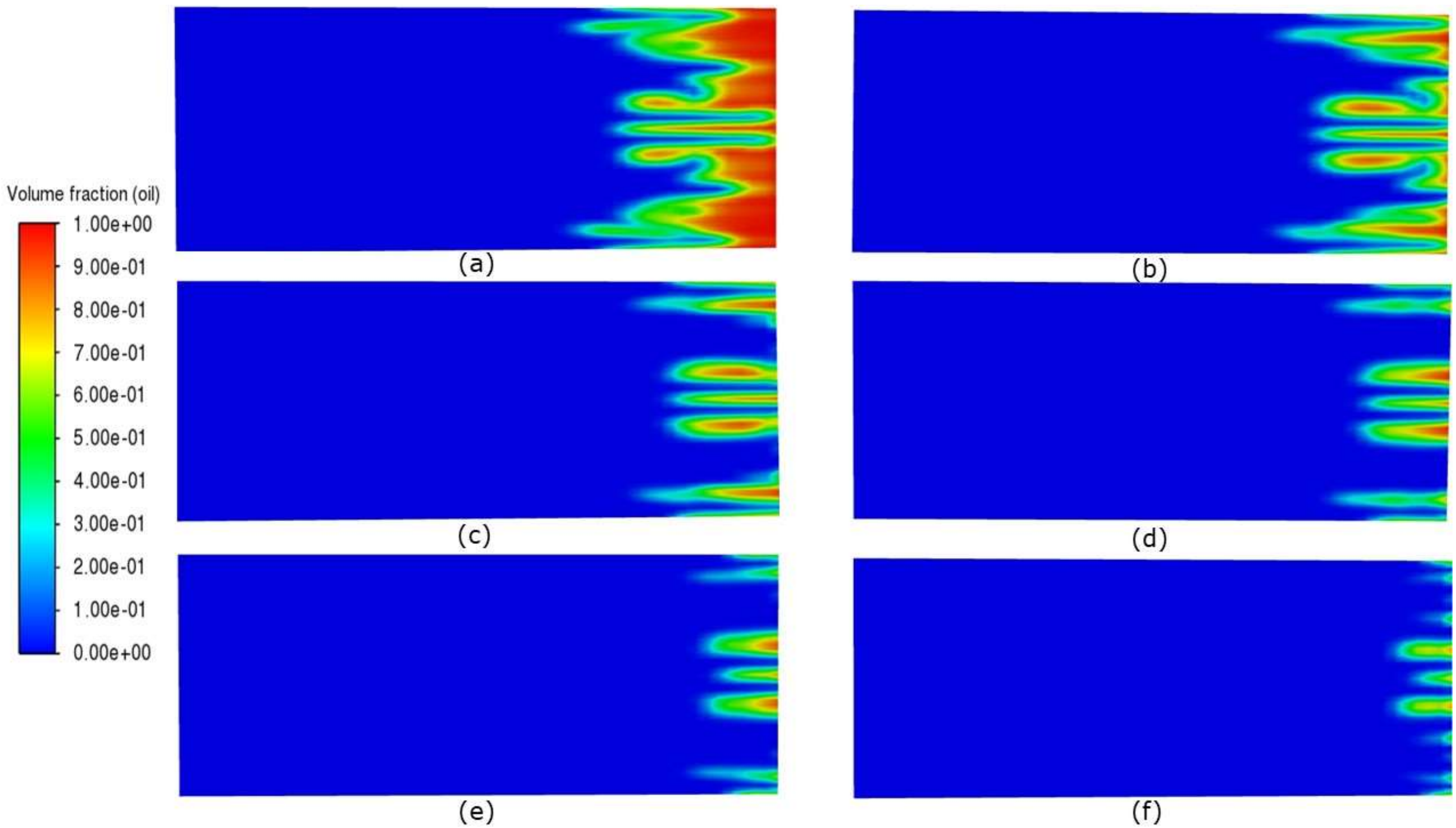

Figure 5.13 Variations in oil saturation at the fracture-matrix interface for 70 % of injected water volume and stress loading of (a) 6.9 MPa (b) 9 MPa (c) 11 MPa (d) 13.1 MPa (e) 15.2 MPa (f) 17.2 MPa

5.9 Stress-dependent Capillary Pressure

Figure 5.14 shows the capillary pressure (*Pc*) variations for injected water volume (V_w) at different stress loading conditions. The capillary pressure has been plotted against the injected water volume here as the capillary pressure is a function of water saturation. The capillary pressure has been computed based on Brooks and Corey method, as discussed in chapter 3. It can be seen in the figure that as the injected water volume increases, the capillary pressure decreases nonlinearly. The same trend has been observed previously in chapter 4 (Figure 4.11). This is due to the fact that as more and more water enters the fractured reservoirs, S_w increases, which results in the decrease of capillary pressure. With regards to the stress loading, for V_w=0.1 (or 10 %), *Pc*=5.46 kPa at a stress loading of 6.9 MPa. At the same V_w, as stress loading increases to 9 MPa, 11 MPa, 13.1 MPa, 15.2 MPa, and 17.2 MPa, *Pc* decreases to 4.96 kPa, 4.47 kPa, 4.01 kPa, 3.47 kPa, and 2.98 kPa, respectively. Similarly, for V_w=0.3, *Pc*=1.45 kPa at a stress loading of 6.9 MPa. As the stress loading increases to 9 MPa, 11 MPa, 13.1 MPa, 15.2 MPa, and 17.2 MPa, *Pc* decreases to 1.28 kPa, 1.16 kPa, 1.06 kPa, 0.98 kPa, and 0.93 kPa, respectively. Figure 5.15 further highlights this be plotting the capillary pressure against the stress loading for V_w=0.1. It can be seen that the decrease in the capillary pressure, with increasing stress loading, exhibits an almost linear pattern.

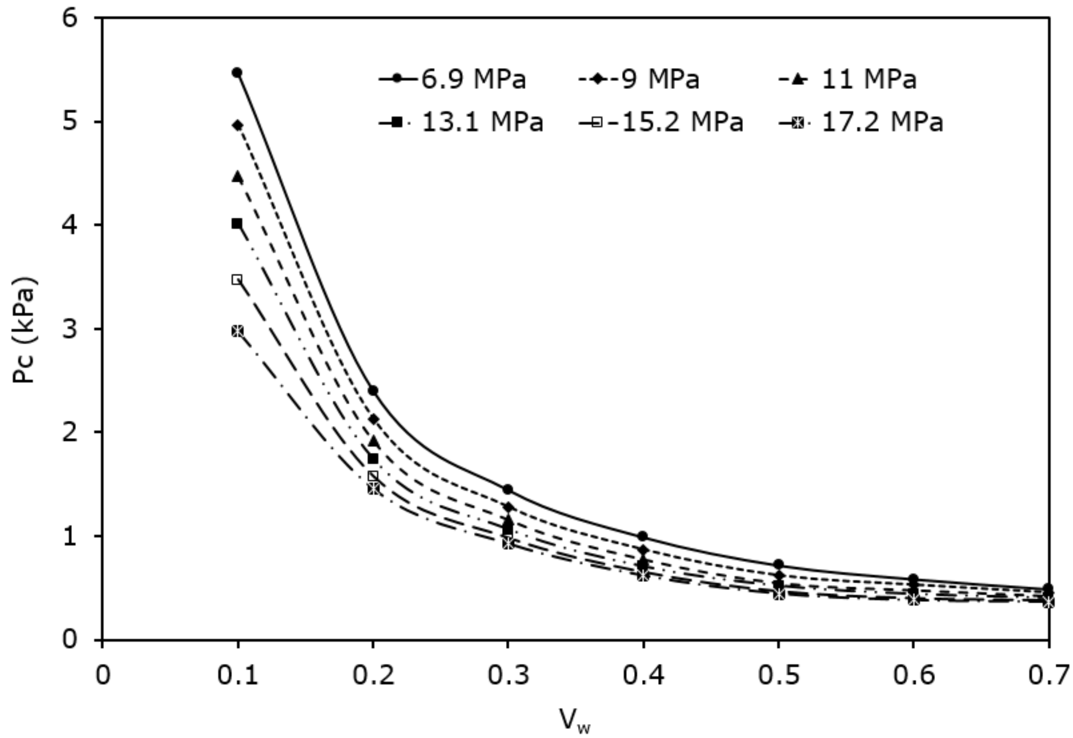

Figure 5.14. Capillary pressure variations w.r.t injected water volume

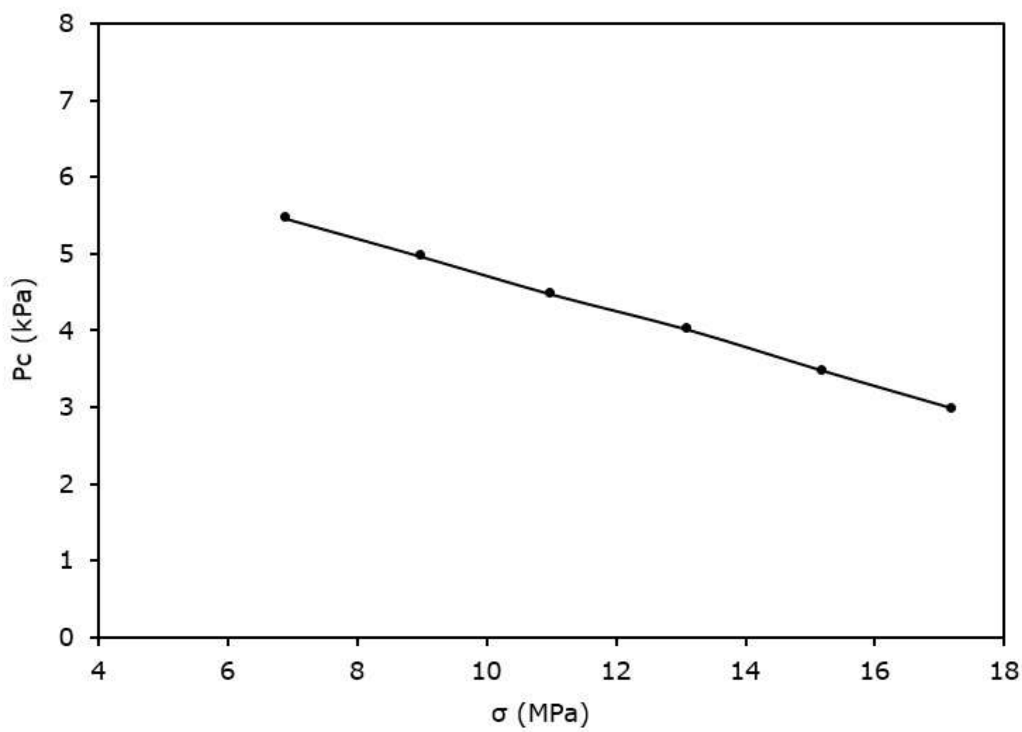

Figure 5.15. Capillary pressure variations w.r.t. stress loading at V_w=0.1

5.10 Stress-dependent Relative Permeability

The variations in relative permeabilities of water (Kr_w) and oil (Kr_o) at the fracture-matrix interface for water saturation (S_w), at different stress loading conditions, is shown in Figure 5.16. The relative permeabilities have been calculated using Brooks and Corey's method, while the water saturation values for corresponding V_w values are shown in Figure 5.10. It can be clearly seen that the oil relative permeability decreases nonlinearly as water saturation increases. The trends observed for water relative permeability are opposite to that of oil relative permeability i.e. water relative permeability increases nonlinearly as water saturation increases.

It is noteworthy that *Kr* changes as applied stress changes. With the application of stress, S_w also changes. Thus, *Kr* is dependent on both the stress loading and the water saturation. It has already been discussed in section 5.9 that S_w is a function of V_w. Hence, *Kr* is dependent on the applied stress (σ), water saturation (S_w) and also indirectly on the injected water (V_w) as S_w is dependent on V_w. It is thus evident that the accurate depiction or explanation of stress-dependent relative permeability is very challenging unless all the relevant parameters are appropriately defined.

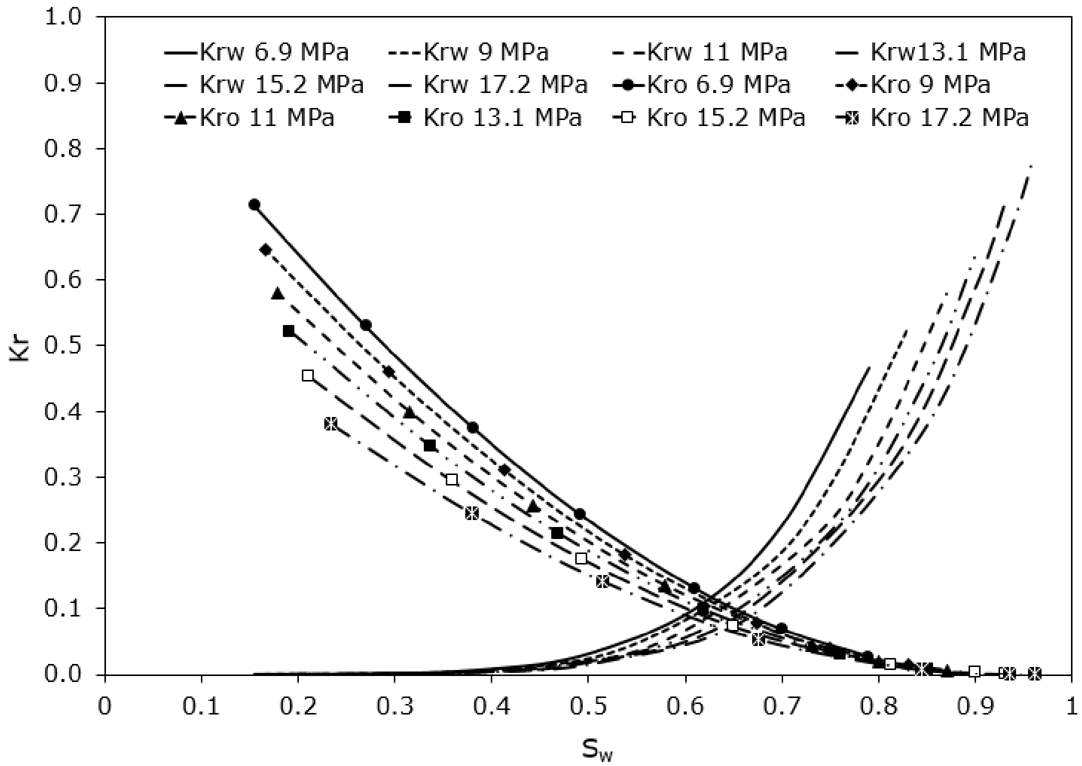

Figure 5.16. Relative permeability variations w.r.t water saturation

5.11 Summary of key findings

Based on extensive parametric investigations carried out in this chapter regarding the effects of geomechanical parameters on multiphase flow characterisation in naturally fractured tight reservoirs, the following key conclusions can be drawn:

- Increase in stress loading decreases the porosity of the rock matrix (see figure 5.4)
- Increase in stress loading decreases the rock matrix permeability (see figure 5.5)

- Increase in stress loading decreases the fracture aperture (see figures 5.6, 5.7, and 5.8)
- Increase in stress loading decreases the fracture permeability (see figure 5.9)
- Increase in stress loading increases the water saturation and decreases the oil saturation, thus increasing oil recovery (see figures 5.10, 5.11, 5.12, and 5.13)
- Increase in stress loading decreases the capillary pressure (see figure 5.15)
- Increase in water saturation decreases the oil relative permeability and increases the water relative permeability (see figure 5.16)

Chapter 6
Development of a Novel Geomechanical-Multiphase Flow Coupling Model

This chapter presents the results of fully coupled geomechanics and multiphase flow in tight reservoirs. The details of the numerical modelling appropriate for full coupling have been presented, along with model validation. Qualitative and quantitative analyses of the geomechanical effects on the transient multiphase flow properties at the fracture-matrix interface have been carried out. Key findings from the results obtained are outlined at the end of the chapter.

6.1 Introduction

Multiphase flow in naturally fractured tight reservoirs is a complicated physical phenomenon especially when the rock is subjected to external stresses. Numerical modelling based on one-way coupling between the geomechanical parameters and multiphase flow characteristics are relatively accurate in predicting the flow behaviour within the stress loaded reservoir however, these numerical predictions are often inaccurate at the fracture-matrix interface. There is a need to develop a novel numerical approach for accurate predictions at the fracture-matrix interface. For this purpose, this study presents a fully coupled numerical model.

There are two main shortcomings of one-way coupling which have been addressed while developing a fully coupled numerical model. Firstly, one-way coupling transfer information in one direction only i.e. from FEA to CFD, whereas in fully coupled model, the flow of information is in both directions, and is instantaneous. This means that not only CFD is informed by FEA, FEA is also informed by CFD predictions, and this coupling occurs at every time step of the transient numerical calculations. Secondly, as discussed in section 3.2.3, pore pressure is neglected in one-way coupling, which is not an accurate representation of real-world scenario. In the fully coupled numerical model developed in this chapter, the pore pressure has been considered. It is envisaged that the fully coupled FEA-CFD model developed in this chapter will results in more accurate numerical predictions, especially at the fracture-matrix interface, which will become evident later in the chapter when the fully coupled model is validated.

Fully coupled model developed is computationally very expensive, and thus is prohibitive for practical purposes. This issue has been resolved by considering a two-dimensional model instead of a three-dimensional model considered in chapters 4 and 5. As the flow within naturally fractured tight reservoirs is dictated by viscous effects (flow laminarity), this approximation doesn't result in unrealistic numerical predictions, as will be observed later in the chapter.

6.2 Fully Coupled Numerical Model

With the implementation of 2D modelling approach, it is prudent to provide details of the numerical model preparation. However, in contrast to chapter 3 where extensive numerical modelling details were provided, the aim here is to highlight only the differences in the model compared to the 3D model developed in chapter 3. It is also noteworthy that COMSOL Multiphysics 6.0 has been used to build the fully coupled FEA-CFD model. This facility is not available in ANSYS®.

6.2.1 Geometry and Meshing

The 2D geometric model of the naturally fractured tight reservoir sample is shown in Figure 6.1. As in chapter 5, the geometric model is based on Clashach core flooding experiments (Stalker et al., 2009) and thus, the diameter (*D*) and length (*L*) of the core are 3.79 cm and 7.54 cm respectively. The rectangular-shaped fracture in the middle of the core sample has an initial aperture size (*h*) of 130 μm.

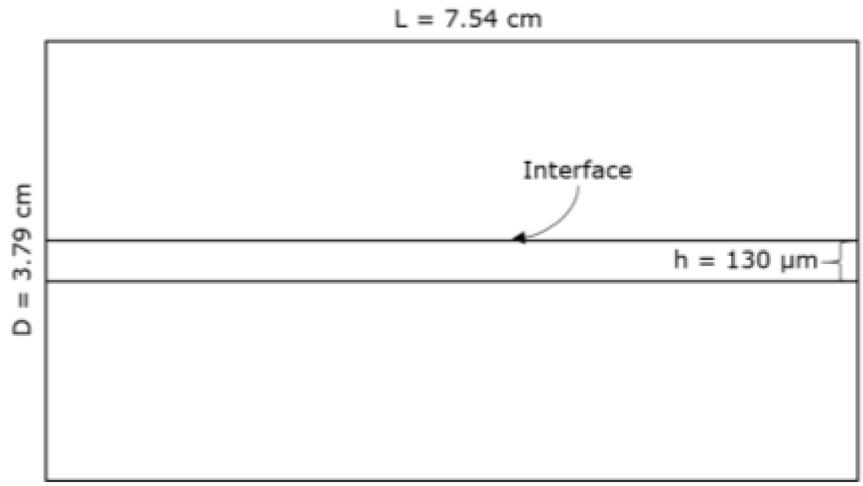

Figure 6.1. 2D model of naturally fractured tight reservoir

With the generation of a simplified geometric model of the tight reservoir, it has now become possible to generate a structured quadrilateral mesh for enhancing the accuracy and precision of the numerical model. Thus, both the inlet edges have been meshed with 40 elements each, while the number of divisions in the fracture region are 5 (in Y direction). The resulting mesh is depicted in Figure 6.2.

Figure 6.2. Meshing

6.2.2 Initial and Boundary Conditions

The rock core sample is assumed here to contain 80 % oil and 20 % water before the application of external stress and water injection into the sample for oil recovery. This initial condition for numerical solution purposes is based on realistic estimation of oil and water saturation in tight reservoirs (Baker et al., 2015). The macroscopic saturation of various phases is frequently discontinuous, where the porous regions with higher and lower permeability meet, particularly in fractured tight reservoirs. The following condition is thus implemented on the fracture-matrix interface via the Porous Medium Discontinuity boundary condition:

$$P^l{}_{c\beta}\left(S_\beta^l\right) = \begin{cases} P^l{}_{ec,\beta} & if \quad P^h{}_{c\beta}(S_\beta^h) \leq P^l{}_{ec,\beta} \\ P^h{}_{c\beta}\left(S_\beta^h\right) & if \quad P^h{}_{c\beta}(S_\beta^h) > P^l{}_{ec,\beta} \end{cases} \tag{6.1}$$

where the superscript *h* shows the high permeability side of the boundary, and the saturation and capillary pressure on the low permeable side of the barrier is shown by the superscript l. The first case demonstrates that the saturation of phase β on low permeable side is equal to zero, if the capillary pressure on the high permeable side is less than the entrance capillary pressure on the low permeable side (or the residual saturation). The second case indicates that phase β is present on both sides of the interface if the capillary pressure on high permeable side is more than the entry capillary pressure on the low permeable side, and that the capillary pressure is continuous over the interface.

6.2.3 Solver Settings

This study investigates coupled geomechanics and transient two-phase fluid flow in naturally fractured tight reservoirs using COMSOL Multiphysics 6.0, where both the core and the fracture regions have been modelled as porous media. Poroelastic module and the multiphase module have been used i.e. coupled modules for Darcy's law, solid mechanics and phase transportation. In the solid mechanic's module, a fracture in a porous medium is regarded as a thin elastic layer border element with various rock properties. Thus, integrated fracture boundary condition has been used for the fractures in Darcy's law module.

Petrophysical and geomechanical property variations (i.e., Eqs. (3.26) to (3.28)) are taken explicitly into account as dynamic local variables. After the convergence of each time step, the generated strain in the rock matrix and fracture is taken into account for updating porosity values (Eq. (3.26)); the updated porosity values are then utilized to determine the elastic modulus spatially (Eq. (3.26)). The permeability of the rock matrix depends on volumetric strain (Eq. 3.27). In contrast, the permeability of fractures depends on the stresses (Eq. 3.28). After each time step $(t + \Delta t)$, these updated values are input in the section that defines the property.

The Backward Differentiation Formula (BDF) solver is an implicit solver (Gudala and Govindarajan, 2020) that employs backward differentiation formulas, ranging from one to five depending on the accuracy level. Lower-order approaches can have significant dampening effects. Backward Euler severely muffles any high frequencies. Due to the damping in Backward Euler, even though anticipated, a solution with abrupt gradients may eventually obtain a reasonably smooth solution. Thus, variable order is used in COMSOL's BDF implementation. In other words, high demand will be used whenever possible, and a lesser charge will be automatically selected to achieve stability. Therefore, the implicit backward differentiation formula (BDF) has been used for time step discretization. The Newton nonlinear approach has been combined with the MUMPS (Multifrontal Massively Parallel Direct Solver) solver to solve the nonlinear system of equations with a pivoting perturbation of 3.28-3.26.

6.2.4 Validation of the Numerical Model

The FEA-CFD full-coupling based numerical model has been validated against the Clashach Core flooding experimental data (Stalker et al., 2009) for the single-phase flow of oil in the fractured tight reservoir. The differential pressure (ΔP) applied over the sample reservoir is used to calculate the cumulative discharge of oil (Qc) and thus, the same solver settings have been utilised for validation here. Figure 6.3 depicts the results of numerical model validation. It can be seen that both the numerically predicted and experimentally recorded Qc values increase with increasing differential pressure. The two Qc curves match well with an average difference of 4.2 %, indicating significantly higher accuracy compared to the numerical model considered in chapter 5 where the average difference was around 9 %. Hence, the fully coupled numerical model developed here is superior to the one-way coupled numerical model, significantly enhancing the accuracy of the numerical predictions in naturally fractured tight reservoirs, due to the fact that pore pressure is considered in the fully coupled model. In terms of time duration, each numerical simulation took fifteen days.

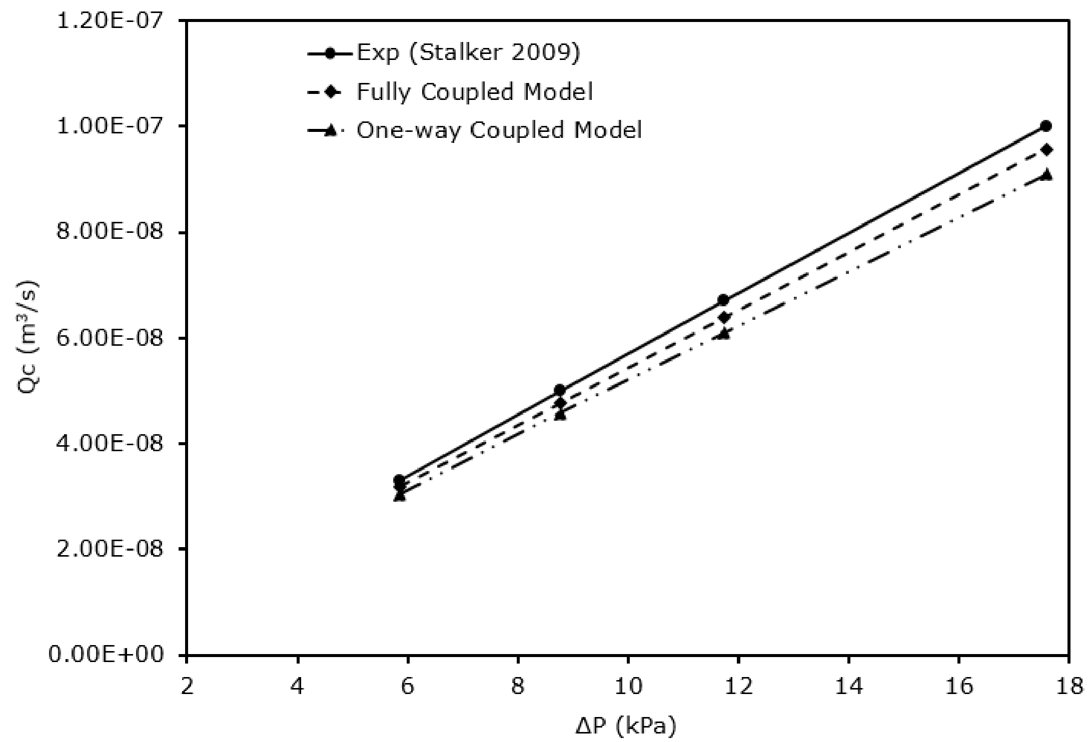

Figure 6.3. Validation of the numerical model w.r.t. the experimental data

6.3 Stress-dependent Matrix Porosity

Figure 6.4 shows the stress-dependent porosity (φ) variations for stress loading (σ). The porosity decreases linearly as the stress loading increases, as opposed to one-way coupled model where this trend was nonlinear. The porosity is 15.386 % at a stress loading of 6.9 MPa. As the stress loading increases to 9 MPa, the porosity decreases by 0.022 % to 15.383 %. The porosity decreases to 15.380 % as the stress loading increases to 11 MPa. Further increasing the stress loading to 13.1 MPa, 15.2 MPa, and 17.2 MPa, the porosity reduces on average by 0.022 %.

It is noteworthy that the effect of pore fluid compression (or expansion) is considered here, which wasn't considered in case of one-way coupled model.

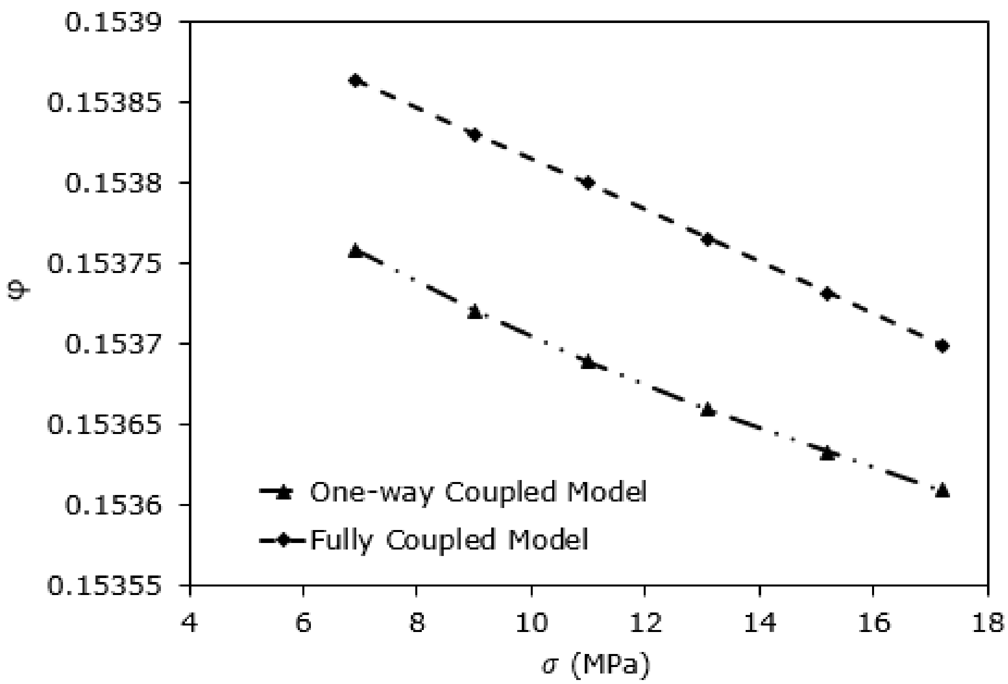

Figure 6.4. Porosity variations w.r.t stress loading

6.4 Stress-dependent Matrix Permeability

Figure 6.5 depicts the stress-dependent matrix permeability (k_{mat}) variations for stress loading (σ). The matrix permeability reduces almost linearly as the stress loading increases. The same trend observed in case of one-way coupled model. At a stress loading of 6.9 MPa, the matrix permeability is 311.8 mD. The matrix permeability reduces to 311.2 mD, a decrease of 0.20 %, as stress loading increases to 9 MPa. Increasing stress loading to 11 MPa, the matrix permeability reduces to 310.7 mD. Further increasing stress loading to 13.1 MPa, 15.2 MPa, and 17.2 MPa, the matrix permeability decreases by 0.17 %, 0.16 %, and 0.15 %, respectively.

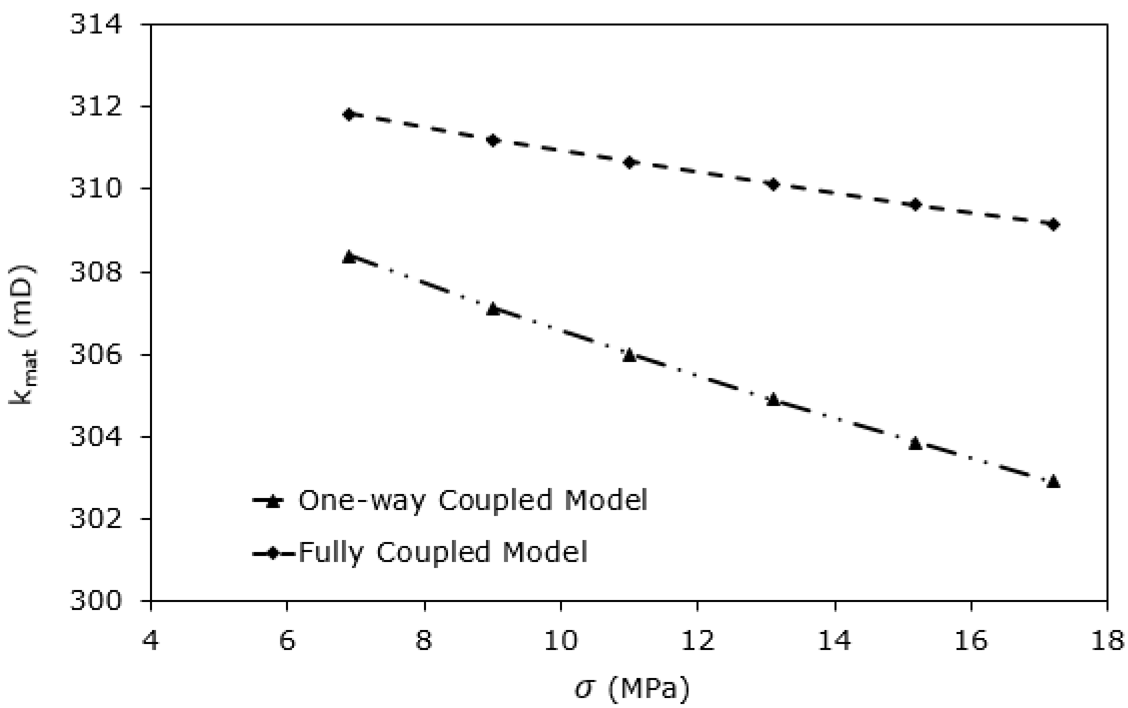

Figure 6.5. Matrix permeability variations w.r.t stress loading

It is worth mentioning that although the difference in the matrix permeability between one-way and fully coupled numerical models at stress loading of 6.9 MPa is negligibly small (< 1 %), the matrix permeability predicted by the fully coupled model at stress loading of 17.2 MPa is 2 % higher than predicted by one-way coupled model. It can be clearly seen that the fully coupled model under-predicts the matrix permeability. The reason behind this is, unlike the one-way coupled model, the fully coupled model considers the influence of pore fluid pressure.

6.5 Stress-dependent Fracture Aperture

Figure 6.6 depicts the variations in fracture aperture (h) for stress loading (σ). It can be seen that as stress loading increases, the fracture aperture decreases linearly until the fracture is completely closed. The same trend was observed in case of one-way coupled model. The fracture aperture decreases from 130 μm (under no-load condition) to 126.3 μm (0.87 % decrease) when a stress of 6.9 MPa is applied. The fracture aperture reduces to 125.2 μm as the stress loading increases to 9 MPa. Increasing stress loading to 11 MPa, the fracture aperture decreases to 124.2 μm, a decrease of 0.82 %. Further increasing stress loading to 13.1 MPa, 15.2 MPa, and 17.2 MPa decreases fracture aperture by 0.89 %, 0.82 %, and 0.84 %, respectively. In comparison with one-way coupled model where the fracture aperture reduced to 94.8 μm at stress loading of 17.2 MPa, in case of fully coupled model, the fracture aperture reduces to 121 μm. Thus, the fracture closure predicted by the fully coupled model is 27 % less than one-way coupled model, due to the pore pressure considered, and thus, it is expected that the fracture permeability will be significantly higher in the fully coupled model.

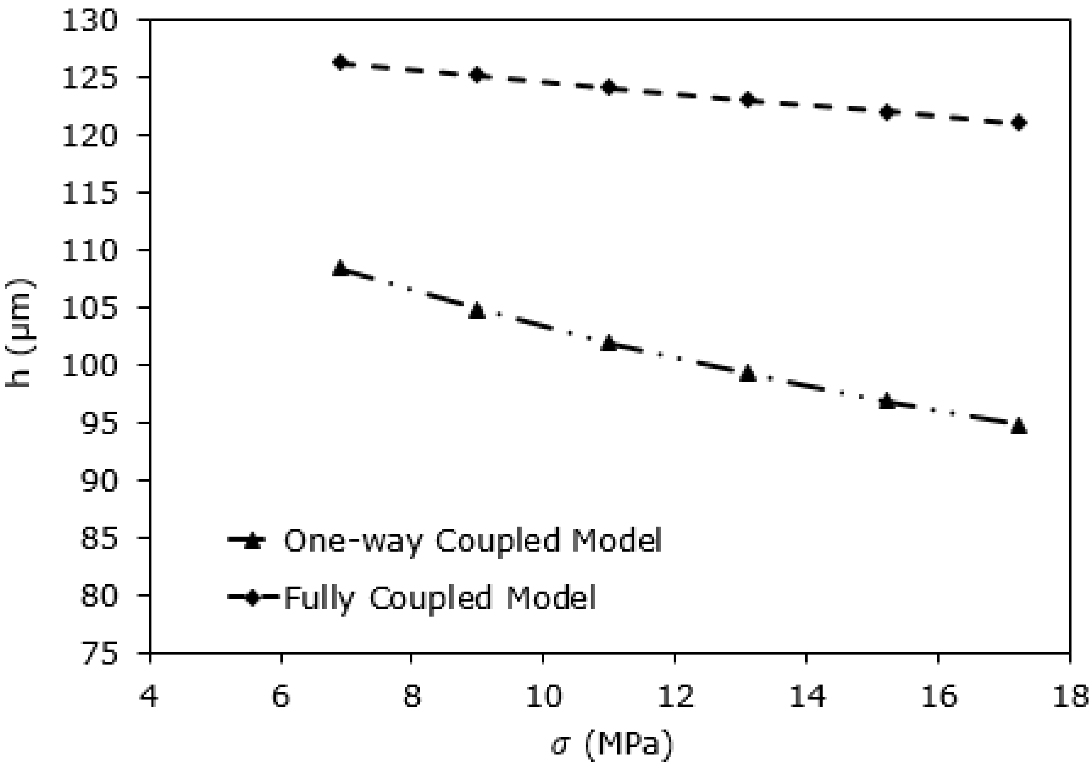

Figure 6.6. fracture aperture variations w.r.t stress loading

6.6 Stress-dependent Fracture Permeability

Figure 6.7 shows the stress-dependent fracture permeability (k_f) variations for stress loading (σ). It can be seen that fracture permeability decreases linearly as stress loading increases. In case of one-way coupled model, a nonlinear behaviour was observed. The fracture permeability is 285 D at a stress loading of 6.9 MPa, which was 180 D in case of one-way coupled model. The fracture permeability decreases to 277 D (2.6 % decrease) when stress loading increases to 9 MPa, while it was 163 D in case of one-way coupled model. Further increasing stress loading to 11 MPa, 13.1 MPa, 15.2 MPa, and 17.2 MPa reduces the fracture permeability by 2.4 %, 2.6 %, 2.4 %, and 2.5 %, respectively. Under stress loading of 17.2 MPa, in case of one-way coupled model, the fracture permeability was 120 D. Thus, on average, the fracture permeability predicted by the fully coupled model is 84.6 % higher than the one-way coupled model. The reason is the considering of the pore pressure in fully coupled model that increases the effective stress in the flow domain.

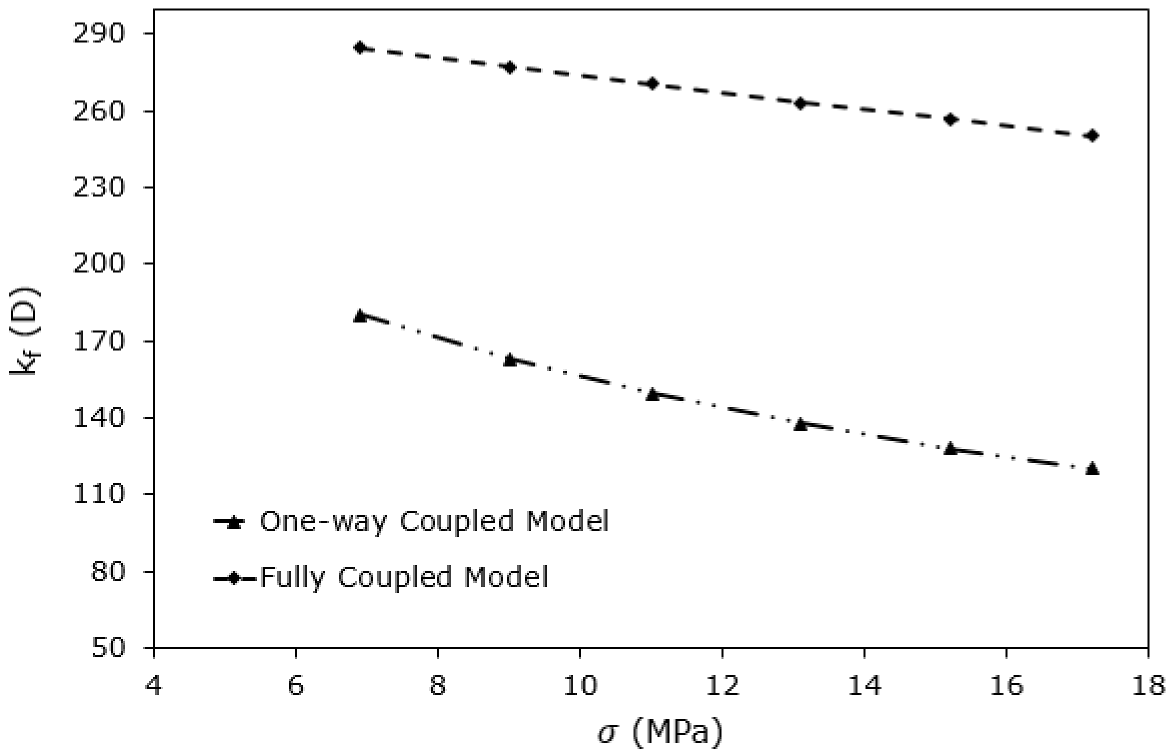

Figure 6.7. Variations in fracture permeability w.r.t stress loading

6.7 Stress-dependent Water and Oil Saturation

Figure 6.8 shows the stress-dependent water saturation (S_w) variations at the fracture-matrix interface for different injected water volumes (V_w) under various stress loading conditions considered. It can be seen that for all the stress loadings, as V_w increases, S_w also increases. This increase can be seen to be nonlinear from

V_w=0.1-0.4, and then linear from V_w=0.4-0.7. In comparison, this trend was linear from V_w=0.1-0.5, and then non-linear afterwards in case of one-way coupled model. It can be seen that at V_w=0.1, S_w=0.7 at a stress loading of 6.9 MPa. Increasing the stress loading to 9 MPa, 11 MPa, 13.1 MPa, 15.2 MPa, and 17.2 MPa, S_w increases to 0.57, 0.58, 0.59, 0.60, and 0.61, respectively. Similarly, for V_w=0.7, S_w=0.71 at a stress loading of 6.9 MPa. As the stress loading increases to 9 MPa, 11 MPa, 13.1 MPa, 15.2 MPa, and 17.2 MPa, S_w increases to 0.72, 0,73, 0.738, 0.746, and 0.752, respectively.

The minimum and maximum S_w predicted by the fully coupled model are 0.55 and 0.78 respectively, whereas in case of one-way coupled model, the minimum and maximum recorded S_w values were 0.15 and 0.96 respectively. Thus, it is clear that there is a significant difference between the two models with regards to predicting water saturation. A potential reason for this significant difference is that fully coupled model has been initialised with 20 % water saturation, while the one-way coupled model was initialised with 0 % water saturation. The main reason for initialising with a particular value of water saturation is the different types of tight reservoirs being tested. In carbonate reservoirs, water saturation starts from 0 to 15 % and in clastic rock reservoirs, water saturation is between 20 to 25 % (Ibrahim et al., 2022; Islam, 2015).

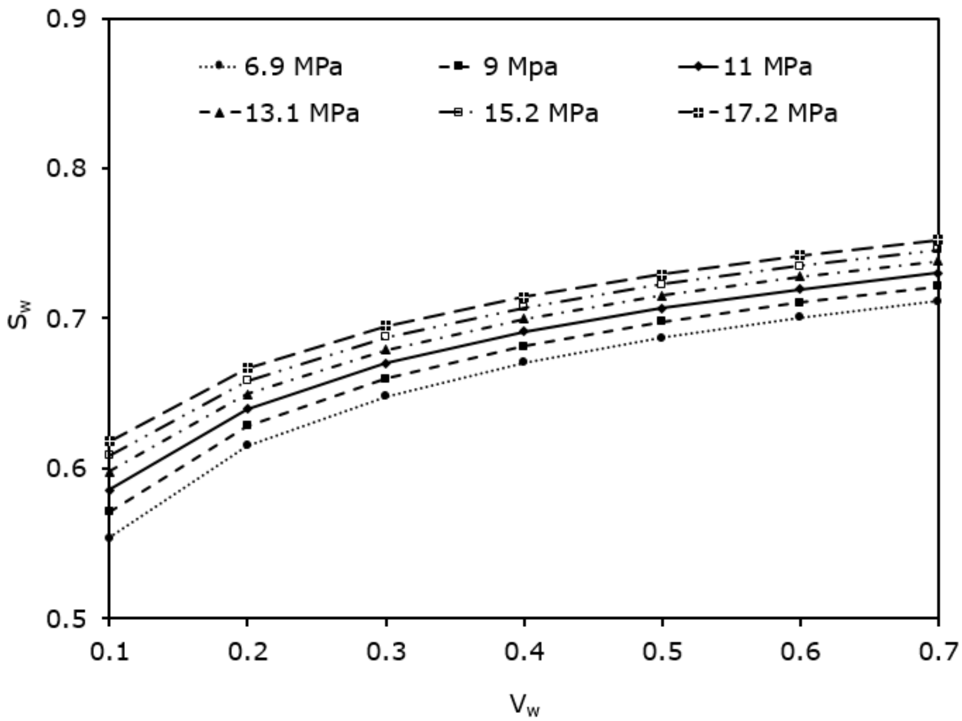

Figure 6.8. Variations in water saturation at the fracture-matrix interface for different water volume injection and stress loading

Figure 6.9 depicts variations in stress-dependent oil saturation (S_o) at the fracture-matrix interface for different injected water volumes (V_w) under various stress loading conditions. It can be seen that S_o decreases nonlinearly as V_w increases, for all stress loadings. For V_w=0.1, S_o=0.446 at a stress loading of 6.9 MPa. Increasing the stress loading to 9 MPa, 11 MPa, 13.1 MPa, 15.2 MPa, and 17.2 MPa, S_o decreases to 0.429, 0.415, 0.402, 0.392, and 0.382, respectively. Similarly, for V_w=0.7, S_o=0.289 at a stress loading of 6.9 MPa. As the stress loading increases to 9 MPa, 11 MPa, 13.1 MPa, 15.2 MPa, and 17.2 MPa, S_w increases to 0.279, 0.270, 0.262, 0.254, and 0.248, respectively. Note that S_o is decreasing because S_w is increasing within the reservoir model i.e. water is pushing oil out of the rock.

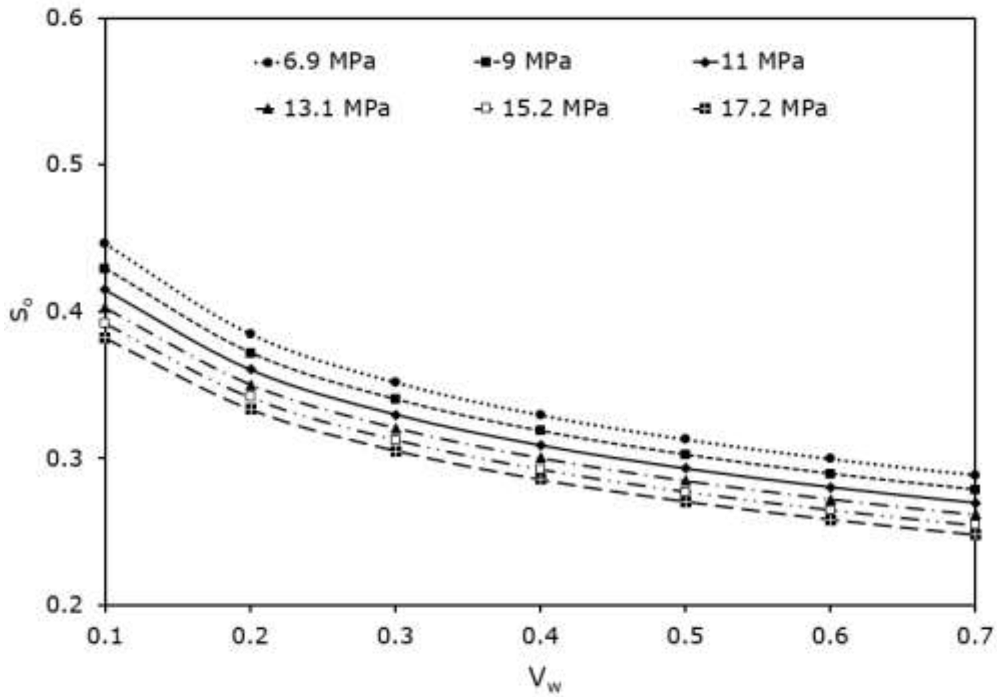

Figure 6.9. Variations in oil saturation at the fracture-matrix interface for different water volume injection and stress loading

Figures 6.10 and 6.11 depict the spatial variations in oil saturation for different injected V_w values at stress loading of 6.9 MPa and 17.2 MPa respectively. As the numerical model considered in this chapter is 2D, oil saturation variations are shown in the whole flow domain rather than at the fracture-matrix interface (as in chapter 5). The direction of flow is from left to right in the figure. It can be seen that as water is being injected into the tight reservoir model, oil is being displaced by it, and is recovered at the exit of the flow domain. With regards to the effects of stress loading on oil recovery, it can be seen that as stress loading increases, the volume of oil recovered at the exit increases due to the decrease in oil saturation, as shown in Figure 6.9.

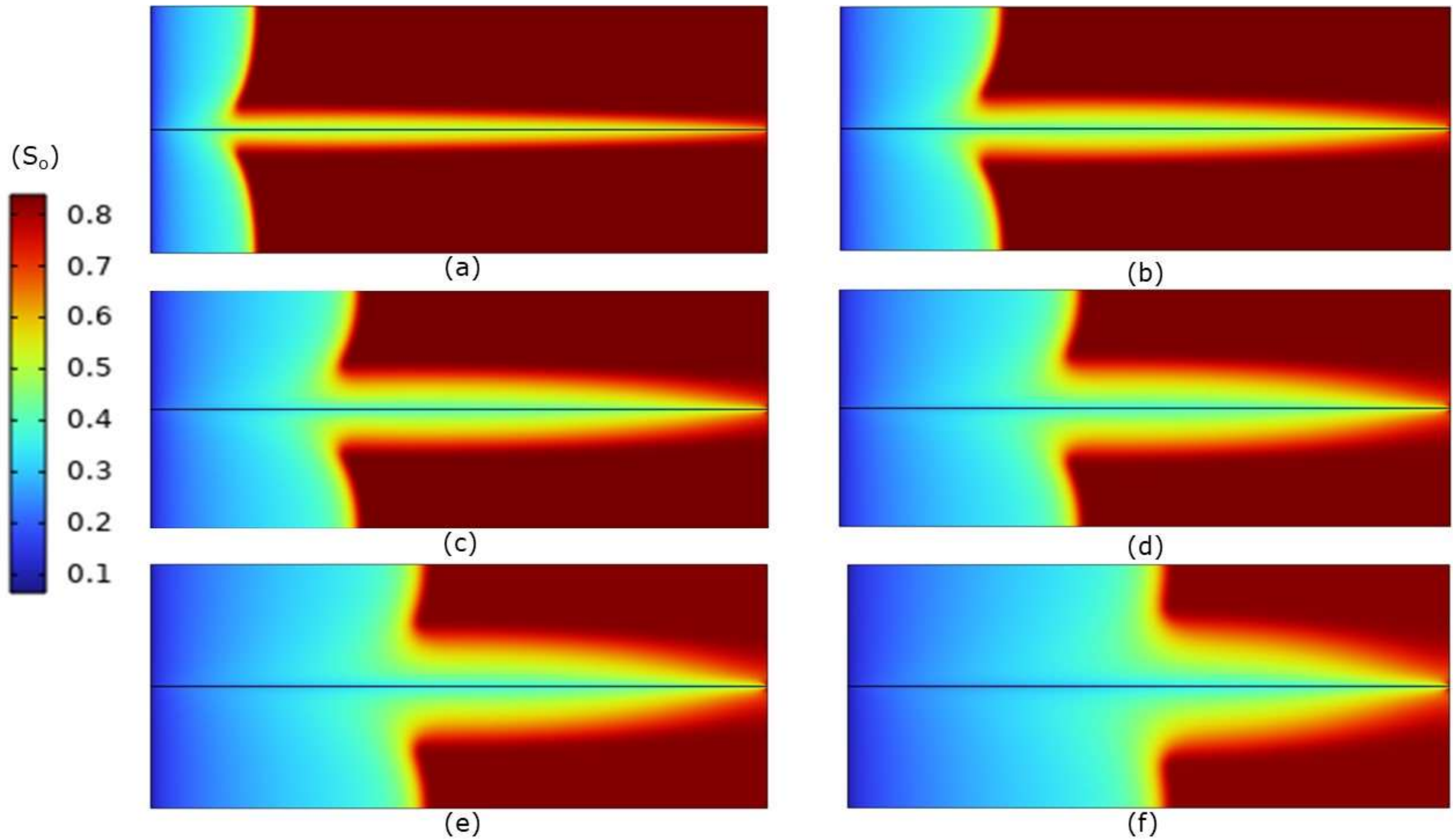

Figure 6.10. Variations in oil saturation at stress loading of 6.9 MPa and for injected water volume of (a) 10 % (b) 20 % (c) 30 % (d) 40 % (e) 50 % (f) 70 %

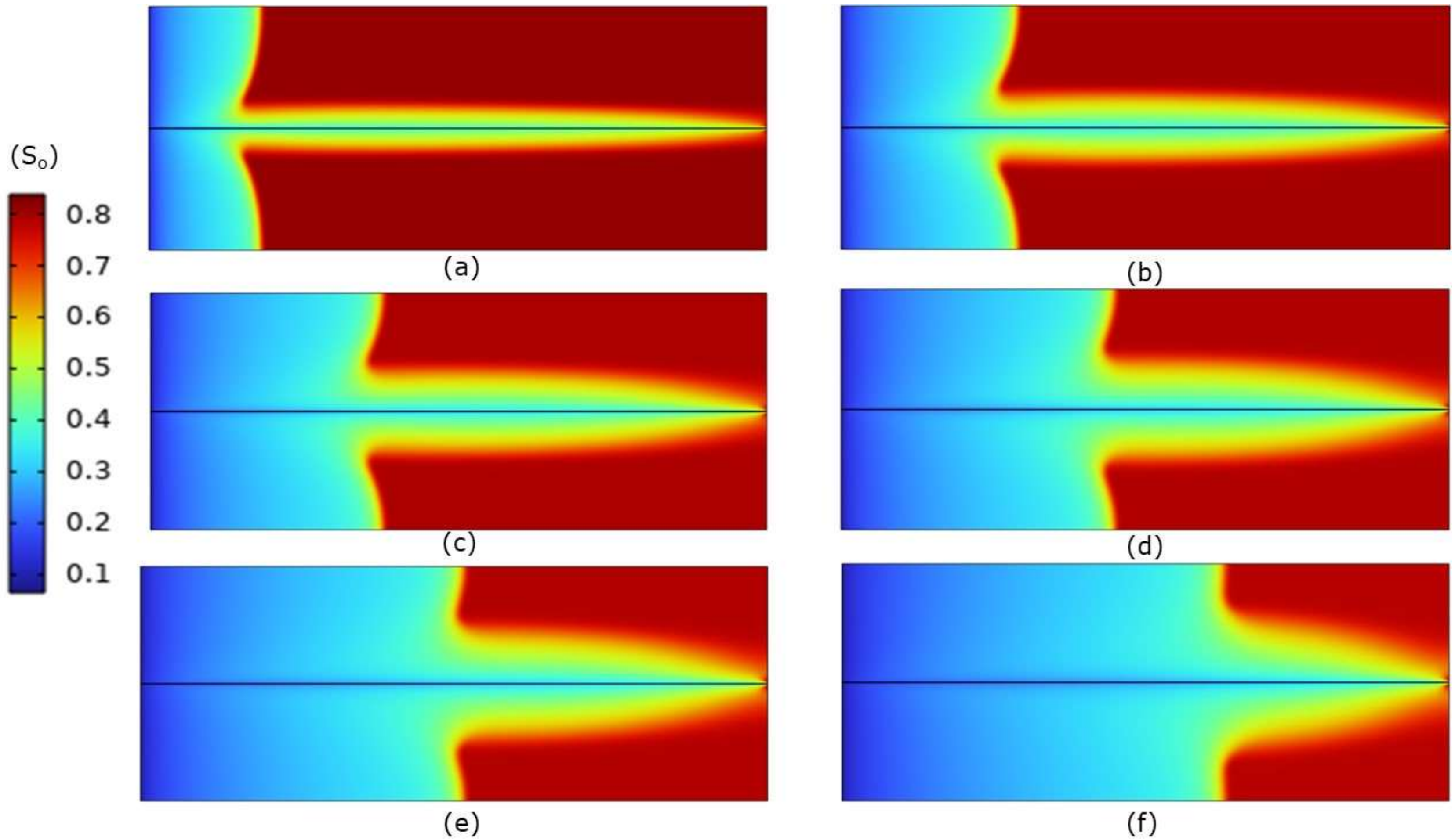

Figure 6.11. Variations in oil saturation at stress loading of 17.2 MPa and for injected water volume of (a) 10 % (b) 20 % (c) 30 % (d) 40 % (e) 50 % (f) 70 %

6.8 Stress-dependent Capillary Pressure

Figure 6.12 depicts the capillary pressure (*Pc*) variations for injected water volume (V_w) at different stress loading conditions. Since capillary pressure is a function of water saturation, it has been displayed against the volume of injected water. It can be seen in the figure that as the injected water volume increases, the capillary pressure decreases nonlinearly. The same trend has been observed previously in chapter 5 (Figure 5.14). With regards to the stress loading, for V_w=0.1, *Pc*=0.829 kPa at a stress loading of 6.9 MPa. At the same V_w, as stress loading increases to 9 MPa, 11 MPa, 13.1 MPa, 15.2 MPa, and 17.2 MPa, *Pc* decreases to 0.793 kPa, 0.764 kPa, 0.741 kPa, 0.721 kPa, and 0.705 kPa, respectively. Similarly, for V_w=0.3, *Pc*=0.572 kPa at a stress loading of 6.9 MPa. As the stress loading increases to 9 MPa, 11 MPa, 13.1 MPa, 15.2 MPa, and 17.2 MPa, *Pc* decreases to 0.560 kPa, 0.550 kPa, 0.541 kPa, 0.533 kPa, and 0.526 kPa, respectively. Thus, it is clear that as the stress loading increases for all V_w values, the capillary pressure decreases. Figure 6.13 further illustrates this by showing the capillary pressure versus the stress loading for V_w=0.1. It can be seen that the decrease in capillary pressure follows an almost linear pattern with increasing stress loading for one-way and fully coupled scheme. The capillary pressure remains high with increasing stress loading for a one-way coupled scheme, while it decreases reasonably for a fully coupled scheme. This is due to the difference in the two modelling approaches used here and the consideration of the pore pressure in case of fully coupled model.

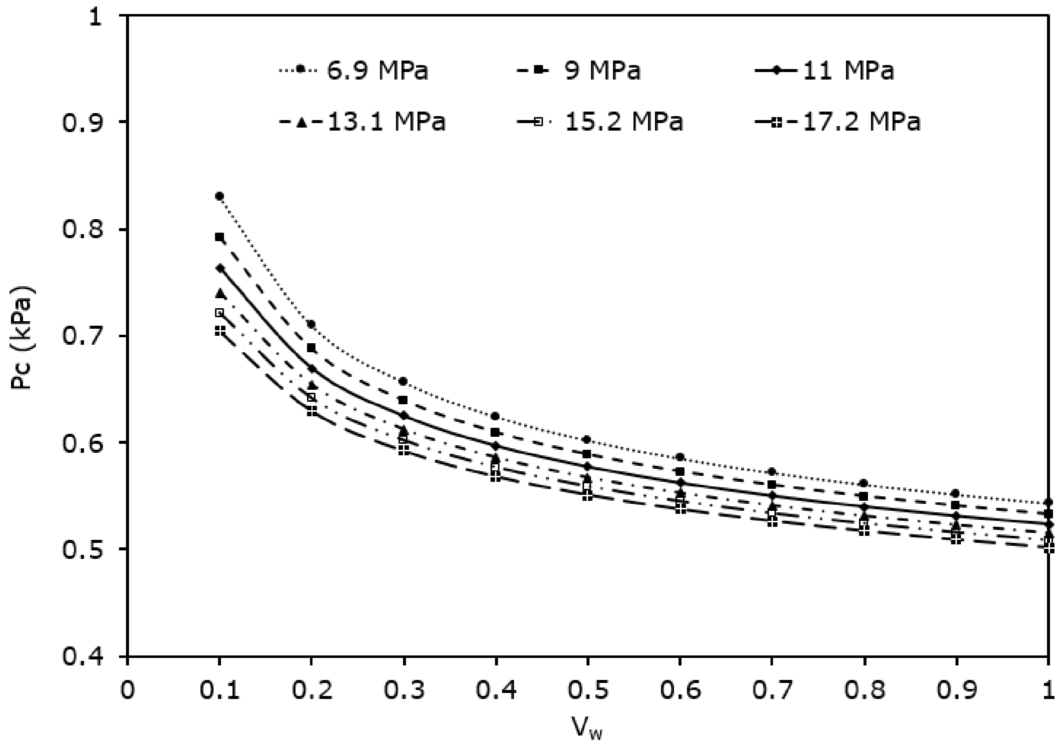

Figure 6.12. Capillary pressure variations w.r.t water volume injection

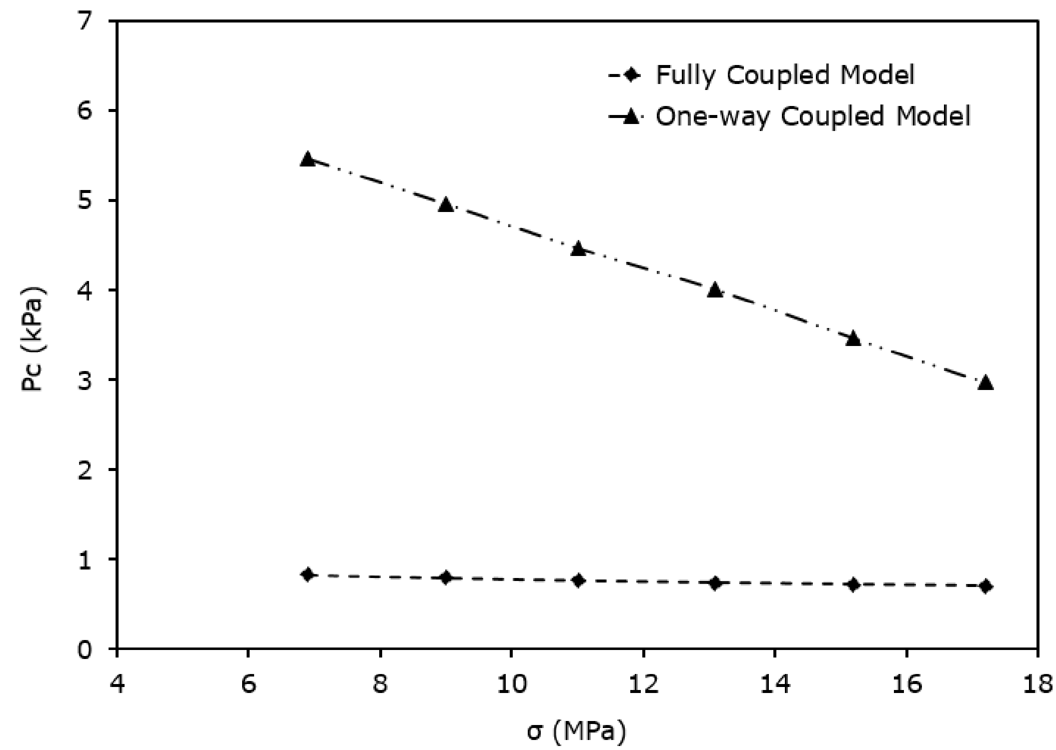

Figure 6.13. Capillary pressure variations w.r.t. stress loading at V_w=0.1

6.9 Stress-dependent Relative Permeability

Figure 6.14 depicts the fluctuations in relative permeabilities of water (Kr_w) and oil (Kr_o) at the fracture-matrix interface for water saturation (S_w) under various stress loading conditions. It is evident that when water saturation increases, the relative permeability of the oil reduces nonlinearly. The trends for water relative permeability are the opposite of those for oil relative permeability, meaning that as water saturation increases, water relative permeability increases nonlinearly. Both these trends have been observed in case of one-way coupled model as well however, the values are quite different. The relative permeability of water predicted by the fully coupled model is significantly less than predicted by the one-way coupled model because of the variations in the permeability and the pore sizes. The variations in *Kr* provide petroleum engineers with a measurable criterion to make decisions regarding the effectiveness of the oil recovery process, which is especially helpful for predicting the oil recovery from fractured tight reservoirs.

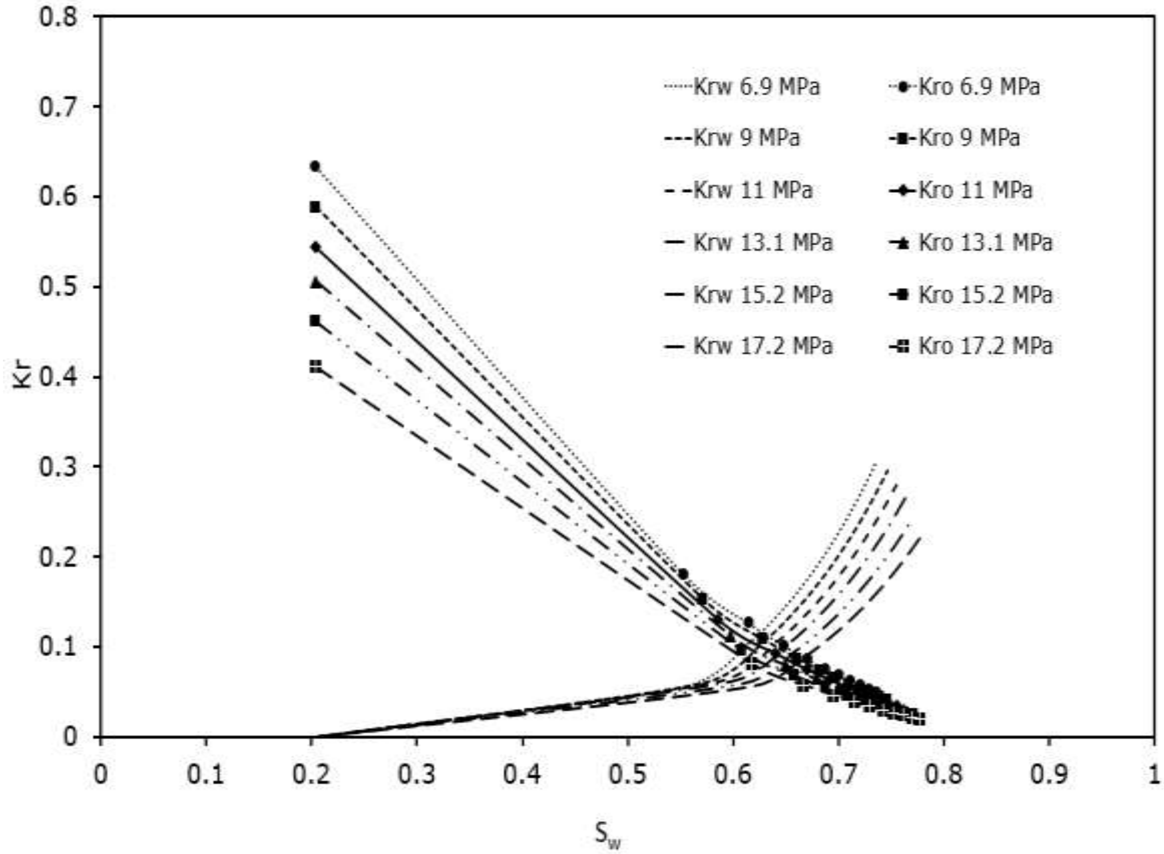

Figure 6.14. Relative permeability w.r.t water saturation

6.10 Summary of key findings

Extensive parametric investigations have been carried out in this chapter regarding the effects of geomechanical parameters on multiphase flow characterisation in naturally fractured tight reservoirs, utilising the concept of full coupling between the two. A summary of the key findings obtained is:

- Increase in stress loading decreases the porosity of the rock matrix. The difference in numerically predicted rock porosity is negligibly small compared to one-way coupled model (see figure 6.5)

- Increase in stress loading decreases the rock matrix permeability. The difference in numerically predicted matrix permeability is small compared to one-way coupled model (< 3 %) (see figure 6.6)
- Increase in stress loading decreases the fracture aperture. The difference in numerically predicted fracture aperture is 27 % higher compared to one-way coupled model (see figure 6.6)
- Increase in stress loading decreases the fracture permeability. The difference in numerically predicted fracture permeability is 84.6 % higher compared to one-way coupled model (see figure 6.7)
- Increase in stress loading increases water saturation and decreases oil saturation, thus increasing oil recovery. The variations in water saturation are less compared to one-way coupled model (see figures 6.8 and 6.9)
- Increase in stress loading decreases the capillary pressure (see figure 6.13)
- Increase in water saturation decreases the oil relative permeability and increases the water relative permeability (see figure 6.14)

Chapter 7
Conclusions

Through this chapter, specific inferences have been made based on the findings from the earlier chapters regarding the transient multiphase flow modelling, application of one-way coupling scheme, and the development of a novel full coupling methodology. The most significant accomplishments and novel contributions to the existing knowledge are presented and, whenever possible, linked to the study's research objectives. Finally, some recommendations have been provided for future research on coupling geomechanical parameters and multiphase flow characteristics in naturally fractured tight reservoirs.

7.1 Research Problem Synopsis

Conventionally, research studies on multiphase phase characterisation in naturally fractured tight reservoirs, from the point-of-view of estimating oil recovery from the reservoirs, have been carried out independent of any geomechanical aspects, and vice versa. More recently, with the advent of advanced numerical solvers and availability of higher computational power, research studies on coupling these two have started to emerge. However, these studies are still in their infancy period, focusing primarily on the global/overall behaviour of fluid flow and geomechanics of tight reservoirs. From critical review of published literature, it is clear that the fracture-matrix interface has a significant importance in oil recovery from tight reservoirs and thus, unless it is appropriately modelled and its characteristics (both fluid dynamics and geomechanical) are accurately predicted, numerical estimation of oil recovery from tight reservoirs will remain inaccurate.

In the present study, detailed numerical investigations have been carried out to address the aforementioned challenges. Independent multiphase flow models have been analysed in order to identify the most appropriate flow modelling techniques for accurate oil recovery predictions. The identified flow model has then been coupled with a geomechanical model, using one-way coupling scheme, to investigate the effects of external stress loading on the multiphase flow characteristics within naturally fractured tight reservoirs. In order to accurately capture multiphase flow phenomena at the fracture-matrix interface, a novel fully coupled model has been developed in this study.

Comparative analysis with one-way coupled model clearly show that the developed fully coupled model is far superior in predicting oil recovery from naturally fractured tight reservoirs.

7.2 Research Aims and Major Achievements

Major achievements of this research study, mapped against the research aims, are presented here.

Research Aim # 1: Evaluation of multiphase flow characteristics at the fracture-matrix interface in naturally fractured tight reservoirs.

Achievement # 1: The multiphase flow diagnostics in naturally fractured tight rocks are thoroughly investigated using CFD in this study, focusing on the prediction of complex flow features at the fracture-matrix interface. Two distinct multiphase flow models of the fractured reservoir have been developed in order to identify the most appropriate numerical modelling technique for the estimation of oil recovery. The numerical models have been validated against the experimental data, from published literature, on recovered oil volume recovery in naturally fractured rocks. A novel viscous loss term has been embedded into the momentum conservation equations for accurate prediction of multiphase flow phenomena at the fracture-matrix interface. Brooks and Corey method has been used to evaluate to evaluate relative permeabilities.

Based on the extensive numerical investigations of multiphase flow in naturally fractured tight reservoirs, both qualitative and quantitative analyses have been carried out on a wide range of flow parameters. These parameters include oil saturation, capillary pressure and relative permeability at the fracture-matrix interface. It has been identified that the most accurate method of modelling fracture region is to model it as a porous medium, rather than a duct. This is a major achievement of this work because a fracture, in real-world, resembles a duct. The porous media-based modelling technique has been shown to perform with superior accuracy and thus, this study paves the way for further scientific research in the area of oil recovery from tight reservoirs, with a special attention towards fracture-matrix interface.

Research Aim # 2: Establishment of interdependency between external loading and multiphase flow at the fracture-matrix interface in tight reservoirs for accurate oil recovery predictions.

Achievement # 2: One-way FEA-CFD coupling scheme has been employed in this study to investigate the effects external stress loading on the multiphase flow characteristics at the fracture-matrix interface. As geomechanical characteristics are essential to all naturally fractured rocks, they significantly affect the multiphase fluid flow behaviour at the fracture-matrix interface. A numerical model, based on one-way coupling scheme and the findings for research aim 1 above, has been created and validated against the experimental data. Systematic set of parametric investigations have been carried out in order to critically evaluate the effects of geomechanical parameters on multiphase flow characteristics at the fracture-matrix interface.

Detailed analyses of the results obtained in the present study reveal the intricate dependency of multiphase flow variables on the geomechanical parameters naturally fractured tight reservoirs. The major achievement of this study is to accurately predict the effects of external stress loading on the geomechanical parameters i.e. fracture aperture and matrix porosity, and on the multiphase flow parameters i.e. fracture and matrix permeabilities and relative permeabilities, capillary pressure and oil saturation, at the fracture-matrix interface. The study also reveals the intricate relationship between injected water volume, water saturation and relative permeability of the matrix and the fracture.

Research Aim # 3: Development of a novel approach for accurate characterisation of geomechanics and multiphase flow in naturally fractured tight reservoirs.

Achievement # 3: A novel numerical methodology has been developed in the present study to evaluate the relationships between the geomechanical and multiphase flow characteristics in naturally fractured tight reservoirs. The novel methodology is based on full coupling between geomechanics and fluid flow, where the governing equations of both these are solved simultaneously. With the inclusions of pore pressure as a variable, as observed in real-world situations, the fully couple methodology is significantly more accurate in predicting geomechanical and fluid flow behaviour in naturally fractured tight reservoirs. Thus, the novel coupling methodology developed here is a major achievement of the present study.

Based on extensive numerical investigations employing fully coupled model, the estimation of recovered oil from the tight reservoir is has considerably improved. Stress-dependent geomechanical and multiphase flow parameters have been extensively investigated and the numerically predicted results compared with the ones obtained from one-way coupled model. It has been observed that the novel fully coupled model significantly enhances the prediction capability of the numerical solver. Thus, this study opens the door for further cutting-edge scientific research for further developments in numerical modelling of naturally fractured tight reservoirs.

7.3 Thesis Conclusions

An extensive numerical study has been conducted to support the body of knowledge regarding coupled geomechanics and transient multiphase flow characterisation at the fracture-matrix interface, and to offer unique insights to advance the scientific understanding of the oil recovery process in naturally fractured tight reservoirs. The following are the conclusions of the main findings from each research objective of this research study.

Research Objective # 1: Comparative analysis of numerically modelling natural fracture in tight reservoirs as a duct and as a porous medium, leading to the identification of the most appropriate modelling technique.

Conclusion # 1: From the investigations regarding the appropriate numerical modelling of multiphase flow of naturally fractured tight reservoirs, it can be concluded that the fracture region is of key importance and needs special attention for accurate prediction of complex flow behaviour in it. Two CFD based modelling techniques have been employed and comparative analyses between them carried out. It has been found that modelling the fracture region as a porous media yields more accurate results in representing multiphase flow, compared to modelling it as a duct. This is because the flow resistance offered by the porous media yields more realistic results, along with the flow in the core region.

Research Objective # 2: Transient multiphase flow diagnostics at the fracture-matrix interface of naturally fractured tight reservoirs through the introduction of a novel source terms in the momentum governing equations.

Conclusion # 2: A viscous loss term has been embedded in the momentum conservation equations while numerically solving for transient multiphase flow in naturally fractured tight reservoirs. The numerical results have been validated against Berea Sandstone core flooding experiments. Detailed analyses on multiphase flow characteristics, such as relative permeability, capillary pressure and fluid saturations, are computed at the fracture-matrix interface to evaluate the multiphase flow behaviour. Based on the results obtained, it can be concluded that the addition of the loss term has resulted in enhanced accuracy of the numerical predictions regrading multiphase flow characteristics at the fracture-matrix interface. This is because the viscous source term adds further resistance to the flow in the fractured reservoir, which yields more realistic results.

Research Objective # 3: Implementation of one-way coupling scheme on the geomechanical and multiphase flow parameters for realistic estimation of oil recovery from naturally fractured tight reservoirs.

Conclusion # 3: One-way FEA-CFD coupling between geomechanical parameters and multiphase flow characteristics has been numerically implemented in order to accurately predict oil recovery in naturally fractured tight reservoirs. The dependency of multiphase flow characteristics on the geomechanical parameters has been critically evaluated, based on key hydraulic parameters of naturally fractured tight reservoirs. The results obtained clearly indicate significant enhancement in the accuracy of numerical predictions, on parameters such as capillary pressure, fluid saturation, permeability etc, when the reservoir sample is modelled using one-way coupling scheme. The reason for the enhanced accuracy is the consideration of external stress loading on the geomechanical and multiphase flow characterisations during oil production, in the naturally fractured tight reservoirs.

Research Objective # 4: Numerical investigations on the effects of geomechanical parameters on multiphase flow characteristics at the fracture-matrix interface of naturally fractured tight reservoirs.

Conclusion # 4: Systematic numerical investigations have been carried out to evaluate the effects of externally applied stress loading (on the core sample) on the multiphase flow characteristics. Based on the results obtained it can be concluded that stress loading significantly impacts multiphase flow parameters at the fracture-matrix interface. The porosity and permeability of the rock matrix has been observed to decrease as the stress loading increases because external stresses cause the pore size and the fracture aperture to decrease. The capillary pressure decreases due to increase in stress loading at the fracture-matrix interface. The fracture-matrix interface area becomes more water wet when the stress loading increases. Moreover, as the stress loading increases, the relative permeability curves shift towards right because of pore size deformations and capillary pressure changes.

Research Objective # 5: Development of a novel fully coupled scheme for enhanced oil recovery predictions from naturally fractured tight reservoirs.

Conclusion # 5: A novel fully coupled numerical model has been developed for enhanced accuracy in predicting oil recovery from naturally fractured tight reservoirs. The simultaneous coupling between the geomechanical and transient multiphase flow characteristics takes into consideration the pore pressure within the reservoir. The porous medium discontinuity boundary condition is added to accurately capture the complicated multiphase flow behaviour at the fracture-matrix interface. The numerically predicted results indicate that the oil volume reduces significantly at the fracture-matrix interface, while the water volume increases, as the stress loading increases on the core sample. This is because the application of external stress loading decreases the fracture aperture, thus increasing oil recovery from the reservoir.

Research Objective # 6: Comparative analysis of one-way and novel fully coupled schemes for the estimation of oil recovery from naturally fractured tight reservoirs.

Conclusion # 6: The numerically predicted geomechanical and multiphase flow characteristics obtained through the use of fully coupled model have been compared against the one-way coupled model. Based on the results obtained, it can be concluded that water saturation from the fully coupled model is considerably less than from one-way coupled model. The same is observed in case of oil saturation. This is because the pore pressure is considered in case of fully coupled model. One-way coupled model over predicts oil recovery from naturally fractured tight reservoirs. When compared against the experimental data, fully coupled model, in comparison to one-way coupled model, improves the accuracy in predicting cumulative oil discharge from 9 % to 4 %. Thus, the fully coupled model is more accurate and the full coupling methodology adopted is more suitable for further scientific investigations. The reason behind this enhanced accuracy is that the effect of pore fluid compression, or expansion, is considered in the fully coupled model.

7.4 Novel Contributions to Knowledge

This study presents a number of novel contributions to the knowledge regarding geomechanics, multiphase flow and oil recovery from naturally fractured tight reservoirs. These novel contributions are presented below.

Contribution # 1:

A significant novel contribution of the present study is the establishment of complex multiphase flow characteristics within naturally fractured tight reservoirs, especially at the fracture-matrix interface. The published literature clearly indicates that multiphase flow characterisation at fracture-matrix interface is quite intricate and needs a lot more attention. With a clear disparity between physical understanding and numerical interpretation of the fracture regions, the author was able to conduct detailed and well-validated numerical investigations using both the approaches. Moreover, with the introduction of the viscous loss term in the momentum equations ensured accurate representation of multiphase flow behaviour at the fracture-matrix interface. The identification of the most appropriate (and accurate) modelling technique, based on porous medium approach for the fracture region, is a significant novel contribution to the existing knowledge.

Contribution # 2:

A significant novel contribution of this study is the implementation of one-way coupling scheme to investigate the effects of geomechanical parameters on multiphase flow characteristics at the fracture-matrix interface of naturally fractured tight reservoirs, leading to realistic oil recovery predictions. The published literature lacks severely in coupling strategies to accurately model the complex flow behaviour at the fracture-matrix interface. The effects of geomechanical parameters on transient multiphase flow characteristics have been extensively investigated in the present study. The effects of externally applied stress loading on the porosity, permeability, relative permeability, capillary pressure and fluid saturation at the fracture-matrix interface have been numerically investigated. This has led to a better understanding of the complexities involved in modelling fracture-matrix interface and its impact on oil recovery prediction in naturally fractured tight reservoirs.

Contribution # 3:

A novel full coupling methodology has been developed in the present study to significantly enhance the accuracy of numerical predictions regarding the geomechanical behaviour and stress-dependent multiphase flow characterisation of naturally fractured tight reservoirs. Special attention has been given towards accurate modelling of the fracture-matrix interface while developing the fully coupled model. Comparative analysis with one-way coupled model clearly indicates enhanced accuracy of the fully coupled model in predicting geomechanical and multiphase flow behaviour at the fracture-matrix interface. The development of a fully coupled model is a significant scientific advancement as no such models exist in the published literature for modelling naturally fractured tight reservoirs.

7.5 Future Recommendations

The current study provides novel insights into geomechanics and multiphase flow characterisation in naturally fractured tight reservoirs, focusing on accurate modelling of fracture-matrix interface and allowing knowledge gaps in the published literature to be bridged. Based on the concluding remarks in the preceding section, a number of areas with considerable potential for further scientific research and development have been uncovered.

Recommendation # 1: Another recommendation for future scientific research is to investigate the effects of stress on solute transport in three-dimensional fracture networks. The FEM-CFD model's nonlinear behaviour in predicting fracture parameters, like opening/closing, shearing, and dilation, in response to externally applied stress, can result in complicated multiphase flow fields in the fracture networks. Extensive parametric investigations are required to accurately model solute transport in naturally fractured tight reservoirs.

Recommendation # 2: Experimental data on multiphase flow in naturally fractured tight reservoirs, under the application of external stress loading, is non-existent in the published literature. Thus, there is a need to carry out systematic set of empirical investigations on this and the recorded data to be published.

Recommendation # 3: Another unexplored area of potential future work is the use of advance analytical models, like Proper Orthogonal Decomposition, leading to the development of Reduced Order Models for rapid estimation of oil recovery from naturally fractured tight reservoirs, without the need of extensive and time consuming numerical modelling.

Recommendation # 4: The effects of temperature change (thermal effects) during the application of external stress loading on the rock matrix, on the geomechanical and multiphase flow characterisations at the fracture-matrix interface in naturally fractured tight reservoirs can be considered.

References

Abbas, F., 2000. Recovery Mechanisms in Fractured Reservoirs and Field Performance. J. Can. Pet. Technol. 39, 13–17. https://doi.org/https://doi.org/10.2118/00-11-DAS

Abdel Azim, R., 2022. Finite Element Model to Simulate Two-Phase Fluid Flow in Naturally Fractured Oil Reservoirs: Part i. ACS Omega 7, 27278–27290. https://doi.org/10.1021/acsomega.2c02223

Abdelazim, R., Rahman, S.S., 2016. Journal of Petroleum Science and Engineering Estimation of permeability of naturally fractured reservoirs by pressure transient analysis : An innovative reservoir characterization and fl ow simulation Fractur Matrix block. J. Pet. Sci. Eng. 145, 404–422. https://doi.org/10.1016/j.petrol.2016.05.027

Ahmed, B.I., Al-Jawad, M.S., 2020. Geomechanical modelling and two-way coupling simulation for carbonate gas reservoir. J. Pet. Explor. Prod. Technol. 10, 3619–3648. https://doi.org/10.1007/s13202-020-00965-7

Ahmed, T., 2019. Reservoir Engineering Handbook, Fifth. ed, Gulf Professional Publishing. Elsevier Inc. https://doi.org/https://doi.org/10.1016/C2016-0-04718-6

Ahmed, T., 2001. Reservoir Engineering Handbook.

Ahmed, T., Mckinney, P., 2004. Advanced Reservoir Engineering. Gulf Professional

Publishing.

Akin, S., 2001. Estimation of fracture relative permeabilities from unsteady state corefloods. J. Pet. Sci. Eng. 30, 1–14. https://doi.org/https://doi.org/10.1016/S0920-4105(01)00097-3

Alyafei, N., 2021. Fundamentals of reservoir rock properties, second. ed, Fundamentals of Reservoir Rock Properties. https://doi.org/10.1007/978-3-030-28140-3

Alymann, J.B., 2010. Poroelastic effects in reservoir modelling. Universität Karlsruhe.

Bagheri, M., Settari, A., 2005. Modeling of geomechanics in naturally fractured reservoirs. SPE Reserv. Simul. Symp. Proc. 11, 235–246. https://doi.org/SPE-93083-PA

Bai, J., Sierra, L., Martysevich, V., 2019. Recompletion with Consideration of Depletion Effect in Naturally Fractured Unconventional Reservoirs, in: 53rd U.S. Rock Mechanics/Geomechanics Symposium. American Rock Mechanics Association, New York City, New York. https://doi.org/ARMA-2019-0321

Bai, M., Elsworth, D., 1994. Modeling of subsidence and stress-dependent hydraulic conductivity for intact and fractured porous media. Rock Mech. Rock Eng. 27, 209–234. https://doi.org/10.1007/BF01020200

Bai, M., Meng, F., Elsworth, D., Zaman, Z., Roegiers, J.C., 1997. Numerical modeling of stress-dependent permeability. Int. J. rock Mech. Min. Sci.

Geomech. Abstr. 34, 446. https://doi.org/10.1016/S1365-1609(97)00056-7

Baker, R.O., Yarranton, H.W., Jensen, J.L., 2015. Special Core Analysis—Rock–Fluid Interactions, in: Practical Reservoir Engineering and Characterization. pp. 239–295. https://doi.org/10.1016/b978-0-12-801811-8.00008-0

Baran, I., Cinar, K., Ersoy, N., Akkerman, R., Hattel, J.H., 2017. A Review on the Mechanical Modeling of Composite Manufacturing Processes. Arch. Comput. Methods Eng. 24, 365–395. https://doi.org/https://doi.org/10.1007/s11831-016-9167-2

Barth, T., Jespersen, D., 1989. The design and application of upwind schemes on unstructured meshes, AIAA 27th Aerospace Sciences Meeting. Reno, Nevada. https://doi.org/10.2514/6.1989-366

Bauer, J.F., Krumbholz, M., Meier, S., Tanner, D.C., 2017. Predictability of properties of a fractured geothermal reservoir: the opportunities and limitations of an outcrop analogue study. Geotherm. Energy 5:24. https://doi.org/10.1186/s40517-017-0081-0

Berge, R.L., Berre, I., Keilegavlen, E., Nordbotten, J.M., 2019. Viscous fingering in fractured porous media 1–15.

Berre, I., Doster, F., Keilegavlen, E., 2019. Flow in Fractured Porous Media: A Review of Conceptual Models and Discretization Approaches. Transp. Porous Media 130, 215–236. https://doi.org/10.1007/s11242-018-1171-6

Bertels, S.P., DiCarlo, D.A., Blunt, M.J., 2001. Measurement of aperture distribution, capillary pressure, relative permeability, and in situ saturation in a rock fracture using computed tomography scanning. Water Resour. Res. 37, 649–662. https://doi.org/10.1029/2000WR900316

Biot, M.A., 1962. Mechanics of deformation and acoustic propagation in porous media. J. Appl. Phys. 33, 1482–1498. https://doi.org/10.1063/1.1728759

Biot, M.A., 1956. Theory of Propagation of Elastic Waves in a Fluid-Saturated Porous Solid. J. Acoust. Soc. Am. 28, 168–178. https://doi.org/10.1121/1.1908239

Biot, M.A., 1941. General theory of three-dimensional consolidation. J. Appl. Phys. 12, 155–164. https://doi.org/https://doi.org/10.1063/1.1712886

Bogdanov, I.I., Mourzenko, V. V., Thovert, J.F., Adler, P.M., 2003. Effective permeability of fractured porous media in steady state flow. Water Resour. Res. 39, 1–16. https://doi.org/10.1029/2001WR000756

British Petroleum Company, 2017. BP Energy Outlook Energy 2017. BP Stat. Rev. World Energy 1–103. https://doi.org/10.1017/CBO9781107415324.004

Brooks, R.H., Corey, A.T., 1966. Properties of Porous Media Affecting Fluid Flow. J. Irrig. Drain. Div. 92, 61–88.

Cai, Y., Sun, H., 2017. Basic Equations and Governing Equations, in: Solutions for Biot ’s Poroelastic Theory in Key Engineering Fields. Elsevier Ltd., pp. 1–8. https://doi.org/https://doi.org/10.1016/B978-0-12-812649-3.00001-0.

Cao, N., Lei, G., Dong, P., Li, H., Wu, Z., Li, Y., 2019. Stress-Dependent

Permeability of Fractures in Tight Reservoirs. Energies 12. https://doi.org/10.3390/en12010117

Carrillo, F.J., Bourg, I.C., Soulaine, C., 2020. Multiphase flow modeling in multiscale porous media: An open-source micro-continuum approach. J. Comput. Phys. X 8, 100073. https://doi.org/10.1016/j.jcpx.2020.100073

Cervera, M., Codina, R., Galindo, M., 1996. On the computational efficiency and implementation of block-iterative algorithms for nonlinear coupled problems. Eng. Comput. (Swansea, Wales) 13, 4–30. https://doi.org/10.1108/02644409610128382

Chapman, R.E., 1983. Chapter 8 The Nature of Petroleum Reservoirs. Dev. Pet. Sci. 16, 155–178. https://doi.org/10.1016/S0376-7361(08)70092-X

Charoenwongsa, S., Kazemi, H., Miskimins, J., Fakcharoenphol, P., 2010. A Fully-Coupled Geomechanics and Flow Model for Hydraulic Fracturing and Reservoir Engineering Applications, in: Canadian Unconventional Resources and International Petroleum Conference 2010. Society of Petroleum Engineers, Calgary, Alberta, Canada, pp. 1460–1490. https://doi.org/10.2118/137497-ms

Chen, Z., Narayan, S.P., Yang, Z., Rahman, S.S., 2000. An experimental investigation of hydraulic behaviour of fractures and joints in granitic rock. Int. J. Rock Mech. Min. Sci. 37, 1061–1071. https://doi.org/10.1016/S1365-1609(00)00039-3

Cheng, P., Shen, W., Xu, Q., Lu, X., Qian, C., Cui, Y., 2022. Multiphysics coupling study of near-wellbore and reservoir models in ultra-deep natural gas reservoirs. J. Pet. Explor. Prod. Technol. https://doi.org/10.1007/s13202-021-01424-7

Cheng, S., Zhang, M., Zhang, X., Wu, B., Chen, Z., Lei, Z., Tan, P., 2022. Numerical study of hydraulic fracturing near a wellbore using dual boundary element method. Int. J. Solids Struct. 239–240, 111479. https://doi.org/10.1016/j.ijsolstr.2022.111479

Chiaramonte, L., Zoback, M., Friedmann, J., Stamp, V., Zahm, C., 2011. Fracture characterization and fluid flow simulation with geomechanical constraints for a CO2–EOR and sequestration project Teapot Dome Oil Field, Wyoming, USA. Energy Procedia 4, 3973–3980. https://doi.org/10.1016/j.egypro.2011.02.337

Chin, L.Y., Thomas, L.K., Sylte, J.E., Pierson, R.G., 2002. Iterative coupled analysis of geomechanics and fluid flow for rock compaction in reservoir simulation. Oil Gas Sci. Technol. 57, 485–497. https://doi.org/10.2516/ogst:2002032

Craig, J., Gerali, F., Macaulay, F., Sorkhabi, R., 2018. The history of the European oil and gas industry (1600s-2000s). Geol. Soc. Spec. Publ. 465, 1–24. https://doi.org/10.1144/SP465.23

Curnow, J.S., Tutuncu, A.N., 2015. Coupled geomechanics and fluid flow model for production optimization in naturally fractured shale reservoirs. SEG Tech. Progr. Expand. Abstr. 34, 399–403. https://doi.org/10.1190/segam2015-5928833.1

Dandekar, A.Y., 2013. Petroleum reservoir rock and fluid properties, second edition, Second. ed, Petroleum Reservoir Rock and Fluid Properties, Second Edition.

CRC Press, New York.

Daniel, E.J., 1954. FRACTURED RESERVOIRS OF MIDDLE EAST. Am. Assoc. Pet. Geol. Bull. 38, 774–815. https://doi.org/https://doi.org/10.1306/5CEADF0E-16BB-11D7-8645000102C1865D

Darcy, H., 1856. Les fontaines publiques de la ville de Dijon : exposition et application des principes à suivre et des formules à [...]. Paris, Dijon.

Dazel, O., Dauchez, N., 2009. The Finite Element Method for Porous Materials, in: Materials and Acoustics Handbook (Eds M. Bruneau and C. Potel). pp. 327–338. https://doi.org/10.1002/9780470611609.ch12

de Hoop, S., Voskov, D. V., Bertotti, G., Barnhoorn, A., 2022. An Advanced Discrete Fracture Methodology for Fast, Robust, and Accurate Simulation of Energy Production From Complex Fracture Networks. Water Resour. Res. 58. https://doi.org/10.1029/2021WR030743

Dean, R.H., Gai, X., Stone, C.M., Minkoff, S.E., 2006. A comparison of techniques for coupling porous flow and geomechanics. SPE J. 11, 132–140. https://doi.org/10.2118/79709-PA

Diomampo, G.P., 2001. Relative Permeability Through Fractures. USA. https://doi.org/https://doi.org/10.2172/896520

Doonechaly, N.G., Rahman, S.S., Kotousov, A., 2013. A New Approach to Hydraulic Stimulation of Geothermal Reservoirs by Roughness Induced Fracture Opening, in: Bunger, A. P. , McLennan, J. , Jeffrey, R. (Ed.), Effective and Sustainable

Hydraulic Fracturing. IntechOpen, London. https://doi.org/http://dx.doi.org/10.5772/56447

Doster, F., Nordbotten, J.M., 2015. Full Pressure Coupling for Geo-mechanical Multi-phase Multi-component Flow Simulations, in: SPE Reservoir Simulation Symposium. Society of Petroleum Engineers, Houston, Texas, USA, pp. 742–753. https://doi.org/SPE-173232-MS

Dubinya, N., Lukin, S., Chebyshev, I., 2015. Two-Way Coupled Geomechanical Analysis of Naturally Fractured Oil Reservoir’s Behavior Using Finite Element Method, in: SPE Russian Petroleum Technology Conference. Society of Petroleum Engineers, Moscow, Russia. https://doi.org/SPE-176631-MS

Falode, O., Manuel, E., 2014. Wettability Effects on Capillary Pressure, Relative Permeability, and Irredcucible Saturation Using Porous Plate. J. Pet. Eng. 2014, 1–12. https://doi.org/10.1155/2014/465418

Fanchi, J.R., 2018. Chapetr 6: Fluid Properties and Model Initialization, in: Principles of Applied Reservoir Simulation. pp. 101–120. https://doi.org/10.1016/b978-0-12-815563-9.00006-9

Federico, S., Grillo, A., 2012. Elasticity and permeability of porous fibre-reinforced materials under large deformations. Mech. Mater. 44, 58–71. https://doi.org/10.1016/j.mechmat.2011.07.010

Feng, X., Peng, X., Li, L., Yang, X., Wang, J., Li, Q., Zhang, C., Deng, H., 2019. Influence of reservoir heterogeneity on water invasion differentiation in carbonate gas reservoirs. Nat. Gas Ind. B 6, 7–15.

https://doi.org/10.1016/j.ngib.2019.01.002

Fernø, M., 2008. A study of capillary pressure and capillary continuity in fractured rocks. University of Bergn.

Fjær, E., Holt, R.M., Horsrud, P., Raeen, A.M., Risens, R., 2008. PETROLEUM RELATED ROCK MECHANICS, 2nd ed. Elsevier B.V. https://doi.org/10.1016/0148-9062(93)92632-Z

Fourar, M., Bories, S., Lenormand, R., Persoff, P., 1993. Two-phase flow in smooth and rough fractures: Measurement and correlation by porous-medium and pipe flow models. Water Resour. Res. 29, 3699– 3708. https://doi.org/doi:10.1029/93WR01529

Fredrich, J.T., Arguello, J.G., Deitrick, G.L., De Rouffignac, E.P., 2000. Geomechanical Modeling of Reservoir Compaction, Surface Subsidence, and Casing Damage at the Belridge Diatomite Field. SPE Reserv. Eval. Eng. 3, 348–359. https://doi.org/10.2118/65354-PA

Fredrich, J.T., Arguello, J.G., Thorne, B.J., Wawersik, W.R., Deitrick, G.L., de Rouffignac, E.P., Myer, L.R., Bruno, M.S., 1996. Three-Dimensional Geomechanical Simulation of Reservoir Compaction and Implications for Well Failures in the 8elridge Diatomite, in: SPE Annual Technical Conference and Exhibition. Society of Petroleum Engineers, Denver, Colorado, pp. 13–28. https://doi.org/10.2523/36698-ms

Fung, L.S., 1991. Simulation of Block-to-Block Processes in Naturally Fractured Reservoirs. SPE Res Eng 6, 477–484.

https://doi.org/https://doi.org/10.2118/20019-PA

Ganat, T.A.A.O., 2019. Fundamentals of reservoir rock properties, Fundamentals of Reservoir Rock Properties. https://doi.org/10.1007/978-3-030-28140-3

Gangi, A.F., 1978. Variation of whole and fractured porous rock permeability with confining pressure. Int. J. Rock Mech. Min. Sci. 15, 249–257. https://doi.org/10.1016/0148-9062(78)90957-9

Garg, S.K., Nur, A., 1973. Effective Stress Laws for Fluid-Saturated Porous Rocks. J. Geophys. Res. 78, 5911–5921. https://doi.org/10.1029/jb078i026p05911

Garipov, T.T., Karimi-Fard, M., Tchelepi, H.A., 2016. Discrete fracture model for coupled flow and geomechanics. Comput. Geosci. 20, 149–160. https://doi.org/10.1007/s10596-015-9554-z

Giani, G., Orsatti, S., Peter, C., Rocca, V., 2018. A coupled fluid flow-geomechanical approach for subsidence numerical simulation. Energies 11. https://doi.org/10.3390/en11071804

Glass, R.J., 1993. Modeling gravity-driven fingering in rough-walled fractures using modified percolation theory. High Lev. Radioact. Waste Manag. 2042–2060.

Glass, R.J., Nicholl, M.J., Yarrington, L., 1998. A modified invasion percolation model for low-capillary number immiscible displacements in horizontal rough-walled fractures: Influence of local in-plane curvature. Water Resour. Res. 34, 3215–334. https://doi.org/10.1029/2000wr900060

Golf-Racht, T.D. Van, 1982. Fundamentals of Fractured Reservoirs, 1st ed. Elsevier

B.V.

Gudala, M., Govindarajan, S.K., 2021. Numerical investigations on two-phase fluid flow in a fractured porous medium fully coupled with geomechanics. J. Pet. Sci. Eng. 199, 108328. https://doi.org/10.1016/j.petrol.2020.108328

Gudala, M., Govindarajan, S.K., 2020. Numerical modelling of coupled single-phase fluid flow and geomechanics in a fractured porous media. J. Pet. Sci. Eng. 191, 107215. https://doi.org/10.1016/j.petrol.2020.107215

Guy, N., Enchéry, G., Renard, G., 2012. Numerical Modeling of Thermal EOR: Comprehensive Coupling of an AMR-Based Model of Thermal Fluid Flow and Geomechanics. Oil Gas Sci. Technol. 67, 1019–1027. https://doi.org/10.2516/ogst/2012052

Haghi, A.H., Chalaturnyk, R., 2022. Experimental Characterization of Hydrodynamic Properties of a Deformable Rock Fracture. Energies 15. https://doi.org/10.3390/en15186769

Haghi, A.H., Chalaturnyk, R., Geiger, S., 2018. New Semi-Analytical Insights Into Stress-Dependent Spontaneous Imbibition and Oil Recovery in Naturally Fractured Carbonate Reservoirs. Water Resour. Res. 54, 9605–9622. https://doi.org/10.1029/2018WR024042

Haghi, A.H., Chalaturnyk, R., Talman, S., 2019. Stress-Dependent Pore Deformation Effects on Multiphase Flow Properties of Porous Media. Sci. Rep. 9, 1–10. https://doi.org/10.1038/s41598-019-51263-0

Hernandez-Perez, V., Abdulkadir, M., Azzopardi, B.J., 2011. Grid generation issues in the CFD modelling of two-phase flow in a pipe. J. Comput. Multiph. Flows 3, 13–26. https://doi.org/10.1260/1757-482X.3.1.13

Hirt, C.W., Nichols, B.D., 1981. Volume of Fluid (VOF) Method for the Dynamics of Free Boundaries. J. Comput. Phys. 39, 201–225. https://doi.org/10.1007/s40998-018-0069-1

Hogg, P.W., Gu, X.-J., Emerson, D.R., 2006. an Implicit Algorithm for Capturing Sharp Fluid Interfaces in the Volume of Fluid Advection Method. Eur. Conf. Comput. Fluid Dyn. ECCOMAS CFD 1–20.

Hommel, J., Coltman, · Edward, Class, · Holger, 2018. Porosity-Permeability Relations for Evolving Pore Space: A Review with a Focus on (Bio-)geochemically Altered Porous Media. Transp. Porous Media 124, 589–629. https://doi.org/10.1007/s11242-018-1086-2

Honarpour, M., Koederitz, L., Harvey, A.H., 1986. Relative permeability of petroleum reservoirs, First. ed, Relative Permeability of Petroleum Reservoirs. CRC Press, New York. https://doi.org/10.1201/9781351076326

Huang, N., Jiang, Y., Liu, R., Li, B., Sugimoto, S., 2019. A novel three-dimensional discrete fracture network model for investigating the role of aperture heterogeneity on fluid flow through fractured rock masses. Int. J. Rock Mech. Min. Sci. 116, 25–37. https://doi.org/10.1016/j.ijrmms.2019.03.014

Huo, D., Benson, S.M., 2016. Experimental Investigation of Stress-Dependency of Relative Permeability in Rock Fractures. Transp. Porous Media 113, 567–590.

https://doi.org/10.1007/s11242-016-0713-z

Huo, D., Li, B., Benson, S.M., 2014. Investigating aperture-based stress-dependent permeability and capillary pressure in rock fractures. Proc. - SPE Annu. Tech. Conf. Exhib. 5, 3274–3288. https://doi.org/10.2118/170819-ms

Hussain, S.T., Rahman, S.S., Azim, R.A., Haryono, D., Regenauer-Lieb, K., 2021. Multiphase fluid flow through fractured porous media supported by innovative laboratory and numerical methods for estimating relative permeability. Energy and Fuels 35, 17372–17388. https://doi.org/10.1021/acs.energyfuels.1c01313

Ibrahim, A.F., Elkatatny, S., Al Ramadan, M., 2022. Prediction of Water Saturation in Tight Gas Sandstone Formation Using Artificial Intelligence. ACS Omega 7, 215–222. https://doi.org/10.1021/acsomega.1c04416

Islam, M.R., 2015. Overview of Reservoir Simulation of Unconventional Reservoirs. Unconv. Gas Reserv. 487–547. https://doi.org/10.1016/B978-0-12-800390-9.00007-4

Issa, R.I., 1986. Solution of the Implicitly Discretised Fluid Flow Equations by Operator-Splitting. J. Comput. Phys. 62, 40–65. https://doi.org/https://doi.org/10.1016/0021-9991(86)90099-9

Jacob, A., Peltz, M., Hale, S., Enzmann, F., Moravcova, O., Warr, L.N., Grathoff, G., Blum, P., Kersten, M., 2021. Simulating permeability reduction by clay mineral nanopores in a tight sandstone by combining computer X-ray microtomography and focussed ion beam scanning electron microscopy imaging. Solid Earth 12, 1–14. https://doi.org/10.5194/se-12-1-2021

Jahanbakhsh, A., Wlodarczyk, K.L., Hand, D.P., Maier, R.R.J., Maroto-Valer, M.M., 2020. Review of microfluidic devices and imaging techniques for fluid flow study in porous geomaterials. Sensors (Switzerland) 20, 1–63. https://doi.org/10.3390/s20144030

Jalali, M.R., Dusseault, M.B., 2012. Coupling Geomechanics and Transport in Naturally Fractured Reservoirs. Int. J. Min. Geo-Eng. 46, 105–131.

Jerauld, G.R., Salter, S.J., 1990. The Effect of Pore-Structure on Hysteresis in Relative Permeability and Capillary Pressure: Pore-Level Modeling. Transp. Porous Media 5, 103–151.

Jin, M., Somerville, J., Smart, B.G.D., 2000. Coupled Reservoir Simulation Applied to the Management of Production Induced Stress-Sensitivity, in: International Oil and Gas Conference and Exhibition in China. Society of Petroleum Engineers, Beijing, China, pp. 997–1008. https://doi.org/10.2523/64790-ms

Jing, L., 2003. A review of techniques, advances and outstanding issues in numerical modelling for rock mechanics and rock engineering. Int. J. Rock Mech. Min. Sci. 40, 283–353. https://doi.org/10.1016/S1365-1609(03)00013-3

Kazemi, H, Gilman, J R, and Eisharkawy, A.M., 1992. Analytical and numerical solution of oil recovery from fractured reservoirs with empirical transfer functions. SPE Res Eng 7, 219–227. https://doi.org/doi:10.2118/19849-PA

Kazemi, H., Merrill, L.S., 1979. Numerical Simulation of Water Imbibition in Fractured Cores. Soc. Pet. Eng. J. 19, 175–182. https://doi.org/10.2118/6895-pa

Keller, A.A., 1997. High resolution cat imaging of fractures in consolidated materials. Int. J. Rock Mech. Min. Sci. 34, 3–4. https://doi.org/https://doi.org/10.1016/S1365-1609(97)00181-0

Kim, D.K., Ban, I., Poh, B.Y., Shin, S.C., 2022. A useful guide of effective mesh-size decision in predicting the ultimate strength of flat- and curved plates in compression. J. Ocean Eng. Sci. https://doi.org/10.1016/j.joes.2022.02.014

Kim, J., 2010. Sequential methods for coupled geomechanics and multiphase flow. Stanford University.

Kim, J., Tchelepi, H.A., Juanes, R., 2013. Rigorous coupling of geomechanics and multiphase flow with strong capillarity. SPE J. 18, 1123–1139. https://doi.org/10.2118/141268-PA

Kim, J., Yang, D., Moridis, G.J., Rutqvist, J., 2012. Numerical studies on two-way coupled fluid flow and geomechanics in hydrate deposits. SPE J. 1. https://doi.org/SPE-141304-PA

Kumar, A., Camilleri, D., Brewer, M., 2016. Comparative analysis of dual continuum and discrete fracture simulation approaches to model fluid flow in naturally fractured, low-permeability reservoirs, in: SPE Low Perm Symposium. Society of Petroleum Engineers, Denver, Colorado, USA. https://doi.org/10.2118/180221-ms

Lamur, A., Kendrick, J.E., Eggertsson, G.H., Wall, R.J., Ashworth, J.D., Lavallée, Y., 2017. The permeability of fractured rocks in pressurised volcanic and geothermal systems OPEN. Sci. Rep. 7, 6173. https://doi.org/10.1038/s41598-

017-05460-4

Latham, J.P., Xiang, J., Belayneh, M., Nick, H.M., Tsang, C.F., Blunt, M.J., 2013. Modelling stress-dependent permeability in fractured rock including effects of propagating and bending fractures. Int. J. Rock Mech. Min. Sci. 57, 100–112. https://doi.org/10.1016/j.ijrmms.2012.08.002

Lavrov, A., 2017. Coupling in hydraulic fracturing simulation, Porous Rock Fracture Mechanics: With Application to Hydraulic Fracturing, Drilling and Structural Engineering. Elsevier Ltd. https://doi.org/10.1016/B978-0-08-100781-5.00003-8

Lay, T., Wallace, T.C., 1995. Elasticity and Seismic Waves, in: Modern Global Seismology. Academic Press, pp. 34–69. https://doi.org/https://doi.org/10.1016/S0074-6142(05)80003-8.

Lee, S., Schechter, D.S., 2015. Iteratively coupled fluid flow and geomechanics simulation using estimated equivalent Permeability and porosity by fractal and statistical methods, in: SPE Annual Technical Conference and Exhibition. https://doi.org/10.2118/175113-ms

Lee, S.H., Lough, M.F., Jensen, C.L., 2001. Hierarchical modeling of flow in naturally fractured formations with multiple length scales conventional finite difference On the basis of their length (l f) relative to the finite difference grid size (/ g), fractures are classified as belonging to on. Water Resour. Res. 37, 443–455.

Lenormand, R., Zarcone, C., 1984. Role of Roughness and Edges During Imbibition in Square Capillaries. Soc. Pet. Eng. AIME, SPE. https://doi.org/10.2118/13264-ms

Lewis, R.W., Schrefler, B.A., 1999. The Finite Element Method in the Static and Dynamic Deformation and Consolidation of Porous, 2nd Editio. ed, Meccanica. Wiley. https://doi.org/10.1023/A:1004546808159

Li, K., Wolf, K.H.A.A., Rossen, W.R., 2022. A novel technique to estimate water saturation and capillary pressure of foam in model fractures. Colloids Surfaces A Physicochem. Eng. Asp. 632, 127800. https://doi.org/10.1016/j.colsurfa.2021.127800

Li, W., Frash, L.P., Welch, N.J., Carey, J.W., Meng, M., Wigand, M., 2021. Stress-dependent fracture permeability measurements and implications for shale gas production. Fuel 290, 119984. https://doi.org/10.1016/j.fuel.2020.119984

Lian, P.Q., Cheng, L.S., Ma, C.Y., 2012. The characteristics of relative permeability curves In naturally fractured carbonate reservoirs. J. Can. Pet. Technol. 51, 137–142. https://doi.org/10.2118/154814-PA

Lima, M.G., Schädle, P., Vogler, D., Saar, M.O., Kong, X., 2019. Impact of Effective Normal Stress on Capillary Pressure in a Single Natural Fracture. Eur. Geotherm. Congr. Proc. 11–14.

Liu, J., Jiang, L., Liu, T., Yang, D., 2020. Modeling tracer flowback behaviour for a fractured vertical well in a tight formation by coupling fluid flow and geomechanical dynamics. J. Nat. Gas Sci. Eng. 84, 103656. https://doi.org/10.1016/j.jngse.2020.103656

Longuemare, P., Mainguy, M., Lemonnier, P., Onaisi, A., Gérard, C., Koutsabeloulis, N., 2002. Geomechanics in reservoir simulation: Overview of coupling methods and field case study. Oil Gas Sci. Technol. 57, 471–483. https://doi.org/10.2516/ogst:2002031

Ma, J., Wang, J., 2016. A Stress-Induced Permeability Evolution Model for Fissured Porous Media. Rock Mech. Rock Eng. 49, 477–485. https://doi.org/10.1007/s00603-015-0760-8

Majorana, C.E., Salomoni, V.A., Mazzucco, G., Pomaro, B., Xotta, G., 2015. Mechanical Modelling of Concrete and Concrete Structures. Comput. Technol. Rev. 11, 1–29. https://doi.org/10.4203/ctr.11.1

Maniscalco, R., Fazio, E., Punturo, R., Cirrincione, R., Di Stefano, A., Distefano, S., Forzese, M., Lanzafame, G., Leonardi, G.S., Montalbano, S., Pellegrino, A.G., Raele, A., Palmeri, G., 2022. The Porosity in Heterogeneous Carbonate Reservoir Rocks: Tectonic versus Diagenetic Imprint—A Multi-Scale Study from the Hyblean Plateau (SE Sicily, Italy). Geosci. 12. https://doi.org/10.3390/geosciences12040149

Martin, A., Zhang, H., Tagavi, K.A., 2017. An introduction to the derivation of surface balance equations without the excruciating pain. Int. J. Heat Mass Transf. 115, 992–999. https://doi.org/10.1016/j.ijheatmasstransfer.2017.07.078

McCartney, J.S., Sánchez, M., Tomac, I., 2016. Energy geotechnics: Advances in subsurface energy recovery, storage, exchange, and waste management.

Comput. Geotech. 75, 244–256. https://doi.org/10.1016/j.compgeo.2016.01.002

McDonald, A.E., Beckner, B.L., Chan, H.M., Jones, T.A., Wooten, S.O., 1991. Some important considerations in the simulation of naturally fractured reservoirs. Rocky Mt. Reg. Permeability Reserv. Symp. Exhib. Rocky Mt. Reg. Permeability Reserv. Symp. Exhib. 117–124. https://doi.org/10.2118/21814-ms

Mejia, C., Roehl, D., Rueda, J., Fonseca, F., 2022. Geomechanical effects of natural fractures on fluid flow in a pre-salt field. J. Nat. Gas Sci. Eng. https://doi.org/10.1016/j.jngse.2022.104772

Melchior, P.J., 1983. The Tides of the Planet Earth, 2nd ed. Pergamon Press, New York. https://doi.org/10.1016/0079-6611(83)90003-4

Merrill, L.S., 1975. Two phase flow in fractures. University of Denver, Denver, Colorado.

Mikelić, A., Wang, B., Wheeler, M.F., 2014. Numerical convergence study of iterative coupling for coupled flow and geomechanics. Comput. Geosci. 18, 325–341. https://doi.org/10.1007/s10596-013-9393-8

Minkoff, S.E., Stone, C.M., Bryant, S., Peszynska, M., Wheeler, M.F., 2003. Coupled fluid flow and geomechanical deformation modeling. J. Pet. Sci. Eng. 38, 37–56. https://doi.org/10.1016/S0920-4105(03)00021-4

Mohais, R., Xu, C., Dowd, P.A., Hand, M., 2012. Permeability correction factor for fractures with permeable walls. Res. Lett 39, 3403.

https://doi.org/10.1029/2011GL050519

Mohiuddin, M.A., Korvin, G., Abdulraheem, A., Awal, M.R., Khan, K., Khan, M.S., Hassan, H.M., 2000. Stress-Dependent Porosity and Permeability of a Suite of Samples From Saudi Arabian Sandstone and Limestone Reservoirs, in: International Symposium, Society of Core Analysts. Society of Core Analysts, Abu Dhabi, p. 33.

Muggeridge, A., Cockin, A., Webb, K., Frampton, H., Collins, I., Moulds, T., Salino, P., 2014. Recovery rates, enhanced oil recovery and technological limits. Philos. Trans. R. Soc. A Math. Phys. Eng. Sci. 372. https://doi.org/10.1098/rsta.2012.0320

Nakashima, T., Sato, K., Arihara, N., Yazawa, N., 2000. Effective Permeability Estimation for Simulation of Naturally Fractured Reservoirs. SPE - Asia Pacific Oil Gas Conf. 165–173. https://doi.org/10.2523/64286-ms

Nick, H.M., 2010. Towards large-scale modelling of fluid flow in fractured porous media. Imperial College London.

Nur, A., Simmons, G., 1969. Stress-Induced Velocity Anisotropy in Rock. an Experimental Study. J. Geophys. Res. 74, 6667–6674. https://doi.org/10.1029/jb074i027p06667

Oostrom, M., White, M.D., Porse, S.L., Krevor, S.C.M., Mathias, S.A., 2016. Comparison of relative permeability-saturation-capillary pressure models for simulation of reservoir CO2 injection. Int. J. Greenh. Gas Control 45, 70–85. https://doi.org/10.1016/j.ijggc.2015.12.013

Osorio, J.G., Chen, H., 1999. Numerical Simulation of the Impact of Flow-Induced Geomechanical Response on the Productivity of Stress-Sensitive Reservoirs SPE 51929. Soc. Pet. Eng.

Pan, F., Sepehrnoori, K., Chin, L.Y., 2007. Development of a coupled geomechanics model for a parallel compositional reservoir simulator, in: Proceedings - SPE Annual Technical Conference and Exhibition. Society of Petroleum Engineers, Anaheim, California, U.S.A., pp. 1294–1302. https://doi.org/10.2523/109867-ms

Pettersen, Ø., 2010. Compaction, permeability, and fluid flow in brent-type reservoirs under depletion and pressure blowdown. Open Pet. Eng. J. 3, 1–13. https://doi.org/10.2174/1874834101003010001

Pratt, W.E., Johnson, D.W., 1926. LOCAL SUBSIDENCE OF THE GOOSE CREEK OIL FIELD. J. Geol. 34, 577–590. https://doi.org/10.1086/623352

Pruess, K., Tsang, Y.W., 1990. On two-phase relative permeability and capillary pressure of rough-walled rock fractures. Water Resour. Res. 26, 1915–1926. https://doi.org/https://doi.org/10.1029/WR026i009p01915

Pyrack-Nolte, L.J., Myer, L.R., Cook, N.C.W., Witherspoon, P.A., 1987. Hydraulic and Mechanical Properties of Natural Fractures in low-permeability Rock, in: The Sixth International Conference on Rock Mechanics. Lawrence Berkeley Laboratory, Montreal, Quebec, Canada.

Pyrak-Nolte, L.J., Helgeson, D., Haley, G.M., Morris, J.W., 1992. Immiscible fluid flow in a fracture, in: Rock Mechanics – Proceedings of the 33rd US

Symposium. A.A. Balkema, Rptterdam, Netherlands, pp. 571–578.

Pyrak-Nolte, L.J., Nolte, D.D., Chen, D., Giordano, N.J., 2008. Relating capillary pressure to interfacial areas. Water Resour. Res. 44, 1–14. https://doi.org/10.1029/2007WR006434

Pyrak-Nolte, L.J., Nolte, D.D., Myer, L.R., Cook, N.G.W., 1990. Fluid flow through single fractures, in: Barton, N., Stephanson, O. (Eds.), Proceeding of the International Symposium on Rock Joints. Loen, Norway.

Rahman, M.J., Fawad, M., Mondol, N.H., 2022. 3D Field-Scale Geomechanical Modeling of Potential CO2 Storage Site Smeaheia, Offshore Norway. Energies 15. https://doi.org/10.3390/en15041407

Reitsma, S., Kueper, B.H., 1994. Laboratory measurement of capillary pressure-saturation relationships in a rock fracture. Water Resour. Res. 30, 865–878. https://doi.org/10.1029/93WR03451

Ren, G., Jiang, J., Younis, R.M., 2018. A Model for coupled geomechanics and multiphase flow in fractured porous media using embedded meshes. Adv. Water Resour. 122, 113–130. https://doi.org/10.1016/j.advwatres.2018.09.017

Ren, X., Zhao, Y., Deng, Q., Kang, J., Li, D., Wang, D., 2016. A relation of hydraulic conductivity — void ratio for soils based on Kozeny-Carman equation. Eng. Geol. 213, 89–97. https://doi.org/10.1016/j.enggeo.2016.08.017

Rocca, V., 2009. Development of a Fully Coupled Approach for Evaluation of

Wellbore Stability in Hydrocarbon Reservoirs. Am. J. Environ. Sci. 5, 781–790. https://doi.org/10.3844/ajessp.2009.781.790

Rod, K.A., Um, W., Colby, S.M., Rockhold, M.L., Strickland, C.E., Han, S., Kuprat, A.P., 2019. Relative permeability for water and gas through fractures in cement. PLoS One 14. https://doi.org/10.1371/journal.pone.0210741

Romm, E.S., 1966. Flow Characteristics of Fractured Rocks (in Russian). Nedra, Moscow.

Rossen, W.R., Kumar, A.T.A., 1992. Single- and Two-Phase Flow in Natural Fractures, in: The SPE Annual Technical Conference and Exhibition. Society of Petroleum Engineers, Washington. https://doi.org/https://doi.org/10.2118/24915-MS

Royer, P., Auriault, J.L., Lewandowska, J., Serres, C., 2002. Continuum modelling of contaminant transport in fractured porous media. Transp. Porous Media 49, 333–359. https://doi.org/10.1023/A:1016272700063

Rutqvist, J., Stephansson, O., 2003. The role of hydrochemical coupling in fractured rock engineering. Hydrogeol. J. 11, 7–40. https://doi.org/10.1007/s10040-002-0241-5

Sanaee, R., Oluyemi, G.F., Hossain, M., Oyeneyin, M.B., 2013. Stress effects on flow partitioning in fractured reservoirs: Equivalent porous media versus poro-elasticity coupled modeling, in: 447th U.S. Rock Mechanics/Geomechanics Symposium, 23-26 June 2013. American Rock Mechanics Association, San Francisco, California, pp. 2329–2337. https://doi.org/ARMA-2013-442

Sanaee, R., Oluyemi, G.F., Hossain, M., Oyeneyin, M.B., 2012. Fracture-Matrix Flow Partitioning and Cross Flow : Numerical Modeling of Laboratory Fractured Core Flood, in: COMSOL Conference, 10 – 12 October 2012. Milan. https://doi.org/10.1016/j.jallcom.2009.01.091

Sangnimnuan, A., Li, J., Wu, K., 2018. Development of Efficiently Coupled Fluid-Flow/Geomechanics Model To Predict Stress Evolution in Unconventional Reservoirs With Complex-Fracture Geometry. SPE J. 23, 640–660. https://doi.org/10.2118/189452-pa

Satter, A., Iqbal, G.M., 2016. 3 - Reservoir rock properties, in: Reservoir Engineering. Gulf Professional Publishing, pp. 29–79. https://doi.org/10.1016/B978-0-12-800219-3.00003-6

Saxena, V., Krief, M., Adam, L., 2018. Handbook of Borehole Acoustics and Rock Physics for Reservoir Characterization, Handbook of Borehole Acoustics and Rock Physics for Reservoir Characterization. Elsevier, Amsterdam. https://doi.org/10.1016/c2016-0-03411-3

Settari, A., Mourits, F.M., 1998. A Coupled Reservoir and Geomechanical Simulation System. SPE J. https://doi.org/10.2118/50939-PA

Settari, A., Walters, D.A., 2001. Advances in Coupled Geomechanical and Reservoir Modeling With Applications to Reservoir Compaction. SPE J. 6. https://doi.org/SPE-74142-PA

Shad, S., Gates, I.D., 2010. Multiphase Flow in Fractures : Co-Current and Counter-Current Flow in a Multiphase Flow in Fractures : Co-Current and Counter-

Current Flow in a Fracture. J Can Pet Technol 49, 48–55. https://doi.org/10.2118/2008-147

Shojaei, A.K., Shao, J., 2017. Porous Rock Fracture Mechanics. Elsevier Ltd.

Simo, J.C., Taylor, R.L., Pister, K.S., 1985. Variational and projection methods for the volume constraint in finite deformation elasto-plasticity. Comput. Methods Appl. Mech. Eng. 51, 177–208. https://doi.org/10.1016/0045-7825(85)90033-7

Simulia, 2011. Abaqus 6.11/Theroy Manual. Simulia Corp., Providence, RI, USA.

Smith, R.Y., Lesueur, M., Kelka, U., Poulet, T., Koehn, D., 2022. Using fractured outcrops to calculate permeability tensors: implications for geothermal fluid flow and the influence of seismic-scale faults. Geol. Mag. 1–17. https://doi.org/10.1017/s0016756822000309

Snow, D., 1969. Anisotropic Permeability o[Fractured Media. Water Resour. Res. 5, 1273–1289.

Soares, E.J., Thompson, R.L., Niero, D.C., 2015. Immiscible liquid-liquid pressure-driven flow in capillary tubes: Experimental results and numerical comparison. Phys. Fluids 27. https://doi.org/10.1063/1.4928912

Soeder, D.J., 2021. Fracking and the Environment, Fracking and the Environment. https://doi.org/10.1007/978-3-030-59121-2

Soulaine, C., Quintard, M., Allain, H., Baudouy, B., Van Weelderen, R., 2015. A PISO-like algorithm to simulate superfluid helium flow with the two-fluid model.

Comput. Phys. Commun. 187, 20–28. https://doi.org/10.1016/j.cpc.2014.10.006

Stalker, R., Graham, G.M., Oluyemi, G., 2009. Modelling staged diversion treatments and chemical placement in the presence of near-wellbore fractures. Proc. - SPE Int. Symp. Oilf. Chem. 2, 745–757. https://doi.org/10.2118/121683-ms

Stone, T., Bowen, G., Papanastasiou, P., Fuller, J., 2000. Fully coupled geomechanics in a commercial reservoir simulator, in: SPE European Petroleum Conference, 24-25 October. Society of Petroleum Engineers, Paris, France, pp. 45–52. https://doi.org/10.2523/65107-ms

Tachibana, S., Ito, S., Iizuka, A., 2020. Constitutive model with a concept of plastic rebound for expansive soils. Soils Found. 60, 179–197. https://doi.org/10.1016/j.sandf.2020.02.007

Teimoori, A., Chen, Z., Rahman, S.S., Tran, T., 2003. Calculation of Permeability Tensor Using Boundary Element Method Provides a Unique Tool to Simulate Naturally Fractured Reservoirs. Proc. - SPE Annu. Tech. Conf. Exhib. 5035–5042. https://doi.org/10.2118/84545-ms

Terzaghi, K., Peck, R.B., Mesri, G., 1940. Soil Mechanics in Engineering Practice, 3rd ed. John Wiley & Sons, Inc., New York City, New York.

Torsaeter, O.; Silseth, J.K., 1985. The effects of sample shape and boundary conditions on capillary imbibition ., in: North Sea Chalk Symposium. Stavanger.

Tran, D., Settari, A., Nghiem, L., 2004. New iterative coupling between a reservoir simulator and a geomechanics module. SPE J. 9, 362–369. https://doi.org/10.2118/88989-PA

Versteeg, H K Malalasekera, W., 2007. An Introduction to Parallel Computational Fluid Dynamics: The Finite Volume Method, 2nd ed, IEEE Concurrency. Pearson. https://doi.org/10.1109/mcc.1998.736434

Wang, C., Elsworth, D., Fang, Y., Zhang, F., 2020. Influence of fracture roughness on shear strength, slip stability and permeability: A mechanistic analysis by three-dimensional digital rock modeling. J. Rock Mech. Geotech. Eng. 12, 720–731. https://doi.org/10.1016/j.jrmge.2019.12.010

Wang, C., Jiang, Y., Gao, R., Wang, X., 2021. On the evolution of relative permeability of two-phase flow in rock fractures: The effect of aperture distribution. IOP Conf. Ser. Earth Environ. Sci. 861. https://doi.org/10.1088/1755-1315/861/4/042112

Weishaupt, K., Joekar-Niasar, V., Helmig, R., 2019. An efficient coupling of free flow and porous media flow using the pore-network modeling approach. J. Comput. Phys. X 1. https://doi.org/10.1016/j.jcpx.2019.100011

Whitaker, S., 1969. Advances in theory of fluid motion in porous media. Ind. Eng. Chem. 61, 14–28. https://doi.org/10.1021/ie50720a004

Wilkinson, D., Willemsen, J.F., 1983. Invasion percolation: a new form of percolation theory. J. Phys. 16, 3365–3376.

Wu, Y.-S., 2016. Multiphase Flow in Fractured Porous Media. Gulf Professional Publishing, Oxford, UK. https://doi.org/10.1016/b978-0-12-803848-2.00009-x

Xiao, C.N., Denner, F., van Wachem, B.G.M., 2017. Fully-coupled pressure-based finite-volume framework for the simulation of fluid flows at all speeds in complex geometries. J. Comput. Phys. 346, 91–130. https://doi.org/10.1016/j.jcp.2017.06.009

Xiong, X., Li, B., Jiang, Y., Koyama, T., Zhang, C., 2011. Experimental and numerical study of the geometrical and hydraulic characteristics of a single rock fracture during shear. Int. J. Rock Mech. Min. Sci. 48, 1292–1302. https://doi.org/10.1016/j.ijrmms.2011.09.009

Xu, C., Dong, S., Wang, H., Wang, Z., Xiong, F., Jiang, Q., Zeng, L., Faulkner, L., Tian, Z.F., Dowd, P., Martinez-Frias, J., Hermans, T., 2021. Modelling of Coupled Hydro-Thermo-Chemical Fluid Flow through Rock Fracture Networks and Its Applications. Geosci. 11, 153. https://doi.org/10.3390/geosciences11040153

Yang, L., Ładosz, A., Jensen, K.F., 2019. Analysis and simulation of multiphase hydrodynamics in capillary microseparators. Lab Chip 19, 706–715. https://doi.org/10.1039/C8LC01296B

Yang, X., Yan, J., Shiming, W., Yayun, Z., Jianhua, X., Hua, Z., 2018. Characterization of multi-scale discrete-fracture/matrix interactions in naturally fractured reservoirs using mud loss data, in: 2nd International Discrete Fracture Network Engineering Conference, 20-22 June. American Rock

Mechanics Association, Seattle, Washington, USA. https://doi.org/ARMA-DFNE-18-0294

Yang, Z.D., Wang, Y., Zhang, X.Y., Qin, M., Su, S.W., Yao, Z.H., Liu, L., 2020. Numerical Simulation of a Horizontal Well With Multi-Stage Oval Hydraulic Fractures in Tight Oil Reservoir Based on an Embedded Discrete Fracture Model. Front. Energy Res. 8, 1–12. https://doi.org/10.3389/fenrg.2020.601107

Zhang, J., Standifird, W.B., Roegiers, J.C., Zhang, Y., 2007. Stress-dependent fluid flow and permeability in fractured media: From lab experiments to engineering applications. Rock Mech. Rock Eng. 40, 3–21. https://doi.org/10.1007/s00603-006-0103-x

Zhang, Z., He, S., Gu, D., Gai, S., Li, G., 2018. Effects of stress-dependent permeability on well performance of ultra-low permeability oil reservoir in China. J. Pet. Explor. Prod. Technol. 8, 565–575. https://doi.org/10.1007/s13202-017-0342-2

Zhangxin, C., Guanren, H., Yuanle, M., 2006. Computational Methods for Multiphase Flows in Porous Media. Society for Industrial and Applied Mathematics, Philadelphia.

Zhao, M., Zhang, Q., Li, S., Zhao, H., 2017. Investigation on coupled fluid-flow and stress in dual model rock mass with time-dependent effect and its simulation. Geosci. 7, 1–14. https://doi.org/10.3390/geosciences7030045

Zhao, Y., Liu, H.H., 2012. An elastic stress-strain relationship for porous rock under anisotropic stress conditions. Rock Mech. Rock Eng. 45, 389–399.

https://doi.org/10.1007/s00603-011-0193-y

Zhu, Z., Liu, J., Liu, H., Wu, M., Song, Z., 2021. Numerical investigation of single- And two-phase flow in porous media with a bifurcated fracture. Phys. Fluids 33. https://doi.org/10.1063/5.0052229

Zivar, D., Foroozesh, J., Pourafshary, P., Salmanpour, S., 2019. Stress dependency of permeability, porosity and flow channels in anhydrite and carbonate rocks. J. Nat. Gas Sci. Eng. 70, 102949. https://doi.org/10.1016/j.jngse.2019.102949

Zoback, M.D., 2007. Reservoir Geomechanics, 1st ed, Reservoir Geomechanics. Cambridge University Press, Cambridge. https://doi.org/10.1017/CBO9780511586477

Appendix A

Table A1. Berea Sandstone experimental data (Kazemi and Merrill, 1979)

Rock and fluid properties	
Parameters	Value
Core Diameter (cm)	2.54
Core Length (cm)	7.62
Fracture Aperture (cm)	0.03
Pore Volume (PV) $\left(cm^3\right)$	6.62
Pore Size Distribution Index (λ_p)	0.674
Entry Capillary Pressure (P_{ec}) (Pa)	345
Matrix Permeability (k_{mat}) (mD)	97
Matrix Porosity	0.185
Fracture Porosity	1
Fracture Permeability (k_f)(mD)	10000
Velocity (m/s)	0.000039
Oil viscosity ($Pa.s$)	0.0046
Water viscosity ($Pa.s$)	0.001

Table A2. Clashach core flooding experimental data (Kazemi and Merrill, 1979)

Rock and fluid properties	
Parameters	Value
Core Diameter (cm)	3.79
Core Length (cm)	7.54
Fracture Aperture (μm)	130
Pore Volume (PV) $\left(cm^3\right)$	6.62
Pore Size Distribution Index (λ_p)	0.674
Entry Capillary Pressure (P_{ec}) (Pa)	345
Matrix Permeability (k_{mat}) (mD)	315
Matrix Porosity	0.154
Fracture Porosity	1
Fracture Permeability (k_f)(D)	310
Oil viscosity ($Pa.s$)	0.001
Oil density $\left(kg/m^3\right)$	850
Young's Modulus (Pa)	40e9
Poisson's Ratio	0.14
Density of rock $\left(kg/m^3\right)$	2500
Swell Index	0.0052

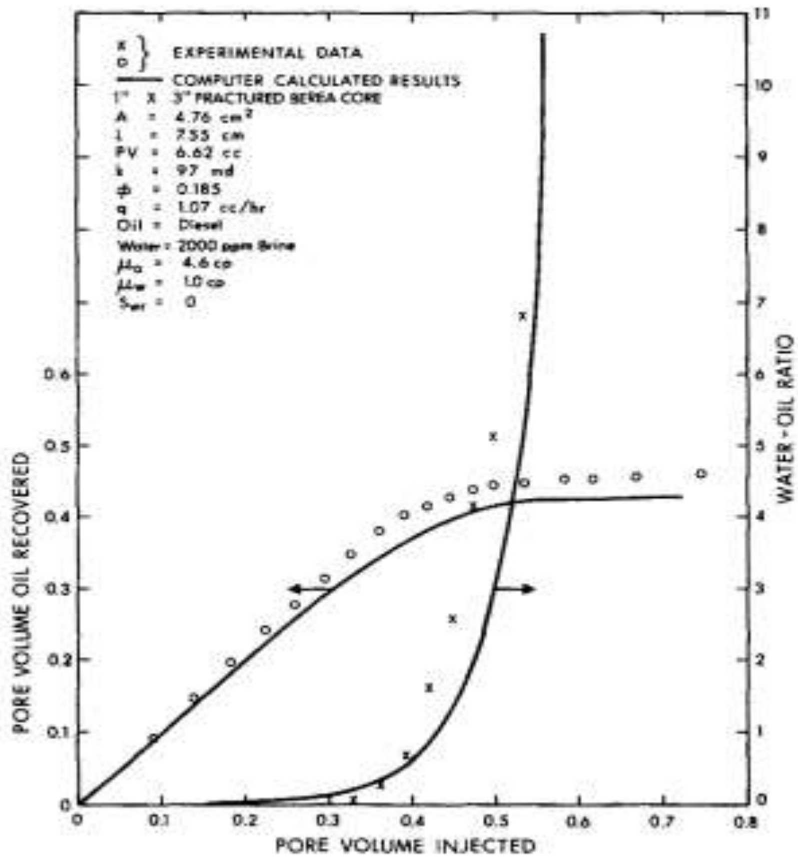

Figure A1. Recovered volume w.r.t volume of water injection (Kazemi and Merrill, 1979)

Appendix B

Table B1. Sensitivity of flow rate calculation to differential pressure under the external stress loading of 21.4 MPa (Stalker et al., 2009)

Differential Pressure (psi)	Flow Rate (cm3/s)	
	Actual	Calculated
0.85	0.033	0.033
2.55	0.100	0.100
1.70	0.067	0.067
1.27	0.050	0.050
0.85	0.033	0.033

Table B2. Calculated matrix and fracture flow rates (Stalker et al., 2009)

Injection Rate		Differential	Fracture Permeability	Flow rate (cm3/s		Combined calculated	Calculated/Actual
ml/h	cm3/s	pressure (psi)	(mD)	Fracture	Matrix	Flow rate (cm3/s)	Flow rate
Overburden Pressure 3100 psi							
120	0.033	0.75		0.0054	0.02399	0.029	0.88
360	0.100	2.47		0.0179	0.07901	0.097	0.97
240	0.067	1.62	72429	0.0117	0.05182	0.064	0.95
180	0.050	1.22		0.0088	0.03903	0.048	0.96
120	0.033	0.79		0.0057	0.02527	0.031	0.93
Overburden Pressure 2800 psi							
120	0.033	0.71		0.0063	0.02271	0.029	0.87
360	0.100	2.36		0.0210	0.07549	0.096	0.96
240	0.067	1.54	82907	0.0137	0.04926	0.063	0.94
180	0.050	1.14		0.0101	0.03647	0.047	0.93
120	0.033	0.75		0.0067	0.02399	0.031	0.92
Overburden Pressure 2500 psi							
120	0.033	0.66		0.0079	0.02111	0.029	0.87
360	0.100	2.2		0.0262	0.07036	0.097	0.97
240	0.067	1.43	100966	0.0171	0.04574	0.063	0.94
180	0.050	1.07		0.0128	0.03422	0.047	0.94
120	0.033	0.69		0.0082	0.02207	0.030	0.91
Overburden Pressure 2200 psi							
120	0.033	0.57		0.0091	0.01838	0.027	0.82
360	0.100	1.99		0.0315	0.06375	0.095	0.95
240	0.067	1.29	121745	0.0204	0.04130	0.062	0.93
180	0.050	0.97		0.0153	0.03091	0.046	0.92
120	0.033	0.61		0.0097	0.01962	0.029	0.88
Overburden Pressure 1900 psi							
120	0.033	0.55		0.0091	0.01764	0.027	0.80
360	0.100	1.93		0.0319	0.06178	0.094	0.94
240	0.067	1.22	125377	0.0202	0.03914	0.059	0.89
180	0.050	0.87		0.0143	0.02779	0.042	0.84
120	0.033	0.57		0.0093	0.01811	0.027	0.82
Overburden Pressure 1600 psi							
360	0.100	1.68		0.0462	0.05356	0.100	1.00
240	0.067	1.11	176594	0.0308	0.03564	0.066	1.00
180	0.050	0.84		0.0231	0.02679	0.050	1.00
120	0.033	0.56		0.0153	0.01776	0.033	0.99
Overburden Pressure 1300 psi							
120	0.033	0.25		0.0135	0.00801	0.022	0.65
360	0.100	1.07		0.0575	0.03404	0.091	0.91
240	0.067	0.65	276053	0.0352	0.02085	0.056	0.84
180	0.050	0.51		0.0273	0.01616	0.043	0.87
120	0.033	0.32		0.0175	0.01034	0.028	0.83
Overburden Pressure 1000 psi							
120	0.033	0.21		0.0134	0.00666	0.020	0.60
360	0.100	0.91		0.0585	0.02905	0.088	0.88
240	0.067	0.52	310397	0.0334	0.01658	0.050	0.75
180	0.050	0.39		0.0248	0.01231	0.037	0.74
120	0.033	0.21		0.0136	0.00676	0.020	0.61